5-2011

Discrete Element Method (DEM) Analyses for Hot-Mix Asphalt (HMA) Mixture Compaction

Jingsong Chen

University of Tennessee - Knoxville, jchen27@utk.edu

To the Graduate Council:

I am submitting herewith a dissertation written by Jingsong Chen entitled "Discrete Element Method (DEM) Analyses for Hot-Mix Asphalt (HMA) Mixture Compaction." I have examined the final electronic copy of this dissertation for form and content and recommend that it be accepted in partial fulfillment of the requirements for the degree of Doctor of Philosophy, with a major in Civil Engineering.

Baoshan Huang, Major Professor

We have read this dissertation and recommend its acceptance:

Eric C. Drumm, Richard M. Bennett, Qiuhong Zhao, Xiang Shu

Accepted for the Council:

Carolyn R. Hodges

Vice Provost and Dean of the Graduate School

(Original signatures are on file with official student records.)

To the Graduate Council:
I am submitting herewith a dissertation written by Jingsong Chen entitled "Discrete Element Method (DEM) Analyses for Hot-Mix Asphalt (HMA) Mixture Compaction." I have examined the final electronic copy of this dissertation for form and content and recommend that it be accepted in partial fulfillment of the requirements for the degree of Doctor of Philosophy, with a major in Civil Engineering.

Baoshan Huang
Major Professor

We have read this dissertation
and recommend its acceptance:

Eric C. Drumm

Richard M. Bennett

Qiuhong Zhao

Xiang Shu

Accepted for the Council:

Carolyn R. Hodges
Vice Provost and Dean of the Graduate School

(Original signatures are on file with official student records.)

Discrete Element Method (DEM) Analyses for Hot-Mix Asphalt (HMA) Mixture Compaction

A Dissertation Presented for
the Doctor of Philosophy
Degree
The University of Tennessee, Knoxville

Jingsong Chen
May 2011

ACKNOWLEDGEMENTS

I would like to express my sincere gratitude to Dr. Baoshan Huang for his support, patience, generosity, and encouragement during my doctoral studies at the University of Tennessee, and his continuous interest and guidance throughout this Ph.D. research.

I would like to extend my sincere thanks to Dr. Eric C. Drumm, Dr. Richard M. Bennett, Dr. Qiuhong Zhao, and Dr. Xiang Shu for serving as committee members and for their help in my Ph.D. research.

I want to express my sincere appreciation to Dr. Feng Chen for his suggestion and help in my Ph.D. research. I would also like to thank Mr. Qiao Dong, Mr. Hao Wu, Mr. Xiaoyang Jia, Mr. Sheng Zhao, Mr. Ximiao Jiang, and Mr. Changjun Zhou for their valuable comments throughout this research program.

Finally, I would like to thank my family and my girl friend Jiaoyan Cui for their supports, understanding, and encouragement during my Ph.D. studies.

ABSTRACT

Asphalt mixture compaction is an important procedure of asphalt mixture construction and can significantly affect the performance of asphalt pavement. Many laboratory compaction methods (or devices), have been developed to study the asphalt mixture compaction. Nevertheless, the whole process from the selection of aggregate to laboratory compaction is still time-consuming and requires significant human and material resources. In order to better understand asphalt mixture compaction, some researchers began to use finite element method (FEM) to study and analyze mixture compaction. However, FEM is a continuum approach and lacks the ability to take into account the slippage and interlocking of aggregates during compaction. Discrete Element Method (DEM) is a discontinuum analysis method, which can simulate the deformation process of joint systems or discrete particle assembly under quasi-static and dynamic condition. Therefore, it can overcome the shortcomings of FEM and is a more effective tool than FEM to simulate asphalt mixture compaction.

In this study, an open source 3D DEM code implemented with the C++ programming language was modified and applied to simulate the compaction of hot-mix asphalt (HMA). A viscoelastic contact model was developed in the DEM code and was verified through comparison with well established analytical solutions. The input parameters of the newly developed contact model were obtained through nonlinear regression analysis of dynamic modulus test results. Two commonly used compaction methods (Superpave gyratory compaction and asphalt vibratory compaction) and one linear kneading compaction based on APA machine were simulated using the DEM code, and the DEM

compaction models were verified through the comparison between the DEM predicted results and the laboratory measured test results. The air voids distribution within the asphalt specimens was also analyzed by post processing virtual DEM compaction digital specimens and the level of heterogeneity of the air void distribution within the specimens in the vertical and lateral directions was studied.

The DEM simulation results in this study were in a relatively good agreement with the experimental data and previous research results, which demonstrates that the DEM is a feasible method to simulate asphalt mixture compaction under different loading conditions and, with further research, it could be a potentially helpful tool for asphalt mix design by reducing the number of physical compactions in the laboratory.

TABLE OF CONTENTS

LIST OF FIGURES

LIST OF TABLES

CHAPTER 1 INTRODUCTION

1.1 Research Background

With the rapid population growth and economic development, humanity's scope of activities have been significantly expanded, the travel frequency has greatly increased and the freight transportation has also sharply risen, which brings huge pressure and challenges to our current transportation systems. Pavement is one of the basic transportation infrastructures and plays an important role in social development and human life. According to the material of surface course, pavements can be divided into two types, Portland cement concrete pavement and Hot Mix Asphalt (HMA) pavement. Compared with cement concrete pavement, HMA is easy to construct, maintain and provides better riding comfort and thus has become the major type of pavement structure in the US. The United States has more than 2 million miles of paved roads and highways, and 94 percent of those are surfaced with asphalt (NAPA, 2010).

HMA mixture consist of asphalt cement binder, coarse and fine aggregates, and mineral filler mixed together at a high temperature and placed and compacted on the road while still hot. Asphalt mixture compaction is an important procedure of asphalt mixture construction and can significantly affect the performance of asphalt pavement. The quality of an asphalt pavement depends largely on the compaction in the field. A well designed and produced asphalt mixture might have bad pavement performance because of poor field compaction. The under compaction of asphalt mixture typically results in

relatively low density. Lower densities mean higher air voids and lower pavement strength, which will likely introduce moisture into the open voids and makes the pavement susceptible to moisture and other failures (Zube 1962; Santucci, 1985). Linden (Linden, 1989) studied the effect of compaction on asphalt concrete performance based on three separate sources and pointed out a 1 percent increase in air voids tends to produce about a 10 percent loss in pavement life. The over compaction of asphalt mixture can also result in some problems. The over compaction can not provide sufficient voids to allow asphalt cement to expand and contract as temperature changes and thus induces rutting (Huber, 1987; Miller, 1988). Brown (1990) pointed out a properly designed and compacted mixture should contain enough air voids to prevent rutting due to plastic flow but low enough air voids to prevent permeability of air and water. The density must be closely controlled to insure that the voids stay within an acceptable range.

In order to study the compaction condition effect and produce a realistic laboratory test specimen that can represent the structure of the paving mixture, many laboratory compaction methods (or devices) have been developed, examples include the Marshall impact hammer, Superpave Gyratory compactor, Linear Kneading Compactor, vibratory-kneading compactor, and the mobile steel wheel simulator. Among these compaction devices, the Marshall Impact hammer and Superpave Gyratory compactor are widely used in asphalt mixture design to obtain asphalt mixture samples for subsequent mix design quality control tests. The kneading compactor can simulate the roller compaction process which is closer to the real field compaction pattern since the asphalt mixture is kneaded and compressed to desired density during compaction. The most important factor of these devices is to adequately simulate field condition. Consuegra (1989)

evaluates the ability of five compaction devices to simulate field compaction. These compaction devices include the mobile steel wheel simulator, the Texas gyratory compactor, the California kneading compactor, the Marshall Impact hammer, and the Arizona vibratory-kneading compactor. After laboratory study of resilient moduli, indirect tensile strengths and strains at failure, tensile creep data of laboratory-compacted samples and field cores, he concluded that the Texas gyratory compactor demonstrated the ability to produce mixture with engineering properties nearest those determined from field cores. Ziauddin (1998) also compared different laboratory compaction methods (Marshall Impact Compaction and Gyratory Shear Compaction) to field compaction and concluded that the Gyratory Shear Compaction (angle of gyration 1.25°) method best represented the engineering properties of the field cores. Sadasivam (2004) investigated the effects of different compaction methods (Superpave Gyratory Compaction and Rolling Wheel Compaction) on the performance of mixture and found that the laboratory compacted mixture tend to be superior in their performance than the field cores.

Compared with field compaction, the scale of these laboratory compaction studies are much smaller and thus can greatly reduce the work of producing asphalt mixture samples, which need less time and also be relatively easy to control. These laboratory methods play important roles in asphalt mixture design and the research of asphalt mixture compaction. However, most of these methods usually require costly compaction devices and the whole process from the selection of aggregate to compaction is still a time consuming process. The laboratory compaction method is also difficult to study the movement of aggregates and the development of internal structure during compaction process. What’s more, it is hard to simulate the real condition of large scale field

compaction condition, like the real compaction boundary. In the laboratory, confinement is provided by the sides and bottom of the mold and the hammer. However, in the field, confinement is provided by the surrounding HMA material, the underlying layer and the compactor area in its zone of influence. In this case, some researchers try to find a more simple and effective way to study and analyze asphalt mixture compaction.

Numerical simulation is an effective tool for finding approximate solutions of complicated engineering and physical systems and has been widely used in aviation, mechanics, material science, chemistry, bioengineering etc. With the fast development of computer technology, the powerful calculation capability of computer makes the numerical simulation of asphalt mixture compaction possible, not only the small scale laboratory compaction but also the large scale field compaction. Compared with laboratory research method, numerical simulation has the advantages of low cost, less time consuming, flexible parameter analysis etc. and has been widely used in engineering analysis. In order to better understand asphalt mixture compaction, some researchers began to utilize numerical methods to study and analyze mixture compaction in recent years.

Koneru (2008) developed a constitutive theory within a thermodynamic setting to study compaction of asphalt mixes and used commercial FEM software ABAQUS to simulate the Superpave gyratory compactor (SGC) compaction process (Koneru, 2008). Zheng (2008) built a mechanical model to simulate pavement vibratory compacting process utilizing the FEM software ANSYS. Ter Huerne (2008) used the Finite Element Model (FEM) with code DiekA to simulate the compaction process of Hot Mix Asphalt under roller compaction conditions. However, hot mix asphalt mixture compaction

happens when mixture is still hot and slippages occur between aggregates. So the above mentioned FEM simulations consider HMA mixture as continuum media and lack the ability to take into account the slippage and interlocking of aggregate particles, which makes FEM asphalt mixture compaction simulation differ greatly from the real situation and thus limits the ability to simulate the true mixture compaction process.

Recently, the discrete element method (DEM) has become popular because it can capture the behaviour of particulate materials better than the finite element method (FEM). Discrete Element Method (DEM) is a discontinuum analysis method, which can simulate the deformation process of joint systems or discrete particles assembly under quasi-static and dynamic condition. Therefore, it can potentially overcome the shortcomings of FEM and is a more effective tool than FEM to simulate asphalt mixture compaction.

1.2 Previous and Related Studies

1.2.1 DEM Application in Asphalt Mixture

Discrete element method is a powerful numerical tool for computing the motion of a large number of particles. With the inherent advantage of DEM, it developed rapidly in the past decades and has been widely used to model the behavior of soils and granular materials (John *et al*, 1989; Jing, 2000; Yao and Anandarajah, 2003; Xie and Zhao, 2009). However, the application of DEM in asphalt concrete is relatively new (Meegoda and Chang, 1994). With the development of computer technology and the appearance of commercial DEM software, researchers began to use discrete element method to

investigate the mechanical behavior of asphalt materials and achieved remarkable results. Most of the current DEM research work mainly includes modulus or dynamic modulus prediction, creep property, fracture behavior etc.

Buttlar and You (2001) applied DEM method to predict creep strains of an HMA laboratory specimen subjected to diametral loads in the Superpave indirect tension test (IDT). They pointed out micromechanical modeling has tremendous potential benefits in the field of asphalt technology for reducing or eliminating costly tests to characterize asphalt-aggregate mixture for the design and control of these materials. Dai and You (2007) established 2D discrete element models for the prediction of viscoelastic creep stiffness of asphalt mixture and acquired reasonable prediction of the creep stiffness across the reduced loading time. Collop *et al.* (2004, 2006) used DEM to simulate the behavior of a highly idealized bituminous mixture (single-sized spherical particles mixed with bitumen) under uniaxial and triaxial compressive creep loading. The DEM predicted results have reasonable agreement with experimental data and are similar to measured curves in magnitude and shape demonstrating the applicability of DEM approach on asphalt mixture.

You and Buttlar (2004, 2006) applied a clustered DEM approach to predict the asphalt mixture complex modulus by using a 2D DEM simulation and found that the DEM approach provides a low modulus prediction compared with the experimental tests for some fine mixes due to insufficient aggregate–aggregate contact in the 2-D model. You and Buttlar (2005) utilized a 2D clustered discrete element modeling approach to simulate hollow cylinder tensile (HCT) test and the DEM simulation results were found to be in good agreement with experimental measurements across a range of test

temperatures and loading frequencies for the coarse-grained mixture investigated. Adhikari and You (2010) further extended the 2D DEM approach and established 3D discrete element models of the hollow cylindrical asphalt concrete specimens and found that the 3D DEM models yielded a better dynamic modulus prediction than 2D DEM models.

Kim (2005, 2008) utilized the discrete element method to investigate fracture mechanisms in asphalt concrete at low temperatures. The DEM simulation results were shown to compare favorably with experimental results and can provide more details of the fracture process in laboratory fracture tests. Abbas *et al.* (2007) analyzed the viscoelastic response of asphalt mixture using the discrete-element method and the DEM model predictions compared favorably with the SPT measurements. DEM approach has also been employed to study the effect of air voids on asphalt mixture. You *et al.* (2010) modeled an idealized asphalt mixture with discrete element method for both two-dimensional (2D) and three-dimensional (3D) cases and proved that the specimens have lower modulus when the air voids are higher in the specimens for both 2D and 3D models.

Most DEM studies have so far mainly focused on the mechanical behavior of cooled asphalt concrete. Little researches have been done in hot and loose asphalt mixture by using DEM. However, during hot mix asphalt mixture compaction, the compaction happens when the mixture is still hot and the slippage occurs between aggregate, which make DEM an ideal method to simulate asphalt mixture compaction. Wang *et al.* (2006) first presented the investigation of the compaction mechanics using Discrete Element Method (DEM). The DEM simulations can provide a micro view of asphalt mixture compaction process in which aggregates particles translate and rotate to positions forming

denser packing. The DEM simulation results indicate that DEM can describe the compaction phenomena consistently with field observations and empirical experience (Wang *et al.*, 2007).

1.2.2 DEM Codes and Open Source Code YADE

With the development of DEM theory, many DEM codes were gradually developed and became important tools for DEM research, such as Trubal, and GRANULA. These DEM codes play an important role in discrete element method research and application. After the 1990s, some commercial DEM software like UDEC, 3DEC, PFC2D, PFC3D began to appear. With the easy operability and strong post processing capability, PFC2D and PFC3D are the most commonly used commercial DEM codes in granular materials analysis (Wang *et al.*, 2003; Buttlar and You, 2001). PFC2D/3D has its own FISH programming language and specific commands for the DEM simulation, which makes the core code a black box for software user and thus restricts the ability of users to extend their applications to other fields as they needed. The commercial DEM codes usually are quite expensive, which makes them unavailable for many research organizations, especially for small research institutions and individual researchers. The open source code generally requires no licensing fees and has been advocated widely in many research areas. A report by Standish Group states that adoption of open-source software models has caused the savings of about $60 billion per year to consumers (Rothwell, 2008).

For commercial software, the research objectives and realizable research contents depend highly on the software's functions provided by software vendors, which

significantly limits researchers' flexibility and capability to do more detailed analysis and handle more complicated research projects. However, open source code is modifiable and allows the user to improve/modify the existing code–base according to the need of research, reducing the dependence on software vendors and enabling the unlimited tuning and improvement of the software for more complicated projects. For the open source code, the code developer/ modifier is also the user of the code. For commercial software, the user's feedback is not so direct and effective for the software developer. In addition, due to the common sharing character of opening resource code, the community of users can share their code and collaborate with each other, which is helpful to dig and solve the early bugs and improve the software. The modifiable character of open source code also makes it possible to couple different codes/methods, like coupled DEM-FEM and DEM-CFD, and thus further enriches researcher's studying means and expands the research scope, which is usually difficult to do with commercial software.

Although convenient, commercial software usually limits one's ability to improve/modify the existing code–base and is usually costly. A common solution is to write one's own software to perform a simulation. In such circumstances, open source DEM codes are catching more and more researchers' attention and have been increasingly used in granular materials analysis in recent years. These open source DEM codes include BALL and TRUBAL (Cundall 1978), YADE (Kozicki and Donzé 2008), Pasimodo (Popp and Schiehlen 2008), LMGC90 (Renouf, 2006), Esys-particle (2008) etc.

YADE Open-DEM is a 3D Open Source GNU/GPL Software framework designed with dynamic libraries and implemented in C++ language, which started as an offspring from SDEC at Grenoble University. It provides a stable and uniform environment for

researchers to implement computational algorithms for DEM and has been successfully used in composite material and geotechnical field (Donzé, 1999; Camborde, 2000; Belheine, 2008; Harthong, 2009; Jerier, 2010). With the extendable and modifiable character of open source code, YADE DEM code could also be coupled with other codes/methods, which expands the research scope. Rousseau (2008) coupled Discrete Element model and Finite Element model to analyze concrete structures and found the coupled FEM/DEM model worked more efficiently than DEM model. Chen *et al.* (2008) used coupled open source code YADE-OpenFOAM to investigate upward seepage flow and obtained reasonable results for the analysis of a particle-fluid system. In this research, the YADE Open-DEM will be modified to simulate the asphalt mixture compaction and the output from virtual digital specimens will be further processed to investigate the heterogeneous air voids distribution.

YADE simulation involves bodies between which interactions occur (Figure 1.1). These interactions can be detected and processed by certain computational algorithms and physical rules. The result of these algorithms can be a moment, a force, a displacement etc., which in general produce a response that affects the body state. Figure 1.2 shows the basic structure of YADE framework which is divided into several layers. Libraries in the lowest layer define functionalities which are not only related to the YADE simulation itself but also can be utilized by other codes. The generic layer represents the core of YADE which defines the most abstract simulation-related classes, such as bodies (particles), interactions, engines. The common layer defines data structures commonly used by various simulation types, such as Newton's law, time integration algorithms, damping methods, classes storing information about bodies or interactions etc.

Specialized layer is based on the common layer and contains functionality for particular simulation methods (DEM, FEM, Lattice Model). The top layer is a Graphical User Interface with an interface based on QT provided (Kozicki and Donze, 2008).

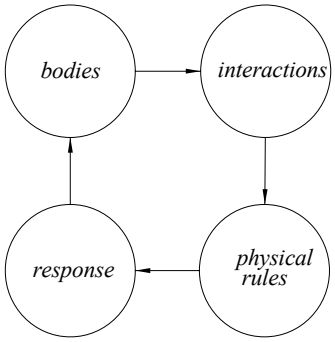

Figure 1.1 Schematics of Simulation Loop (Kozicki and Donze, 2008)

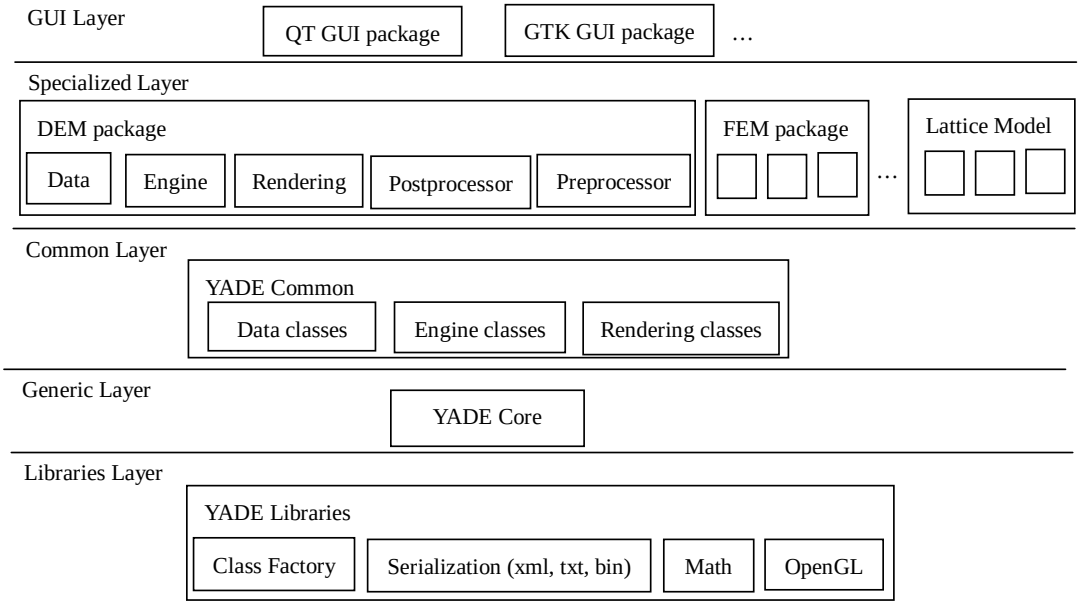

Figure 1.2 Layered structure of YADE framework (Kozicki and Donze, 2008)

1.3 Research Objectives and Significance

The primary objective of the research is to simulate asphalt compaction process by using an open source DEM code and to investigate the heterogeneous air voids

distribution with the help of DEM simulation. The objectives can be divided into the following parts:

1. To develop a viscoelastic DEM contact model for HMA compaction simulation and to validate the viscoelastic contact model code with well established analytical solution (Chapter 2);
2. To determine the input parameters of DEM viscoelastic contact model by fitting Burger's model to dynamic modulus test results (Chapter 3);
3. To establish a DEM Superpave Gyratory Compaction (SGC) model and validate the SGC model by comparing the DEM predicted air voids with laboratory compaction test results, and study the effects of different factors (such as compaction pressure, gyration angle, temperature, aggregate shape) on SGC compaction (Chapter 4);
4. To establish a DEM Vibratory Compaction model and validate the DEM model by comparing the DEM predicted air voids with laboratory compaction test results, and study the effects of different factors (such as vibration pressure, speed) on Vibratory compaction (Chapter 5);
5. To develop a laboratory linear kneading compaction test based on the Asphalt Pavement Analyzer (APA) machine and simulate the APA linear kneading compaction by using open source DEM codes; To evaluate APA linear kneading compaction DEM model through a comparison of the predicted and laboratory measured results and investigate the effects of different factors (such as moving load, speed, boundary conditions) on compaction (Chapter 6);

6. To analyze air voids distribution within asphalt specimen by post processing virtual DEM compaction digital specimen and investigate the level of heterogeneity of the air void distribution within the specimen in the vertical and lateral directions, and study the effect of compaction method, aggregate gradation, specimen height, mold size and shape on air voids distribution (Chapter 7).

Although there are many laboratory compaction methods (or devices) now available to study the asphalt mixture compaction, the compaction devices are pretty expensive and the whole process is also quite time consuming and highly dependent on an engineering's personal experience. Numerical analysis is another important tool to study asphalt mixture compaction. The widely used finite element method (FEM) lacks the ability to account for the slippage between aggregate particles, thus limit their ability to simulate the true mixture compaction process.

In this study, an open source 3D DEM code was first applied to simulate the compaction of hot-mix asphalt (HMA) by using Superpave gyratory compactor, asphalt vibration compactor and self developed APA linear kneading compactor. A viscoelastic contact model was developed for asphalt mixture and the parameters were obtained through nonlinear regression analysis of dynamic modulus test results. The DEM simulation results have a good agreement with lab test results, which prove that DEM can be used to simulate different kinds of compaction methods. Discrete element method provides a new way to study asphalt mixture compaction through internal microscopic view and have tremendous potential to help understand asphalt mixture compaction process. With the advantage of low cost, modifiability and common sharing, open source code significantly reduces researcher's dependence of software vendor, and greatly

enriches researcher's studying means and expands research scope, and has a wide application prospect in scientific research.

Although some assumptions in this paper are not very close to the real situation and the DEM simulation results are still not accurate enough to satisfy the need of asphalt mixture design, it is the first try to study asphalt mixture compaction process using discrete element method. Therefore, this research provides a good starting point for DEM simulation of asphalt mixture compaction and could offer a base studying for further research. The finite element method which was used for simple 2D elastic analysis at the early stage and became a widely used tool in more complicated fields (like nonlinear, viscoelastic, micro 3D analysis etc) later, with further research (combination with other recently developed techniques, like X-ray computed tomography imaging technique, fluid-solid coupling, clump technique etc.), DEM simulation could come closer to describe the reality of asphalt mixture compaction and have tremendous potential to help researchers understand the micro structure of asphalt mixture compaction.

CHAPTER 2 BURGERS CONTACT LAW AND VERIFICATION

2.1 Discrete Element Method

The Discrete Element Method (DEM) is a discontinuous approach and a powerful numerical tool for computing the motion of a large number of particles such as granular material. The DEM was first introduced by Cundall (1971) for the analysis of rock-mechanics problems and then applied to soils by Cundall and Strack (1979). Different from traditional continuum computational method, in DEM each element is separated and can have independent movement. All particles are assumed rigid bodies and the interaction only happens at contacts or interfaces between these bodies. Behavior at the contacts uses a soft-contact approach and rigid particles are allowed to overlap one another at contact points. According to the force-displacement law, the overlap in every contact will generate an interaction force between particles. A set of contact forces acting on the particle and the external stresses (like gravity) will cause the motion of particles which is calculated by the Newton's second law. The motion of particles consequently change the contact situation and results in the changes of contact forces between particles, which continually bring about new motion of particles.

In order to simplify the calculation process, discrete element method usually uses the following assumption:

(1) All particles are considered as rigid bodies and the geometry of particles will not change under the extrusion force between particles. The deformation of particle system is the summation of deformations in contact points of all particles;

(2) The contacts between particles happen at a tiny small area, i.e. contact at point;

(3) The contact behavior of particles is soft contact which allows some overlap in the contact points between rigid particles. The value of the overlap in each contact can be determined by force displacement law. Compared with the size of particles, the overlap between particles is small and it is also much smaller than the translation and rotation of particles;

(4) The interaction only happens at contacts between particles and the time step should be small enough to make sure that each particle only has force effect on its contacted particles and will not affect other particles.

(5) The values of speed and acceleration are constant in each specific time step and single rigid particle motion is predicted by Newton's second law of motion.

(6) Time step chosen is so small that, during a single time step, disturbances cannot propagate from any particle further than its immediate neighbors. Then, at all times, the forces acting on any particle are determined exclusively by its interaction with the particles with which it is in contact.

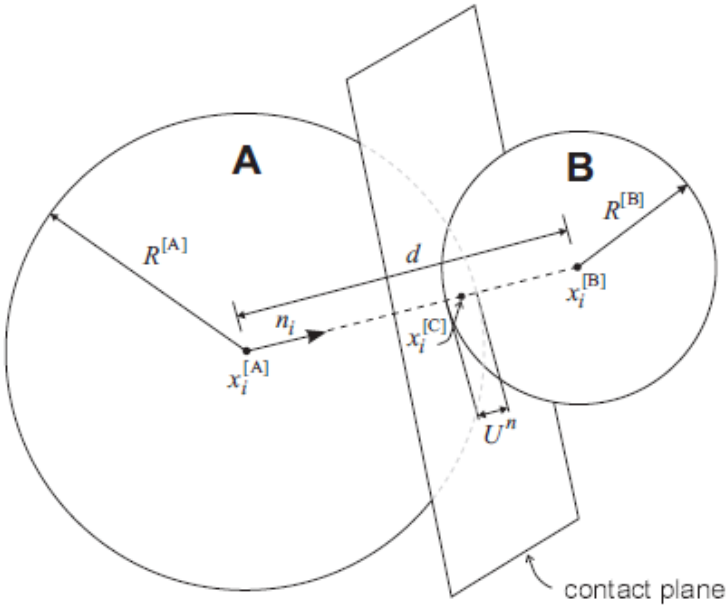

Figure 2.1 Contact between two particles (Itasca, 2004)

In continuum computational method, stress-strain relation is used to describe the physical properties of materials. However, in DEM the overall constitutive behavior of material is reflected through the force-displacement law in each contact, which is the key component of discrete element method and can significantly influence the correctness and rationality of the DEM simulation. The force-displacement law describes the relationship between contact force and relative displacement in each contact point $x_i^{[C]}$ (Figure 2.1), which includes the relationship between normal contact force and normal displacement, shear contact force and shear displacement. Here a simple elastic contact model was presented to explain the concept of force-displacement law. The contact force of elastic contact model can be calculated by following equations:

$$F_i^n = K^n U^n n_i \tag{2.1}$$

$$\Delta F_i^s = -K^s \Delta U^s \tag{2.2}$$

Where F_i^n and ΔF_i^s are the normal contact force and shear contact force increment between particles (or wall), K^n and K^s are the normal stiffness [force/displacement] and shear stiffness at the contact respectively, U^n and ΔU^s are normal displacement and shear displacement increment between particles (or wall), n_i is the unit normal for ball-ball contact, or is directed along the line defining the shortest distance for ball-wall contact.

In each time step, the geometry and motion condition of each particle are known values, then the normal displacement U^n and shear displacement increment ΔU^s can be calculated, and thus the normal contact force F_i^n and shear contact force increment ΔF_i^s between particles can be obtained with force-displacement law. The resultant contact force and external force will result in the new motion of particles and further change particles' geometry and motion condition in next time step.

In DEM the motion of each rigid body follows the Newton's laws of motion which provides the fundamental relationship between particle motion and the forces causing that motion. With Newton's second law, the acceleration $\ddot{x}_i$ and angular acceleration $\dot{\omega}_i$ can be calculated with the following equations:

$$F_i = m(\ddot{x}_i - g_i) \qquad \text{(translational motion)} \qquad (2.3)$$

Where m is the mass of the particle; g_i is the body force acceleration vector; and F_i is the resultant force arising from the contact forces and external forces acting on the particle.

$$M_1 = I_1 \dot{\omega}_1 + (I_3 - I_2)\omega_3\omega_2$$

$$M_2 = I_2 \dot{\omega}_2 + (I_1 - I_3)\omega_1\omega_3 \qquad \text{(rotational motion)} \qquad (2.4)$$

$$M_3 = I_3 \dot{\omega}_3 + (I_2 - I_1)\omega_2\omega_1$$

Where I_1, I_2, I_3 are the principal mass moments of inertia of the particle; $\dot{\omega}_1$, $\dot{\omega}_2$ and $\dot{\omega}_3$ are the angular accelerations about the principal axes; and M_1, M_2, M_3 are the components of the resultant moment to the principal axes arising from the contact forces and external forces acting on the particle.

For a spherical particle and disk-shaped particle, the rotational motion equation can be further simplified as follow:

$$M_3 = I_3 \dot{\omega}_3 + (\beta m R^2)\dot{\omega}_3 \tag{2.5}$$

Where β = 2/5 or 1/2 (spherical or disk-shaped particle).

By using centered finite difference method, the accelerations at time t can be expressed as the following form:

$$\ddot{x}_i^{(t)} = \frac{1}{\Delta t}(\dot{x}_i^{(t+\Delta t/2)} - \dot{x}_i^{(t-\Delta t/2)}) \tag{2.6}$$

$$\dot{\omega}_3^{(t)} = \frac{1}{\Delta t}(\omega_3^{(t+\Delta t/2)} - \omega_3^{(t-\Delta t/2)}) \tag{2.7}$$

Solving these expressions and above Newton's laws of motion simultaneously , the velocities at time (t+Δt/2) are obtained.

$$\dot{x}_i^{(t+\Delta t/2)} = \dot{x}_i^{(t-\Delta t/2)} + (\frac{F_i^{(t)}}{m} + g_i)\Delta t \tag{2.8}$$

$$\omega_3^{(t+\Delta t/2)} = \omega_3^{(t-\Delta t/2)} + (\frac{M_3^{(t)}}{I})\Delta t \tag{2.9}$$

The position of the particle center at time t+Δt can be calculated as follow:

$$x_i^{(t+\Delta t)} = x_i^{(t)} + \dot{x}_i^{(t+\Delta t/2)} \Delta t \tag{2.10}$$

In order to account for energy losses during inter-particle or particle/wall collisions, viscous damping and local non-viscous damping are commonly used in the discrete element method. Local non-viscous damping act on each ball, while viscous damping acts at each contact. In this study, Cundall non-viscous damping was used as local non-viscous damping to dissipate energy by damping the unbalanced force in the system and the damping coefficients α=0.3 were chosen empirically on the basis of simulations of small numbers of particles. In DEM, viscous damping adds normal and shear dashpots at each contact to reflect the energy loss upon collision. In this study, the Burger's contact model was employed and a new viscoelastic contact engine was developed in YADE code to simulate asphalt mixture, which has two dashpot components to provide damping effect.

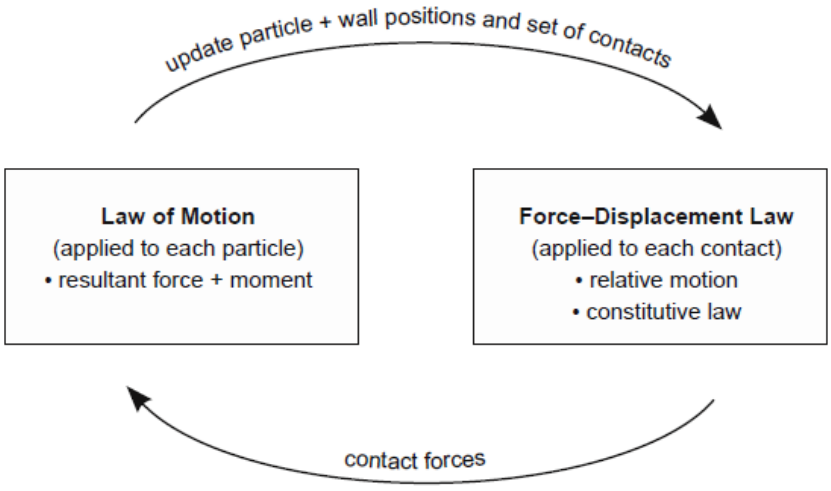

Figure 2.2 Calculation cycle in DEM (Itasca, 2004)

From above content, it can be seen that the calculations performed in the DEM alternate between the application of Newton's second law to the particles and a force-

displacement law at the contacts. The calculation cycle of DEM consists of the repeated application of the law of motion to each particle, a force-displacement law to each contact, and a constant updating of wall positions (Figure 2.2). The steps of DEM calculation can be summarized as followings:

1) Calculate time step for current iteration;
2) Get geometry and motion properties of particles from last time step results;
3) Update the velocity and position of walls based on the specified input wall velocities or boundary conditions.
4) Detect collisions between particles and walls with the new updated particles and wall geometry and motion properties.
5) Calculate the contact force between particles based on the relative deformation between the two entities at each contact and corresponding force-displacement law, and add the force vector to the unbalanced force vector;
6) Calculate the body force (like gravitational force) of each particles and add to the unbalanced force vector;
7) Apply the damping effect (force) to the resultant unbalanced force;
8) Apply the calculated unbalanced force to the particles, and calculate particles' new accelerations and angular accelerations with the Newton's second law;
9) Update its velocity and position based on the new accelerations and angular accelerations
10) Perform time integrations of particles according to their new accelerations;
11) Repeat the loop (step 1-10) until the calculation is terminated.

2.2 Burgers' Contact Model

2.2.1 Contact Model in Asphalt Mixture DEM Simulation

In DEM all particles are assumed rigid bodies and the interaction only happens at contacts or interfaces between these bodies. The overall constitutive behavior of a material is simulated by associating the constitutive model with each contact. Therefore, the contact behavior is an extremely important aspect and critical factor in DEM, which can significantly influence the correctness and rationality of the DEM simulation.

Due to the advantages of easy realization, simple input parameter and fast calculation speed in DEM simulation, elastic contact model has been used to simulate asphalt mixture by many researchers. In 2001, Buttlar and You used elastic contact law in DEM model to predict strains of a hot mix asphalt laboratory specimen subjected to diametral loads in the Superpave Indirect Tension Test (IDT) and did a parametric study on the synthetic IDT specimen (Buttlar and You, 2001). You and Buttlar (2004) employed elastic contact law in discrete element modeling to predict the asphalt mixture complex modulus in extension/compression across a range of test temperatures and load frequencies by invoking the correspondence principle. Their research focused on asphalt materials tested at lower temperatures, where strain levels are chosen to keep response in the linear viscoelastic range. Dai and You (2007) utilized elastic contact model in DEM simulation to predict creep stiffness of asphalt mixture at different loading times and test temperatures. In their study, the elastic–viscoelastic correspondence principle was used to bridge the elastic simulation and mixture viscoelastic response through the input of viscoelastic mastic creep stiffness. Collop *et al.* (2004, 2006) used elastic contact

properties to simulate the behaviour of a highly idealized bituminous mixture under uniaxial and triaxial compressive creep tests and investigated the effect of the shear and normal contact stiffness on bulk material properties. They found that the bulk modulus is linearly dependent on the normal contact stiffness and independent of the shear contact stiffness and Poisson's ratio is dependent on only the ratio of the shear contact stiffness to the normal contact stiffness.

However, asphalt mixture is a thermal rheological material which generally behaves in a viscoelastic or viscoelastoplastic fashion, and its properties depend upon the temperature, loading frequency, and level of strain. Although the elastic contact model has some advantages in DEM simulation and can indirectly study the viscoelastic behavior of asphalt mixture with the help of elastic–viscoelastic correspondence principle, it can not reflect the real viscoelastic property in DEM simulation. In order to truly reflect the viscoelastic behavior of asphalt mixture, viscoelastic contact model have been increasingly used in the DEM simulation of asphalt mixture. Burgers' model is a widely used viscoelastic model to study the rheological behavior of asphalt mixture, which can greatly describe the creep, relaxation and dynamic properties of asphalt mixture and is gaining popularity in the DEM simulation of asphalt mixture.

In order to capture the time dependent behaviour of bitumen, Collop *et al.* (2006) also used Burger's model to predict axial, volumetric and distortional strain for uniaxial creep test and obtained good agreement with measured results. Abbas *et al.* (2007) used Burgers contact law in DEM model which subjected to sinusoidal loads similar to those applied in the simple performance test (SPT) and found the DEM predicted dynamic moduli compared favorably with the experimentally measured values. Liu *et al.* (2009)

developed a viscoelastic discrete element simulation approach for asphalt mixture based on the Burger's model and conducted discrete element (DE) simulations of uniaxial compressive tests. The dynamic moduli and phase angles of asphalt mixture were predicted with 2D discrete element simulations under cyclic loading conditions and got less than 10 % prediction error. Adhikari and You (2010) employed Burger's contact model to characterize the viscoelastic behaviors of the asphalt mixture and calculated the strain response of the asphalt concrete under a tensile haversine load at the inner core of the hollow cylindrical specimen to determine the dynamic modulus which was found within a 5% range of difference compared with laboratory test results.

In this study, in order to simulate the time- and temperature-dependent property of asphalt mixture, Burger's constitutive model was employed and a new constitutive law engine was developed in the YADE code to process the calculation.

2.2.2 Constitutive Behavior of Burger's Model

In rheological model theory, elasticity, viscosity and plasticity are considered as the basic elements to characterize mechanical behavior of materials. These basic elements also known as mechanical constants can be described by using definite mechanical models, i.e. mechanical constitutive relations. The basic mechanical elements can form more complicated models through parallel and series connection with each other and thus can further reflect the real mechanical behaviors of materials. Viscoelastic material has both elastic and viscosity behaviors and can be described by elastic and viscosity mechanical elements. The simplest mathematics models of elastic and viscosity elements are Hooke's spring and dashpot models (Figure 2.3 and 2.4).

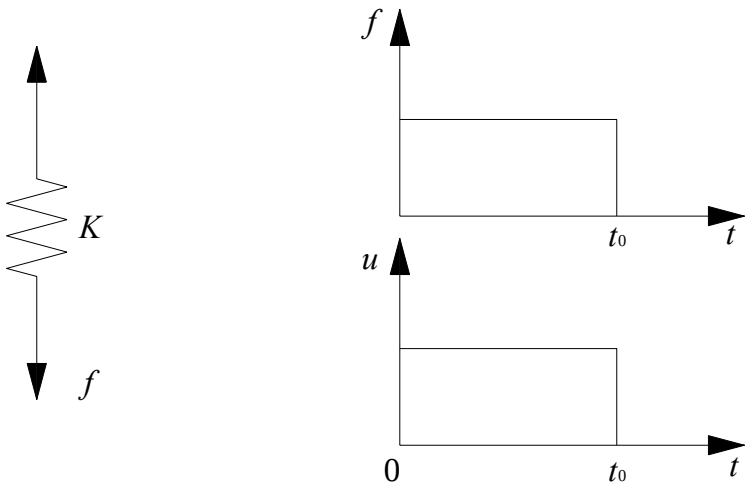

Figure 2.3 Hooke's spring and elastic deformation

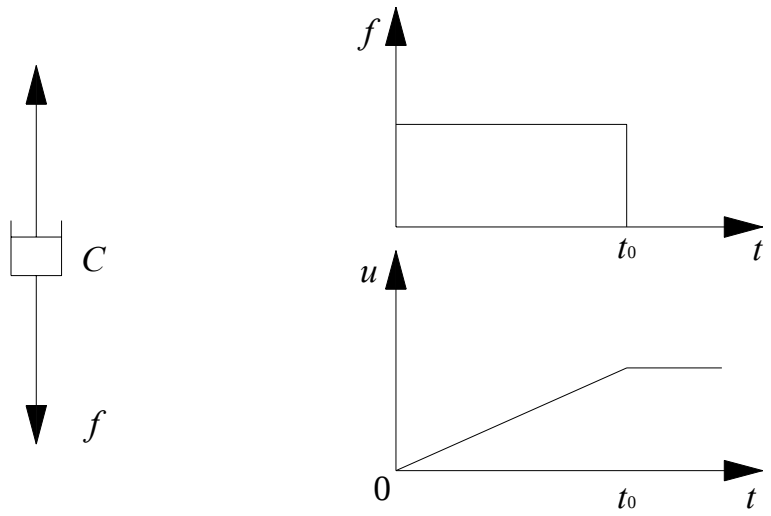

Figure 2.4 Dashpot and viscosity flow

The mechanical constitutive relations of Hooke's spring and dashpot models can be expressed as followings:

$$\sigma = K\varepsilon \qquad \text{Hooke's spring} \qquad (2.11)$$

$$\sigma = C\dot{\varepsilon} \qquad \text{Dashpot} \qquad (2.12)$$

Maxwell and Kelvin model are two commonly used combined models for time dependent materials. Maxwell model can be represented by a viscous Dashpot and an

elastic spring connected in series and is effective for predicting stress relaxation. Kelvin model is composed of a Hooke's spring and a Dashpot connected in parallel and is effective for predicting creep. Asphalt mixture has both stress relaxation and creep characteristics, which can be described by Burgers' model.

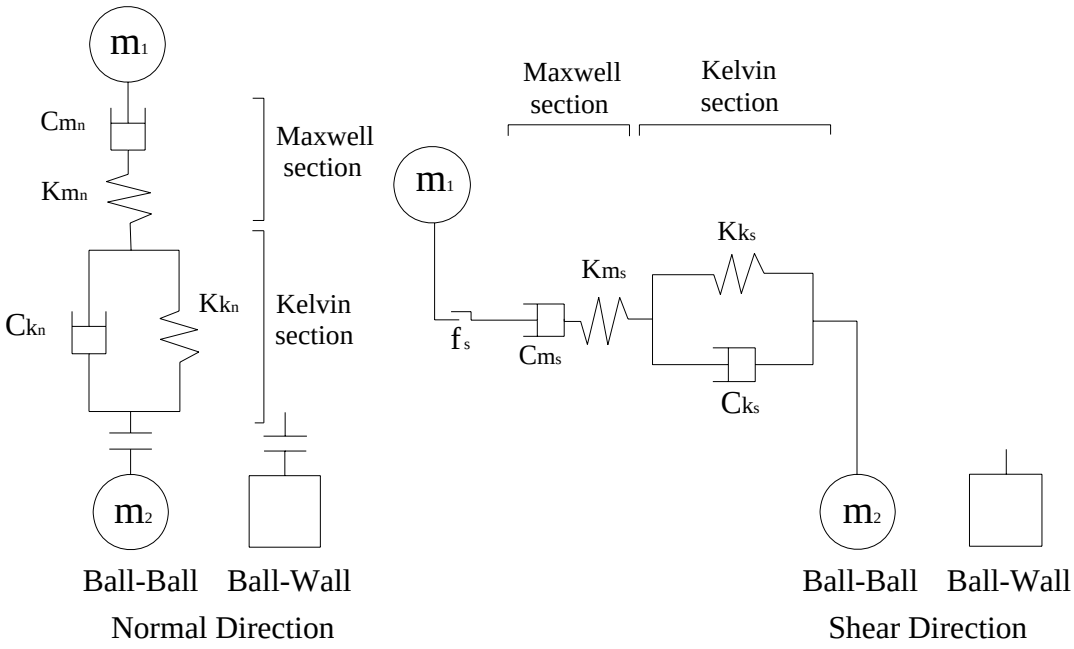

Figure 2.5 Burger's Model (Itasca, 2004)

Burgers model is four elements viscoelastic model and its mechanical constants are shown in Figure 2.5 (both normal and shear directions). It can be seen that this model comprises Maxwell model element and Kelvin model element, which are connected in series in both normal and shear directions, respectively. The deformation of Burgers model consists of three parts: the displacement of the Kelvin section (ε_k) and that of the Maxwell section (ε_{mK}， ε_{mC}) (Ferry 1970; Tschoegl 1989; Itasca, 2004; Abbs, 2004).

$$\varepsilon = \varepsilon_k + \varepsilon_{mK} + \varepsilon_{mC} \tag{2.13}$$

The first and second derivatives of above equation can be expressed as follows:

$$\dot{\varepsilon} = \dot{\varepsilon}_k + \dot{\varepsilon}_{mK} + \dot{\varepsilon}_{mC} \tag{2.14}$$

$$\ddot{\varepsilon} = \ddot{\varepsilon}_k + \ddot{\varepsilon}_{mK} + \ddot{\varepsilon}_{mC} \tag{2.15}$$

The stress σ carried by the mechanistic model and its first derivative can be represented by using the Kelvin section as follows:

$$\sigma = \pm K_k \varepsilon_k \pm C_k \dot{\varepsilon}_k \tag{2.16}$$

$$\dot{\sigma} = \pm K_k \dot{\varepsilon}_k \pm C_k \ddot{\varepsilon}_k \tag{2.17}$$

Where the K_{k} is stiffness for Kelvin section; C_{k} is viscosity for Kelvin section. In the equation the symbols $\pm$ and $\mp$ correspond to the cases of normal direction and shear direction, respectively.

The stress σ carried by the mechanistic model can also be represented by using the Maxwell section as follows:

$$\sigma = \pm K_m \varepsilon_{mK} \tag{2.18}$$

$$\dot{\sigma} = \pm K_m \dot{\varepsilon}_{mK} \tag{2.19}$$

$$\ddot{\sigma} = \pm K_m \ddot{\varepsilon}_{mK} \tag{2.20}$$

$$\sigma = \pm C_m \dot{\varepsilon}_{mC} \tag{2.21}$$

$$\dot{\sigma} = \pm C_m \ddot{\varepsilon}_{mC} \tag{2.22}$$

Where the K_{m} is stiffness for Maxwell section; C_{m} is viscosity for Maxwell section. Using equation 2.14-22, the constitutive behavior of Burger's model can be expressed with the following second-order partial differential equation (Itasca, 2004):

$$\sigma + [\frac{C_k}{K_k} + C_m(\frac{1}{K_k} + \frac{1}{K_m})]\dot{\sigma} + \frac{C_k C_m}{K_k K_m}\ddot{\sigma} = \pm C_m \dot{\varepsilon} \pm \frac{C_k C_m}{K_k}\ddot{\varepsilon} \tag{2.23}$$

This equation also can be expressed as follow simple format:

$$\sigma + p_1 \dot{\sigma} + p_2 \ddot{\sigma} = \pm q_1 \dot{\varepsilon} \pm q_2 \ddot{\varepsilon} \tag{2.24}$$

Where:

$$p_1 = \frac{C_m K_m + C_m K_k + C_k K_m}{K_k K_m}$$

$$p_2 = \frac{C_m C_k}{K_k K_m}$$

$$q_1 = C_m$$

$$q_2 = \frac{C_m C_k}{K_k}$$

2.3 Implement of Burger's Contact Model in DEM

In discrete element method, the constitutive relation is described using force-displacement pattern instead of stress-strain pattern in continuum approach. So equation 2.23 can be expressed as follows for Burger's contact law in DEM:

$$f + [\frac{C_k}{K_k} + C_m(\frac{1}{K_k} + \frac{1}{K_m})]\dot{f} + \frac{C_k C_m}{K_k K_m}\ddot{f} = \pm C_m \dot{u} \pm \frac{C_k C_m}{K_k}\ddot{u} \tag{2.25}$$

Where f is the contact force at contact point and u is the total displacement of the Burger's model (overlap between particles)

Since an explicit time stepping algorithm is employed in DEM simulation, above constitutive equation 2.25 should be further adapted for the realization in DEM codes.

Using a centered finite-difference time-stepping scheme, forces, displacements, and their partial derivatives can be expressed as follows:

$$u_m = \frac{u_m^{t+1} + u_m^t}{2}$$

$$\dot{u}_m = \frac{u_m^{t+1} - u_m^t}{\Delta t}$$

$$u_k = \frac{u_k^{t+1} + u_k^t}{2}$$

$$\dot{u}_k = \frac{u_k^{t+1} - u_k^t}{\Delta t}$$

$$f = \frac{f^{t+1} + f^t}{2}$$

$$\dot{f} = \frac{f^{t+1} - f^t}{\Delta t}$$

Where u_m^t and u_m^{t+1} are the displacement of Maxwell section at time step *t* and *t+1* respectively; u_k^t and u_k^{t+1} are the displacement of Kelvin section at time step *t* and *t+1* respectively; f^t and f^{t+1} are the contact force at time step *t* and *t+1* respectively.

From the equation 2.16, the first derivative of the deformation in Kelvin section can be expressed as follow:

$$\dot{u}_k = \frac{-K_k u_k \pm f}{C_k} \tag{2.26}$$

With a central difference approximation of the finite difference scheme, this equation can be expressed as follow:

$$\frac{u_k^{t+1}-u_k^t}{\Delta t}=\frac{1}{C_k}\left[-\frac{K_k(u_k^{t+1}+u_k^t)}{2}\mp\frac{f^{t+1}+f^t}{2}\right] \tag{2.27}$$

So,

$$u_k^{t+1}=\frac{1}{A}\left[Bu_k^t\pm\frac{\Delta t}{2C_k}(f^{t+1}+f^t)\right] \tag{2.28}$$

Where:

$$A=1+\frac{K_k\Delta t}{2C_k}$$

$$B=1-\frac{K_k\Delta t}{2C_k}$$

The deformation and the first derivative of Maxwell section are represented as follows:

$$u_m=u_{mK}+u_{mC} \tag{2.29}$$

$$\dot{u}_m=\dot{u}_{mK}+\dot{u}_{mC} \tag{2.30}$$

Using equation 2.19, 2.21 and 2.30,

$$\dot{u}_m=\pm\frac{\dot{f}}{K_m}\pm\frac{f}{C_m} \tag{2.31}$$

With a central difference approximation of the finite difference scheme, this equation can be expressed as follow:

$$\frac{u_m^{t+1}-u_m^t}{\Delta t}=\pm\frac{f^{t+1}-f^t}{K_m\Delta t}\pm\frac{f^{t+1}+f^t}{2C_m} \tag{2.32}$$

So,

$$u_m^{t+1}=\pm\frac{f^{t+1}-f^t}{K_m}\pm\frac{\Delta t(f^{t+1}+f^t)}{2C_m}+u_m^t \tag{2.33}$$

The total deformation and the first derivative of Burgers model can be represented as follows:

$$u = u_k + u_m \tag{2.34}$$

$$\dot{u} = \dot{u}_k + \dot{u}_m \tag{2.35}$$

With a central difference approximation of the finite difference scheme, this equation can be expressed as follow:

$$u^{t+1} - u^t = u_k^{t+1} - u_k^t + u_m^{t+1} - u_m^t \tag{2.36}$$

Using equation 2.28, 2.33 and 2.36, the contact force f^{t+1} can be expressed as the follow:

$$f^{t+1} = \frac{1}{C}[u^{t+1} - u^t + (1 - \frac{B}{A})u_k^t \mp Df^t] \tag{2.37}$$

Where:

$$C = \frac{\Delta t}{2C_k A} + \frac{1}{K_m} + \frac{\Delta t}{2C_m}$$

$$D = \frac{\Delta t}{2C_k A} - \frac{1}{K_m} + \frac{\Delta t}{2C_m}$$

It should be noted that in the beginning of iterative computation of Burgers model, there is no deformation in Kelvin section and all the deformation happens in the Maxwell section, so the initial condition of Burgers model at contacts can be expressed as follows:

$$u_k^0 = 0 \tag{2.38}$$

$$u^0 = u_k^0 + u_m^0 = 0 + u_m^0 = \frac{f^0}{K_m} \tag{2.39}$$

$$f^0 = K_m u_m^0 = K_m u^0 \tag{2.40}$$

The initial overlap u^0 can be calculated according to the geometry conditions of particles and then the initial contact force f^0 can be obtained from equation 2.40 with physical conditions of particles. Under the force effect of f^0 and external force (like gravitational force), particles will move to the new positions according to Newton's second law.

In next time step (t =1), the displacement u^1 can be calculated with updated geometry conditions of particles. From equation 2.37, with the known values u^1, u^0, u_k^0 (equal 0) and f^0, the contact force f^1 can be obtained. From equation 2.28, with the known values f^1, f^0, and u_k^0, the displacement of Kelvin section u_k^1 can be obtained, which will be used for the calculation of next step contact force f^2.

By using the similar procedure, the contact force at time step $t+1$ f^{t+1} can be calculated from equation 2.28 and 2.37 through iterative computation. Figure 2.6 presents the flow diagram of newly programmed Burger's contact law engine in YADE. The developed codes for Burger's contact law engine in YADE are presented in Appendices A, which was implemented by C++ language and would be executed in each contact and time step during simulation process. It should be noted that the developed codes are based on version YADE-0.12rc1.

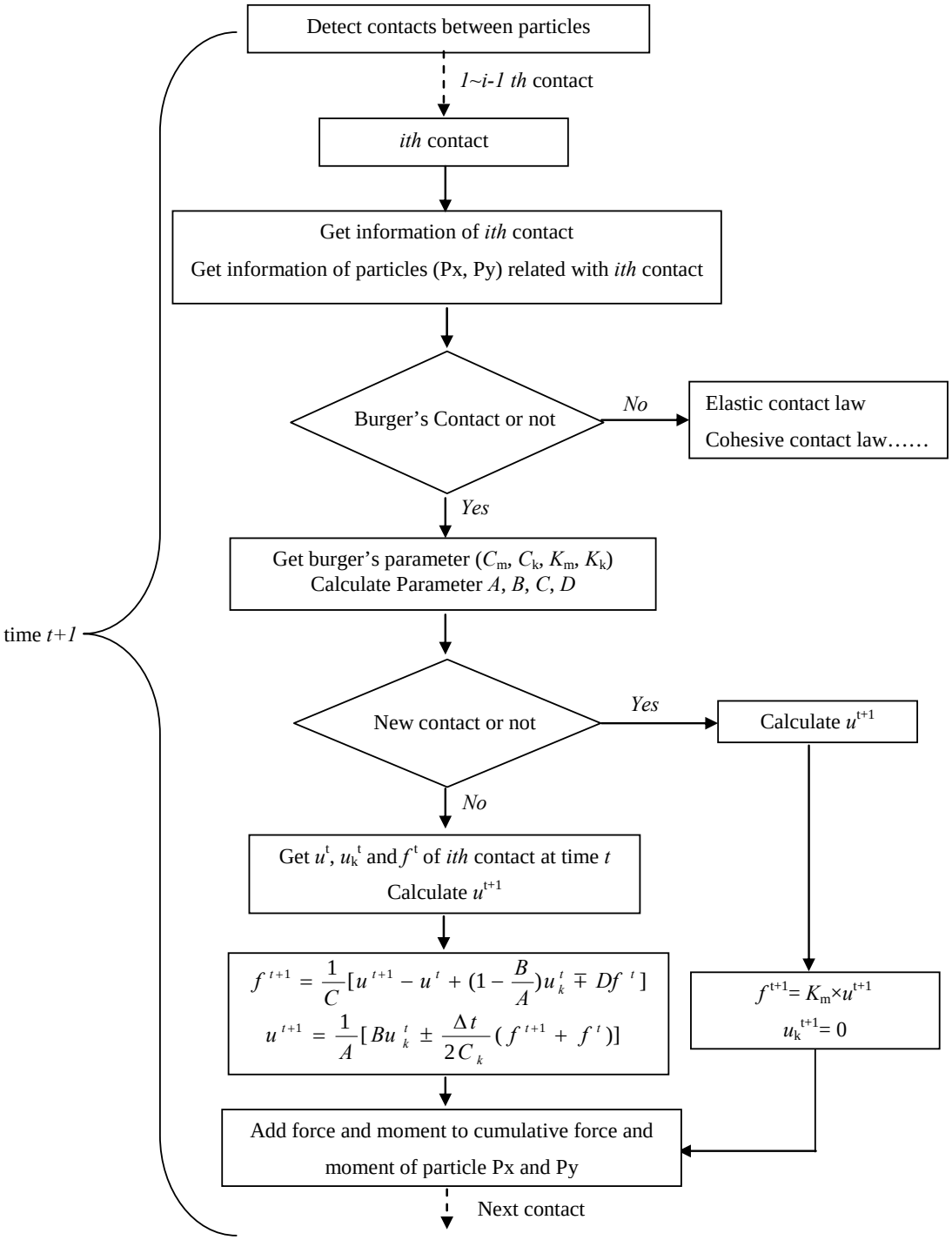

Figure 2.6 Flow diagram of Burger's contact law engine

2.4 Verification of Burgers Contact Model

DEM simulation is a highly intensive computation process, the results of DEM models with a large number of particles usually are very difficult to verify. So in DEM simulation, in order to gain a better understanding of the solution process, and assure the correctness of simulation results, it is often useful to solve simple verification problems with well established analytical solutions, especially for the newly developed or modified DEM codes. These simplified verification problems usually have a small number of particles and have little engineering practice interest, but it can be used to study the effect of parameters and mutual relationship between particles, and can also provide guidance for selecting the input parameters for larger scale problems, which is helpful in debugging, modification and development of DEM codes.

In order to verify the correctness of new Burger's contact law engine in YADE, a simple test was conducted just as in the PFC2D manual (Itasca Consulting Group, 2004) and similar to Chen (Chen *et al.*, 2007). Two balls are created under an overlap condition and fixed in position (Figure 2.7), so the deformation is constant value between the two balls and stress relaxation occurs in such situation. The analytical solution of contact force for this verification problem can be written as following:

$$f(t) = Ae^{z_1 t} + Be^{z_2 t} \tag{2.41}$$

Where:

$$A = \frac{b_2 z_1 + b_1}{a_2 (z_1 + z_2)}$$

$$B = \frac{b_2 z_2 + b_1}{a_2 (z_2 - z_1)}$$

$$a_1 = \frac{C_k}{K_k} + C_m(\frac{1}{K_k} + \frac{1}{K_m})$$

$$a_2 = \frac{C_k C_m}{K_k K_m}$$

$$b_1 = \pm C_m$$

$$b_2 = \pm \frac{C_k C_m}{K_k}$$

z_1 and z_2 are the roots of the quadratic equation $a_2 s^2 + a_1 s + 1 = 0$.

Assuming $K_k = 1.2 \times 10^8$, $K_m = 1.2 \times 10^8$, $C_k = 3 \times 10^8$ and $C_m = 3 \times 10^8$, a comparison of the contact force versus time for the analytical and YADE solution is shown in Figure 2.8. From Figure 2.8, it can be seen that the YADE solution results agree well with the theoretical solution. This simple verification test guarantees the correctness of the calculation results for each contact between particles, and thus gives more confidence in the simulation results of whole DEM model with large number of particles when using Burgers contact model.

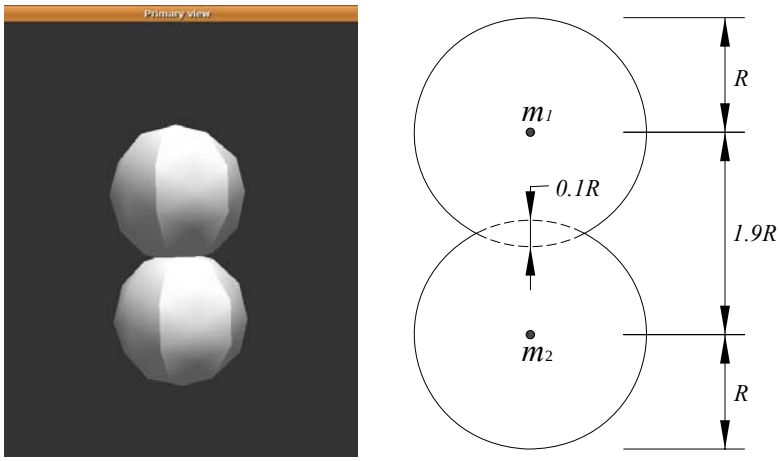

Figure 2.7 Verification of Burger's contact model in YADE Code (R=1)

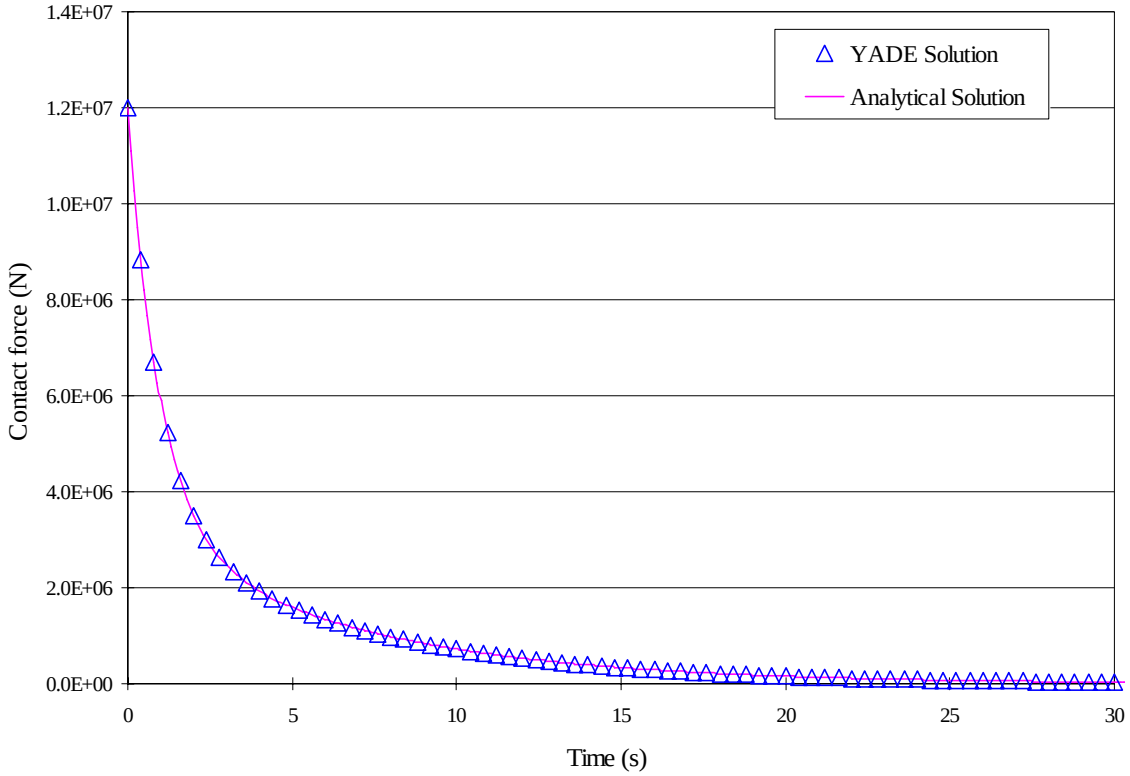

Figure 2.8 Comparison between Analytical and YADE Solution

CHAPTER 3 DETERMINATION OF BURGERS' MODEL INPUT PARAMETERS

3.1 Introduction

Asphalt mixture is a typical viscoelastic material. This kind of viscoelatic property should be considered in viscoelastic contact model of discrete element method. For the determination of input parameters of asphalt mixture, the common method is to obtain contact model's parameters through fitting experimental data set of representative samples of the composite. So in order to obtain input parameters through regression analysis, the rheological relationships should be established between the viscosity behavior of asphalt mixture and the parameters of Burgers' model

3.2 Rheological Relationships for the Burger's Model

In order to establish the rheological relationships for the Burger's Model, the response of asphalt mixture induced by different loading conditions can be investigated through the constitutive equation 2.23 presented in last chapter. Typically, the commonly used loading conditions are a creep load, a constant strain, and dynamic loading conditions (Tschoegl 1989; Ferry 1980; Abbas, 2004).

3.2.1 Creep Compliance of Burgers Model

The response of the Burger model due to the application of a creep load (i.e., constant stress) can be characterized through creep compliance, $D(t)$, which is defined as the resulting strain function divided by the applied stress. The creep loading function can be described as follow:

$$\sigma = \Delta(t) \cdot \sigma_0$$

Where

$$\Delta(t) = \begin{cases} 0 & t < 0 \\ 1 & t > 0 \end{cases}$$

Substituting the creep load function into the constitute equation 2.23 and making laplace transformation results in,

$$\frac{\sigma_0}{s} + p_1\sigma_0 + p_2 s\sigma_0 = q_1 s\hat{\varepsilon}(s) + q_2 s^2\hat{\varepsilon}(s) \tag{3.1}$$

Solving the above equation, results in,

$$\hat{\varepsilon}(s) = \sigma_0\left[\frac{1}{s^2(q_1 + q_2 s)} + \frac{p_1}{s(q_1 + q_2 s)} + \frac{p_2}{q_1 + q_2 s}\right] \tag{3.2}$$

Where $\hat{\varepsilon}(s)$ is laplace transform of total displacement of Burgers model and s is the transformation variable

The creep strain can be obtained by taking the inverse laplace transform of the above equation, which can be expressed as follow and the creep curve is shown in Figure 3.1a:

$$\varepsilon(t) = \sigma_0\left[\frac{p_1 q_1 - q_2}{q_1^2} + \frac{t}{q_1} + \left(\frac{p_2}{q_2} - \frac{p_1 q_1 - q_2}{q_1^2}\right)e^{-\lambda t}\right] \tag{3.3}$$

Where $\lambda = \frac{q_1}{q_2}$

Above equation can also be expressed by using viscoelastic constants as follow:

$$\varepsilon(t) = \sigma_0 \left(\frac{1}{K_M} + \frac{t}{C_M} + \frac{1}{K_K}(1 - e^{\frac{K_K}{C_K}t}) \right) \tag{3.4}$$

Creep compliance is equal to the resulting strain function divided by the applied stress and can be given by the following equation:

$$D(t) = \frac{\varepsilon(t)}{\sigma_0} = \frac{1}{K_M} + \frac{t}{C_M} + \frac{1}{K_K}\left(1 - e^{\frac{K_K}{C_K}t}\right) \tag{3.5}$$

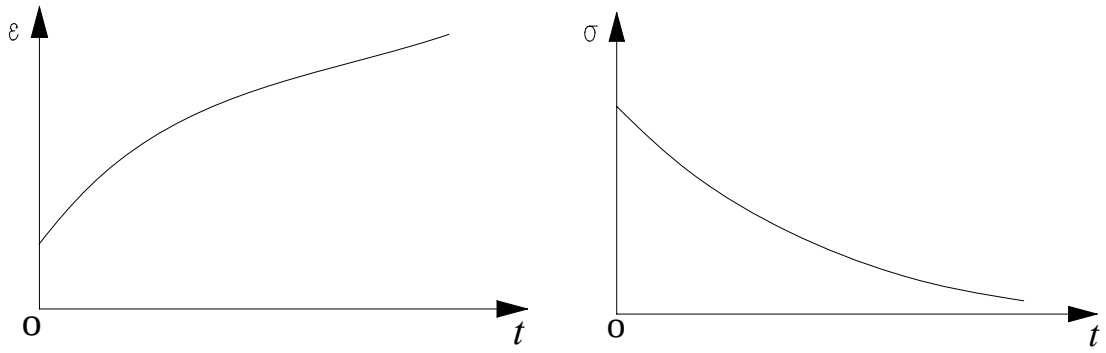

(a) creep curve (b) stress relaxation curve

Figure 3.1 Mechanical response of Burger's Model

3.2.2 Relaxation Modulus of Burgers Model

The response of the Burger model due to the application of a constant strain can be characterized using the relaxation modulus, $E(t)$, which is defined as the resulting stress function divided by the strain value. The constant strain function can be described as follow:

$$\varepsilon = \Delta(t) \cdot \varepsilon_0$$

Where

$$\Delta(t) = \begin{cases} 0 & t < 0 \\ 1 & t > 0 \end{cases}$$

Substituting the constant strain function into the constitute equation 2.23 and making laplace transformation results in,

$$\sigma_0(s) = \varepsilon_0 \frac{q_1 + q_2 s}{1 + p_1 s + p_2 s^2} \tag{3.6}$$

This equation can be expressed in the following format with new parameter α, β:

$$\hat{\sigma}(s) = \frac{\varepsilon_0}{p_2}\left[\frac{q_1}{(s+\alpha)(s+\beta)} + \frac{q_2 s}{(s+\alpha)(s+\beta)}\right] \tag{3.7}$$

Where

$$\alpha = \frac{1}{2p_2}(p_1 + \sqrt{p_1^2 - 4p_2})$$

$$\beta = \frac{1}{2p_2}(p_1 - \sqrt{p_1^2 - 4p_2})$$

Taking the inverse laplace transform, results in the stress relaxation equation (Figure 3.1b),

$$\sigma(t) = \frac{\varepsilon_0}{\sqrt{p_1^2 - 4p_2}}\left[(-4q_1 + \alpha q_2)e^{-\alpha t} + (q_1 - \beta q_2)e^{-\beta t}\right] \tag{3.8}$$

Relaxation modulus is equal to the resulting stress function divided by the strain value and can be given by following equation:

$$E(t) = \frac{\sigma(t)}{\varepsilon_0} = \frac{(-4q_1 + \alpha q_2)e^{-\alpha t} + (q_1 - \beta q_2)e^{-\beta t}}{\sqrt{p_1^2 - 4p_2}} \tag{3.9}$$

3.2.3 Complex Compliance and Complex Modulus of Burger's Model

The response of the Burger's model due to either dynamic stress or dynamic strain can be characterized using the complex modulus, $E^*(\omega)$, which is defined as the ratio of the dynamic stress to the dynamic strain. Complex compliance $D^*(\omega)$ is equal to the reciprocal of complex modulus $E^*(\omega)$ and vise versa. For Burger's model, the application of dynamic load $\sigma(t) = \sigma_0 e^{i\omega t}$ will cause a dynamic strain response $\varepsilon(t) = \varepsilon^* e^{i\omega t}$, where σ_0 and ε^* are the stress and strain at time equals zero, ω is the radial frequency, and *t* is the elapsed time.

Taking the first and second derivatives of the stress and the strain functions with respect to time and substituting them in Equation (3.7), then the complex compliance, $D^*(\omega)$, can be obtained and expressed as the following equation,

$$D^*(\omega) = \frac{\varepsilon^*}{\sigma_0} = \frac{1}{K_m} + \frac{1}{i\omega C_m} + \frac{1}{K_k + i\omega C_k} \tag{3.10}$$

The complex compliance consists of real and imaginary components and can be written in the following format:

$$D^*(\omega) = D'(\omega) - iD''(\omega) \tag{3.11}$$

Where:

$i = \sqrt{-1}$

$D'(\omega)$ is the real component of complex compliance,

$$D'(\omega) = \left(\frac{1}{K_m} + \frac{K_k}{K_k^2 + \omega^2 C_K^2}\right)$$

$D''(\omega)$ is the imaginary component of complex compliance,

$$D''(\omega) = (\frac{1}{\omega C_m} + \frac{\omega C_k}{K_k^2 + \omega^2 C_K^2})$$

The real component $D'(\omega)$ and imaginary component $D''(\omega)$ of complex compliance are also referred to as the storage compliance and loss compliance respectively. The dynamic compliance, $\left|D^*\right|$, is equal to the square root of the sum of squares of storage and loss compliances:

$$\left|D^*\right| = \sqrt{(D')^2 + (D'')^2} \tag{3.12}$$

The phase angle, δ, is the direction of complex compliance and is defined as the tan inverse of the loss compliance divided by the storage compliance.

$$\delta = \tan^{-1}\left(\frac{D''}{D'}\right) \tag{3.13}$$

The complex modulus, E^*, and the dynamic modulus, $\left|E^*\right|$, are equal to the reciprocals of the complex compliance, D^*, and the dynamic compliance, $\left|D^*\right|$, respectively, and can be expressed as follows:

$$E^* = \frac{1}{D^*} = \frac{1}{D' - iD''} = \frac{D'}{\left|D^*\right|^2} + i\frac{D''}{\left|D^*\right|^2} \tag{3.14}$$

$$\left|E^*\right| = \frac{1}{\left|D^*\right|} = \frac{1}{\sqrt{(D')^2 + (D'')^2}} \tag{3.15}$$

Equation 3.15 can also be expressed using mechanical constants of Burger's model as follow:

$$\left|E^*\right| = \frac{1}{\sqrt{(D')^2 + (D'')^2}} = \frac{1}{\sqrt{(\frac{1}{K_m} + \frac{K_k}{K_k^2 + \omega^2 C_K^2})^2 + (\frac{1}{\omega C_m} + \frac{\omega C_k}{K_k^2 + \omega^2 C_K^2})^2}} \tag{3.16}$$

3.3 Dynamic Modulus Test

For the determination of input parameters of asphalt mixture, the commonly used laboratory tests usually include uniaxial creep test, stress relaxation test, and dynamic modulus test. Dynamic modulus test is a conventional asphalt mixture test and has been used to determine the DEM input parameters of Burgers' model by researchers (Liu *et al.*, 2009; Abbas, 2004).

Dynamic modulus $|E^*|$ is one of the fundamental engineering properties widely used to characterize the viscoelastic behavior of HMA mixture and can reflect the temperature and frequency dependency of HMA mixture properties, which is one of the important material property input parameters for flexible pavement design. In the dynamic modulus test, a sinusoidal stress is applied to a cylindrical specimen and a sinusoidal steady-state strain is induced, or vice versa. Due to the viscoelastic effect, the stress always leads the strain, or the strain always lags the stress (Figure 3.2)

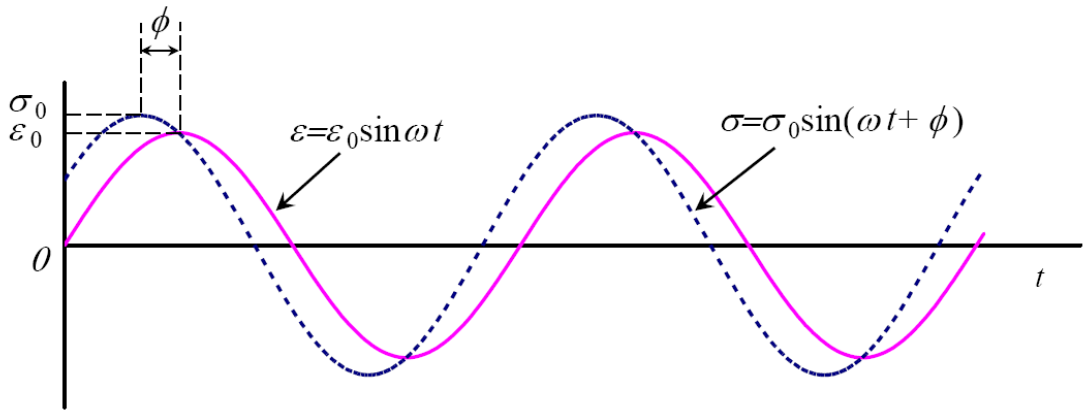

Figure 3.2 Stress and Strain in a Dynamic Modulus Test

During the dynamic modulus testing, a cylindrical specimen (usually 100mm in diameter and 150mm in height) is subjected to a constant lateral confining pressure and a sinusoidal vertical pressure at a range of temperatures and frequencies (Figure 3.3). Depending upon the specimen stiffness, the amplitude of vertical pressure varies between 35 and 2800kPa to keep the strain between 75 and 125 micro-strains. Stresses are measured using a load cell, and axial strains at the middle part of the specimen are measured using three linear variable differential transformers (LVDT) mounted on studs attached to the sides of the specimen. Test specimens were placed in an environmental chamber and allowed to equilibrate to the specified testing temperature ranging from –10 to 54.4^{o}C (14 to 130^{o}F). At each temperature, different frequencies ranging from 0.01Hz to 25Hz are applied.

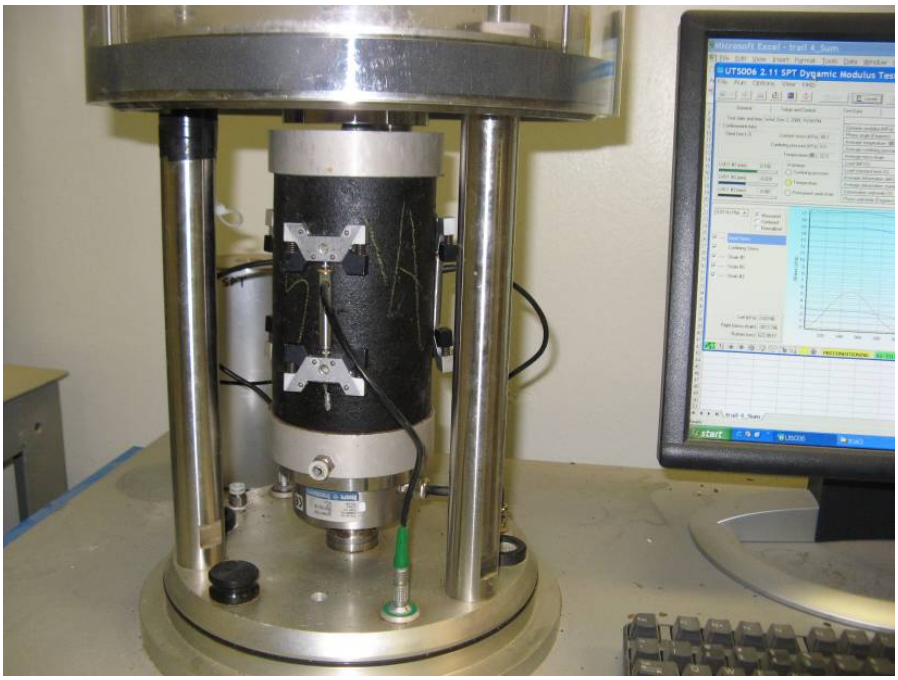

Figure 3.3 Dynamic Modulus Test

Prior to testing, two latex membranes are placed between the specimen ends and loading platens to reduce the end friction. A contact load equal to 5 percent of the dynamic load was first applied to the specimen and a sinusoidal dynamic load was then applied. Usually testing is conducted from the lowest to the highest temperature and from the highest to the lowest frequency. For each combination of testing temperature and frequency, 10 conditioning and 10 testing cycles were applied. A typical rest period between each frequency run is 2 minutes. The rest period should not exceed 30 minutes for any two successive frequency runs. At the end of testing, the specimen should be discarded if excessive deformation greater than 1500 micro strain was accumulated. The data from conditioning cycles were used to adjust the amount of dynamic load and those from testing cycles to calculate the values of dynamic modulus and phase angle. Figure 3.4 presents the typical axial stress and strains from the testing cycles.

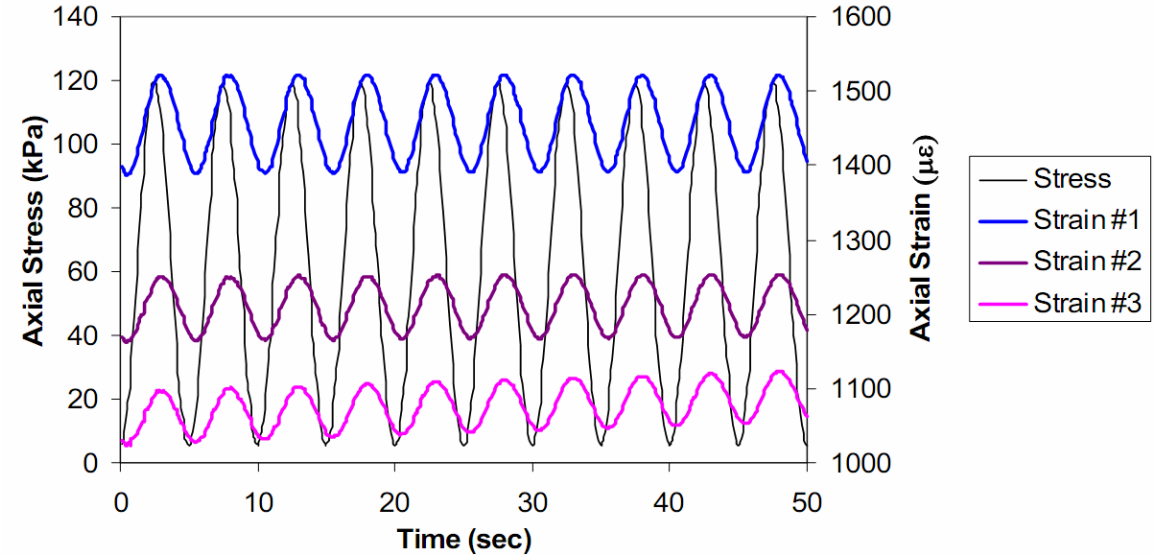

Figure 3.4 Axial Stress and Strains in Dynamic Modulus Test

The dynamic modulus is equal to the ratio of the axial stress amplitude to the axial strain amplitude:

$$\left|E^*\right| = \frac{\sigma_0}{\varepsilon_0} \tag{3.17}$$

Where

$\left|E^*\right|$ = dynamic modulus;

σ_0 = axial stress amplitude; and

ε_0 = axial strain amplitude;

In the complex form, the applied sinusoidal stress $\sigma(t)$ can be expressed as:

$$\sigma(t) = \sigma_0(\cos\omega t + i\sin\omega t) = \sigma_0 e^{i\omega t} \tag{3.18}$$

Where

ω = radian frequency; and

$i = \sqrt{-1}$.

The above loading stress can be calculated using the following equation:

$$\sigma_0 = \frac{\overline{P}}{A} \tag{3.19}$$

Where

$\overline{P}$ = average loading amplitude (from best-fit sinusoid function); and

A = cross sectional area of specimen.

The axial strain can be calculated through measured deformation as follow:

$$\varepsilon_0 = \frac{\overline{\Delta}}{GL} \tag{3.20}$$

Where

$\overline{\Delta}$ = average deformation amplitude (from best-fit sinusoid function) calculated after removal of the underlying baseline drift deformation; and

GL = gauge length.

The phase angle ϕ can be calculated using the following equation:

$$\phi = \frac{t_i}{t_p} \times 360 \tag{3.21}$$

Where

ϕ = phase angle (in degrees);

t_i = average time lag between the peak stress and the peak strain in seconds, calculated as the difference between the best fit load and deformation sinusoid functions; and

t_p = average time for a loading cycle in seconds.

3.4 Construction of Master Curve

The master curve of different viscoelastic material properties as a function of time or frequency can be constructed based on the time-temperature superposition principle (Ferry 1980). The measured curves at other temperatures are shifted horizontally along the time or frequency axis according to respective horizontal shift factor and then form a single master curve at a reference test temperature. If the reference temperature is chosen to be in the middle of all test temperatures, then the test data measured at lower temperatures are shifted to the right, i.e. to higher frequencies until the ends of adjacent temperature curves just meet or partially overlap. In a similar manner, the test data measured at higher temperatures are shifted to the left, i.e. to low frequencies. This constructed master curve covers a much wider range of frequency than the actual

experimental data. The construction process of dynamic modulus master curve of HMA mixture can be found in Figure 3.5 and 3.6 shown in the next section. The horizontal shift factor, α_T, a constant which defines the required horizontal shift from an arbitrary test temperature, T, to the reference temperature of master curve, T_0, can be expressed as:

$$f_T = \alpha_T f_{T_0} \tag{3.22}$$

Where:

α_T = horizontal shift factor;

f_T = frequency at a freely chosen temperature T; and

f_{T_0} = frequency at the reference temperature T_0.

In general, the Sigmoidal function can be used to fit the dynamic modulus data set at a reference test temperature.

$$\log(E^*) = \delta + \frac{\alpha}{1 + e^{\beta + \lambda(\log t_r)}} \tag{3.23}$$

Where

t_r = time of loading at the reference temperature;

δ, α, β, λ = fitting parameters; for a given set of data, δ represents the minimum value of E^* and $\delta + \alpha$ represents the maximum value of E^* ; β, λ describes the shape of the sigmoidal function.

With the time-temperature superposition principle, the master curve at any temperature can be obtained by shifting horizontally according to the corresponding horizontal shift factor at that temperature.

3.5 Regression of Burger's Model Parameters

As presented earlier in this chapter, the dynamic modulus can be expressed using mechanical constants of Burger's model as equation 3.16. With the dynamic modulus test results, the parameters of Buger's model can be obtained by making multi-element non-linear regression analysis according to equation 3.16. The steps of determination of Burger's model parameters can be summarized as follows:

1) Prepare test samples (compaction, coring and cutting);
2) Perform dynamic modulus test at different temperature and frequencies;
3) Calculate dynamic modulus according to equation 3.17;
4) Construct dynamic modulus master curve according to time-temperature superposition principle;
5) Fit the dynamic modulus data set at a reference test temperature with Sigmoidal function;
6) Obtain master curve at required temperature by horizontally shifting curve according to the corresponding horizontal shift factor at that temperature;
7) Determine parameters of Burger's model by fitting Burger's Model to dynamic modulus test results;

Asphalt binder and fine aggregate were assumed to mix together as a special "asphalt mastic" and "asphalt mastic" samples were prepared for dynamic modulus testing (Figure 3.3). Two types of asphalt mixture (Superpave and SMA aggregate gradation shown in Figure 4.3) were investigated in this study. The Asphalt Mixture Performance Tester (AMPT) produced by IPC Global corporation was used to run the dynamic modulus test.

The test was conducted under no confining pressure at 3 temperatures (5°C, 20°C, and 30°C) and 10 frequencies (0.01, 0.1, 0.2, 0.5, 1, 2.5, 10, 20, 25 Hz). After testing, dynamic modulus master curves were constructed by translating the dynamic modulus curves at different temperatures to reference temperature according to time-temperature superposition principle. Figure 3.5 and 3.6 presents the dynamic modulus test results at temperature 5, 20, 30°C and the asphalt mastic master curves of Superpave and SMA asphalt mastic at the reference temperature of 20°C.

The dynamic modulus master curve can be represented by the sigmoidal function and be shifted to any particular temperature with the time-temperature superposition principle. The master curve of Superpave and SMA asphalt mastic at 20°C and 150°C are shown in Figures 3.7 and 3.8.

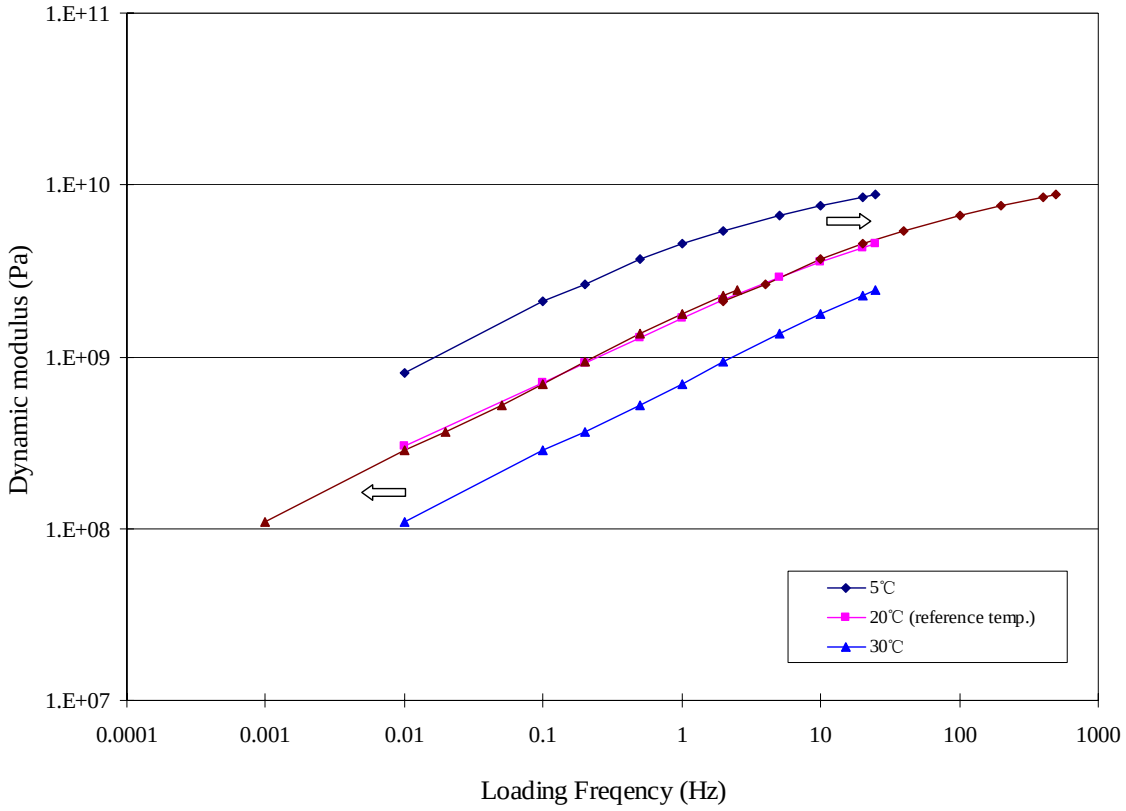

Figure 3.5 Dynamic modulus test results of Superpave mastic

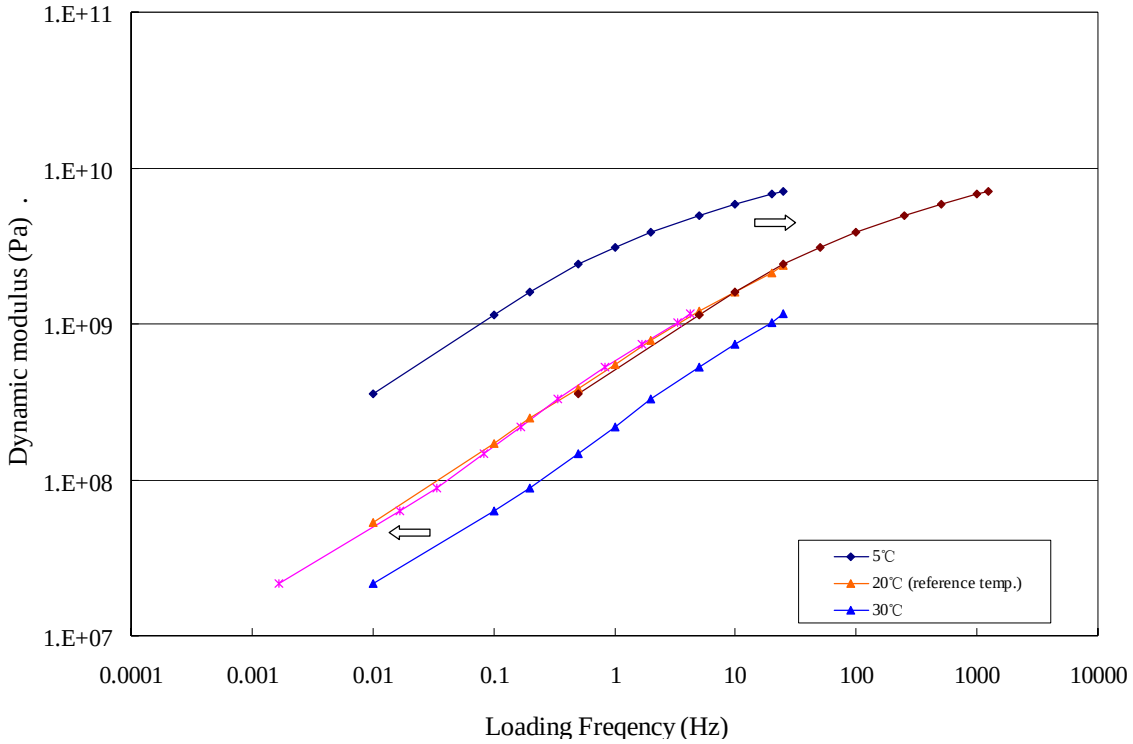

Figure 3.6 Dynamic test results of SMA mastic

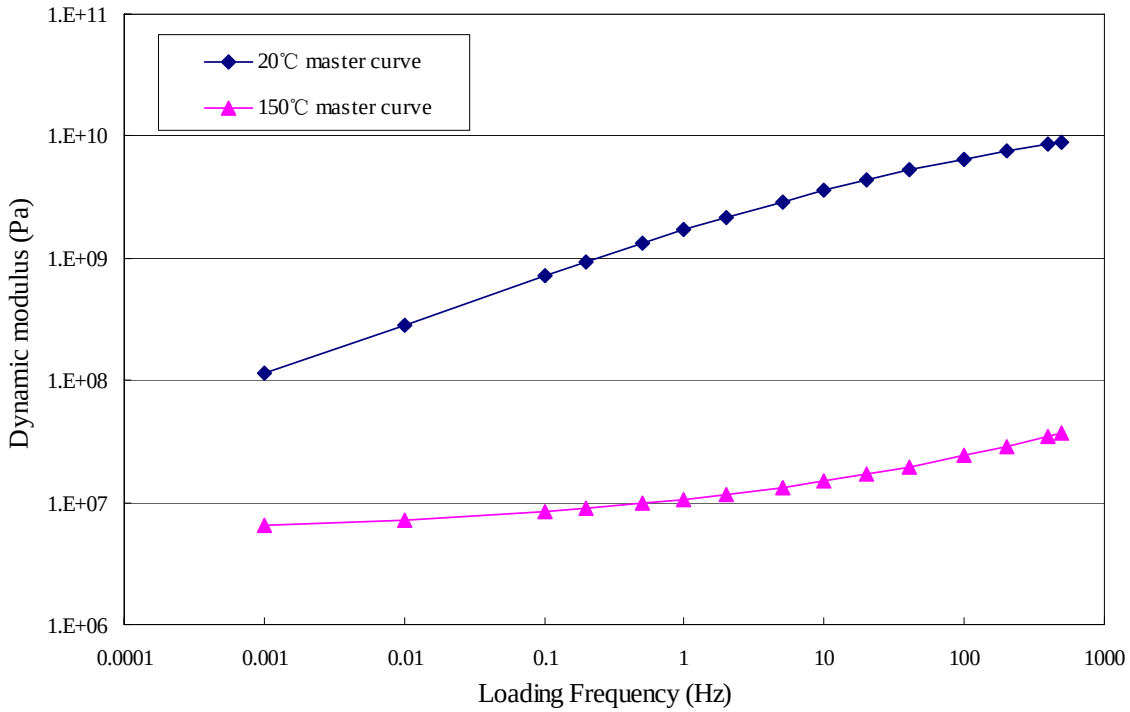

Figure 3.7 Master Curve of Superpave mastic

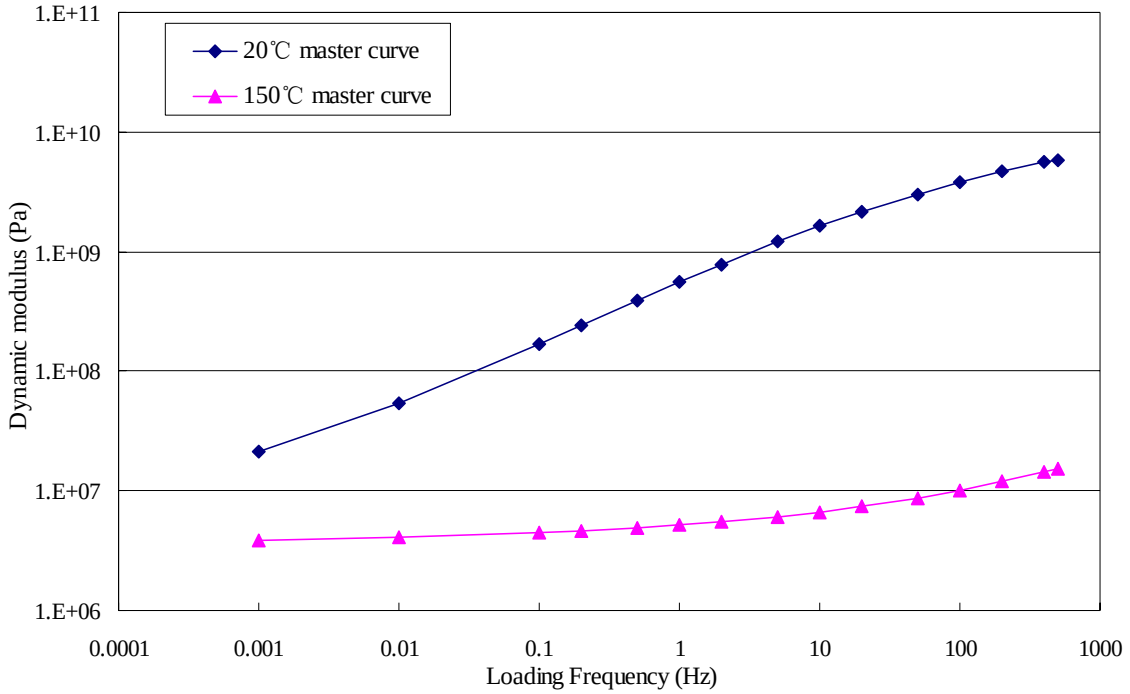

Figure 3.8 Master Curve of SMA mastic

The Equation 3.16 provides the basis for fitting Burger's Model to Data to dynamic modulus test data. The burger's parameter can be obtained using nonlinear regression method and the parameters of Burger's model by fitting dynamic modulus master curve at temperature 150°C and the regression results are shown in Table 3.1.

Table 3.1 Burger's Model Parameter (at 150°c)

Parameters	E_1 (MPa)	η_1 (MPa·s)	E_2 (MPa)	η_2 (MPa·s)
Superpave	19.960	1030.856	19.255	3.717
SMA	15.996	652.714	10.891	1.898

CHAPTER 4 DEM SIMULATION OF GYRATORY COMPACTION

4.1 Introduction

In this chapter, the discrete element method (DEM) was used to simulate the compaction of hot-mix asphalt (HMA) with the Superpave gyratory compactor (SGC). The Open Source discrete element code, YADE, was modified and implemented with the C++ programming language to conduct virtual SGC compaction. The effects of compaction pressure, gyration number, gyration angle, gyration angular velocity and aggregate gradation during the Superpave gyratory compaction were thoroughly investigated. This study showed that the virtual compaction with DEM was potentially very helpful in asphalt mix design by significantly reducing the number of samples prepared of physical gyratory compaction.

4.2 Asphalt mixture Superpave Gyratory Compaction Method

Superpave mix design method is one of the final research products of Strategic Highway Research Program (SHRP) and has been widely used all over the world since the design method was introduced in 1993 (Roberts ea al., 1996). For asphalt mix design, it is very important to simulate the field compaction process in the laboratory. One of the major advantages of the Superpave mix design method is that it can simulate the field compaction with the Superpave Gyratory Compactor (SGC) much better than other mix

design methods (such as the Marshall and Hveem design methods). The Superpave Gyratory Compactor (SGC) is the key component of Superpave mix design procedure and has become a routinely used compactor to prepare specimens for evaluating the mechanical properties of hot mix asphalt (HMA) mixture in lab nowadays.

The Superpave Gyratory Compactor was modified from the Texas Gyratory Compactor with the compaction principles of the French Gyratory Compactor and was developed in SHRP for several goals:

1) Realistically compact mix specimens to densities achieved under actual pavement climate and traffic loading conditions;

2) Capable of accommodating large aggregates;

3) Capable of measuring compactibility so that potential tender mix behavior and similar compaction problems could be identified;

4) Portable enough to allow quality control and quality assurance in mixing facility.

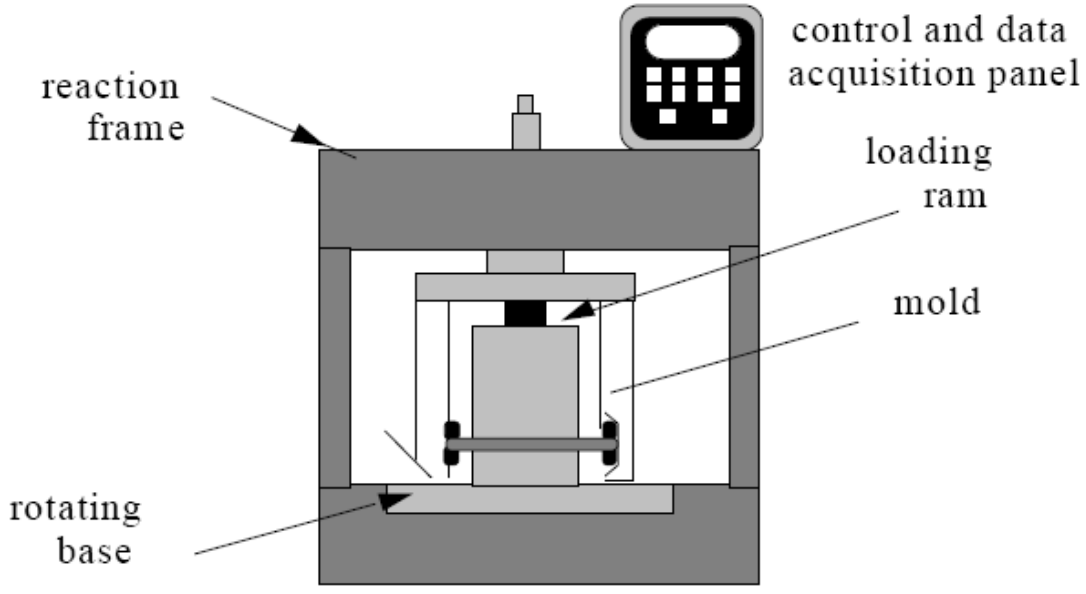

Figure 4.1 Schematic diagram of Superpave Gyratory Compactor (SGC)

Superpave Gyratory Compactor is a mechanical compaction device and is basically composed of the following components (as shown in Figure 4.1):

- Reaction frame, rotating base, and motor;
- Loading system, loading ram, and pressure gauge;
- Specimen height measurement and recording system;
- Specimen molds and base plates;
- Control Panel, initialization, compaction time and height control of the specimen.

Prior to compaction, both the pre-arranged loose mix and compaction mold are placed in an oven at compaction temperature for the specific time. After heating, the pre-determined weight of loose asphalt mixture is poured into the cylindrical compaction mold, and then the mold is moved into the testing chamber of the Superpave Gyratory Compactor and placed on the rotating base. A loading mechanism presses against the reaction frame and applies a load to the loading ram to produce a compaction pressure on the specimen and a pressure gauge measures the ram loading to maintain constant pressure during compaction. With the effect of gyratory motion, the asphalt mixture is subjected to two simultaneous stresses during compaction: one is the constant compression stress and other is a shearing stress which produces a kneading action on the specimen.

The compaction effort applied to the sample by the SGC is controlled by three parameters, namely vertical pressure, angle of gyration and number of gyrations. For the Superpave design procedure, the typical compaction angle is 1.25 degrees, and the applied vertical load to the specimen is 87 psi (600 kPa). The Superpave gyratory

specimens are either 6 inches (150 mm) or 4 inches (100 cm) in diameter. The gyrations are applied at a rate of 30 revolutions per minute and the number of gyrations is varied based on the traffic level. Compaction stops automatically when the desired number of gyrations or height of specimen is reached.

The specimen height is constantly monitored during compaction, which provides a measure of specimen density throughout the compaction procedure. Specimen density can be estimated during compaction by knowing the mass of material placed in the mold, the inside diameter of the mold, and the specimen height. Height is measured by recording the position of the ram throughout the test. Using these measurements, a specimen's compaction characteristics are developed.

A good laboratory compaction technique should be capable of producing pavement with engineering properties very close to those measured from field cores, although there is no single laboratory compaction method that always provided the best match with engineering properties of the field cores. The gyratory compaction was reported more reliable and easy to use for making asphalt mixture specimens, and was identified to be the most suitable method for a Superpave mix design project (Monismith, 1993). The SGC can orient the aggregate particles in a way that is similar to that observed in the field and has the capability to accommodate larger aggregates (up to 50 mm) in the mix (Roberts, et. al., 1996). After comparing the physical properties of laboratory-compacted samples and field cores, Button *et al.* (1994) concluded that the gyratory method most often produced specimens similar to pavement cores and is more convenient for preparing laboratory specimens for routine mixture design and testing of asphalt concrete.

4.3 Assumption of Aggregate Simulation

Due to the limitation of computer processing capability, it is impossible to simulate all the aggregate particles in asphalt mixture compaction (tens of millions of small particles have to be considered in asphalt mixture). According to Simpson and Tatsuoka (2008), DEM analyses to date have been limited to about 10^5 particles, generally circular (2D) or spherical (3D). Although Cundall (2001) has predicted that 10^{11} particles could be available in DEM modeling within 20 years, it is still insufficient to model most real boundary value problems on a particle-by-particle basis. One common method in DEM simulation is to only simulate the aggregates bigger than a certain particular size and assume fine aggregate and asphalt mixing together as mastic which is taken into account by the contact law between particles. Collop *et al.* (2004, 2006) used a 1.18 mm diameter spherical balls to simulate aggregate to study bulk material properties and viscoelastic behavior of asphalt mixture. Kim *et al.* (2008) built a homogeneous DEM model by using 0.35 mm radius particles to simulate asphalt concrete fracture and got reasonable results. In this study, the minimum aggregate particle size 2.36mm was select in DEM simulation.

In fact, coarse aggregates compose the skeleton structure of asphalt mixture, undertake the main traffic load and have significant influence on mechanical behavior of asphalt mixture (Pan *et al.*, 2005; Huang *et al.*, 2009). For coarse grade and stone mastic asphalt mixture, the main role of fine aggregate is to fill the voids between coarse aggregates and increase the density of asphalt mixture. Since in this study the maximum aggregate size 25mm is much bigger than 2.36mm and both gradations have low proportion of fine aggregate smaller than 2.36 mm, only aggregates greater than 2.36mm

were simulated in this DEM simulation, which can greatly reduce the calculation work of the DEM simulation. The fine aggregates and asphalt binder were supposed to be mixed together as special mastic which was taken into account by contact constitutive law between coarse aggregates. The coarse aggregates were assumed to be spherical balls coated with asphalt mastic.

Spherical particle has been generally used in DEM modeling (Simpson and Tatsuoka, 2008), which makes the contact condition simple and greatly eases the calculation difficulty. Irregular shape particles make the particle contact conditions more complicated, and thus it is difficult to get reasonable results. Although spherical particle is not very close to the real shape of aggregates, calculating results by using spherical particles is more reliable and have some reference values for learning asphalt mixture compaction process and valuable guide for future DEM research of asphalt mixture compaction. The spherical particle simplification has also been used in previous asphalt mixture DEM simulation and obtained good results (Collop *et al.* 2004, 2006; Kim *et al.* 2008). Clump technique is a potential tool to simulate irregular-shaped aggregates in DEM simulation. In order to appropriately describe the shape of aggregate, usually tens of spherical balls should be used to model one aggregate. However, all aggregates in asphalt mixture have different shapes, and at least thousands or millions of particles have to be considered in DEM simulation depending on the minimum particle size. So it is difficult to subtly model all those irregular-shaped aggregates by using clump technique, which still has a long way to go before it is put into practice. Therefore, in this study, aggregates are simulated by using spherical particles in most DEM simulation and clump technique was briefly used to investigate the effect of aggregate shape on asphalt mixture compaction.

4.4 SGC Compaction DEM Simulation Process

Gyratory compaction is the commonly used compaction method to make asphalt mixture specimen. In this gyratory compaction DEM simulation, the vertical pressure was set at 600 kPa and the angle of gyration was set at 1.25^{o}. The gyration was applied at a rate of 30 revolutions per minute. The gyratory kneading action in YADE code was applied by a rotary compression plate which is controlled by two separate DEM simulation engines, rotation plate engine and constant pressure engine. The rotation plate engine applies a constant rotation speed on the compression plate around a specific axis and the code of rotation plate engine in YADE code is presented in Appendices B, which is an existing engine of original YADE code. The function of constant pressure engine is to apply a specific pressure to the underneath particles by specified plate and the code of constant pressure engine in YADE code is presented in Appendices C.

The procedures of the DEM simulation process is summarized as follows:

- Generate compaction cylinder and funnel (Figure 4.2a);
- Calculating particle numbers of each particle size according to gradation curve;
- Randomly generate particles in specific space (Figure 4.2b);
- Packing of spheres under gravity force until it is stable (Figures 4.2c and 4.2d);
- Generate compression plate and gyratory compact asphalt mixture by constant pressure (Figures 4.2e and 4.2f);
- Record the position of compression plate and spheres during compaction process;
- Calculate air void of the whole mixture or each layer.

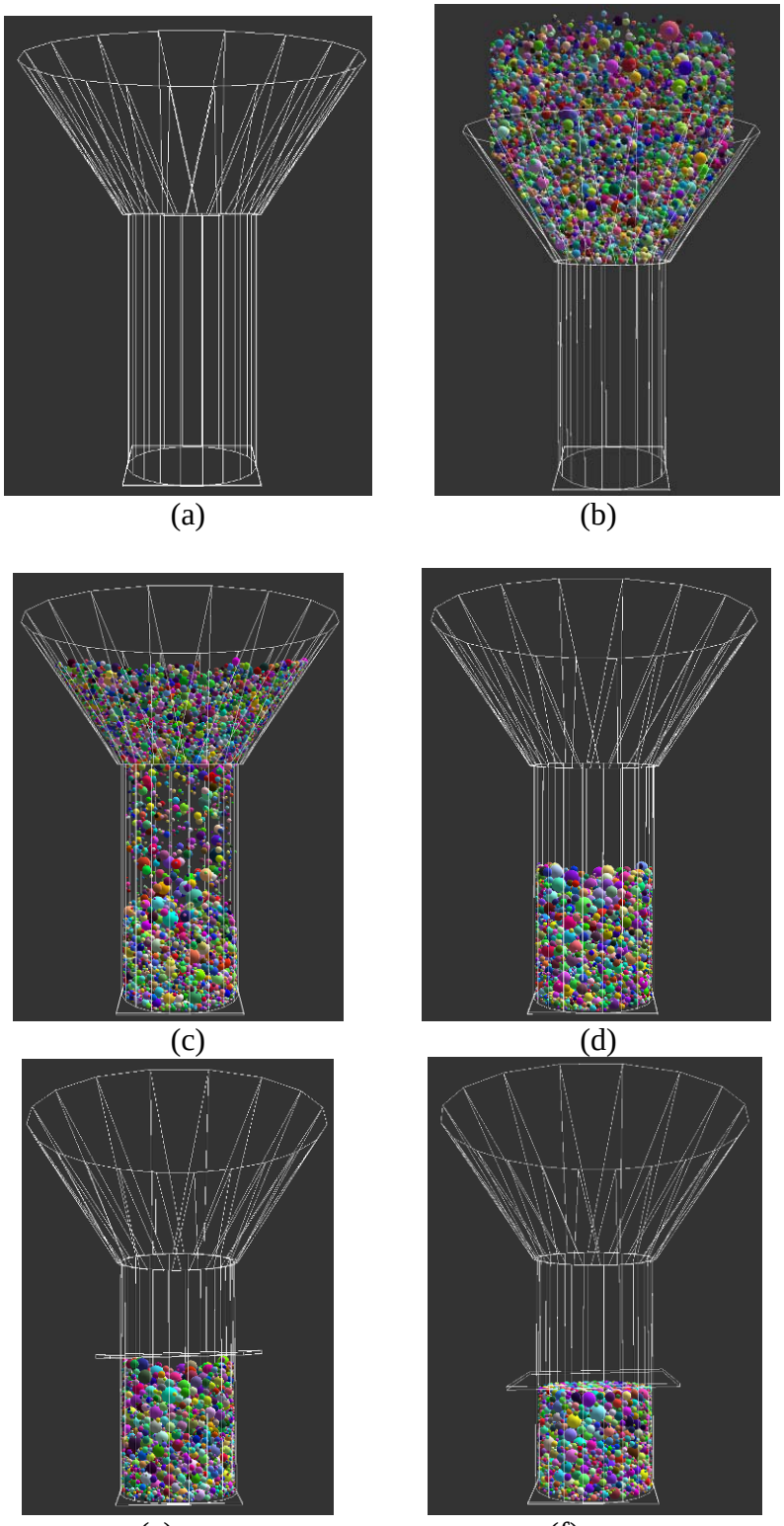

(a) (b)

(c) (d)

(e) (f)

Figure 4.2 DEM Simulation Process of SGC

4.5 Air Voids Prediction and Verification

As mentioned earlier, the position of the gyratory plate and particles can be recorded at specified time steps during the virtual simulations of compaction process and then the coarse aggregate compaction density (V_{CA}) can be calculated. Although aggregate particles smaller than 2.36mm was not considered as individual particles in DEM simulation, the air voids can be roughly estimated according to the proportional relationships between compositions. It was assumed all fine aggregates and asphalt binder were filled into the voids between coarse aggregates. According to the proportional relationship between coarse and fine aggregates, the volume of fine aggregate (V_{FA}) in the whole mixture can also be calculated and the volume of asphalt ($V_{asphalt}$) can be calculated from the asphalt content in the whole mixture. With the known value V_{CA}, V_{FA} and $V_{asphalt}$, the air voids (V_v) can be roughly estimated through following Equation 4.

$$V_v = 1 - V_{CA} - V_{FA} - V_{asphalt} \tag{4-1}$$

4.5.1 SGC DEM Simulation Results

Two types of aggregate gradations (Superpave and SMA) were selected for DEM simulation in this paper and the gradation curves are shown in Figure 4.3. The coarse aggregate compaction density curves are shown in Figure 4.4. The DEM predicted air voids of Superpave and SMA mixtures at 208 gyrations are presented in table 4.1.

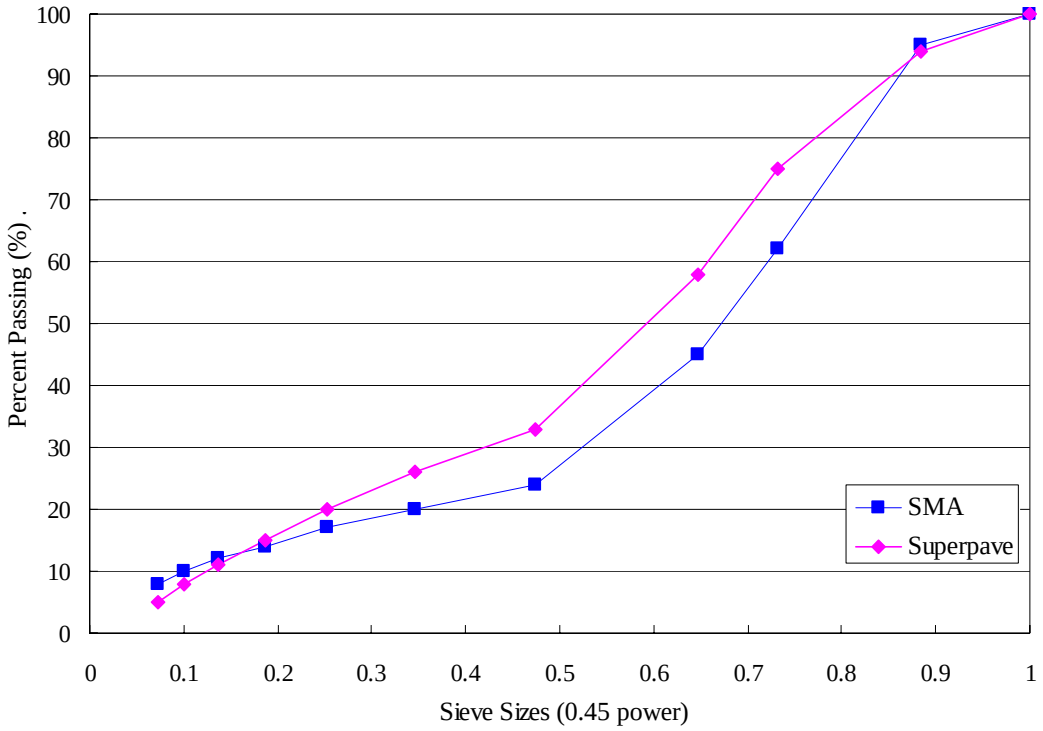

Figure 4.3 Aggregate Gradation Chart (maximum size 1 inch)

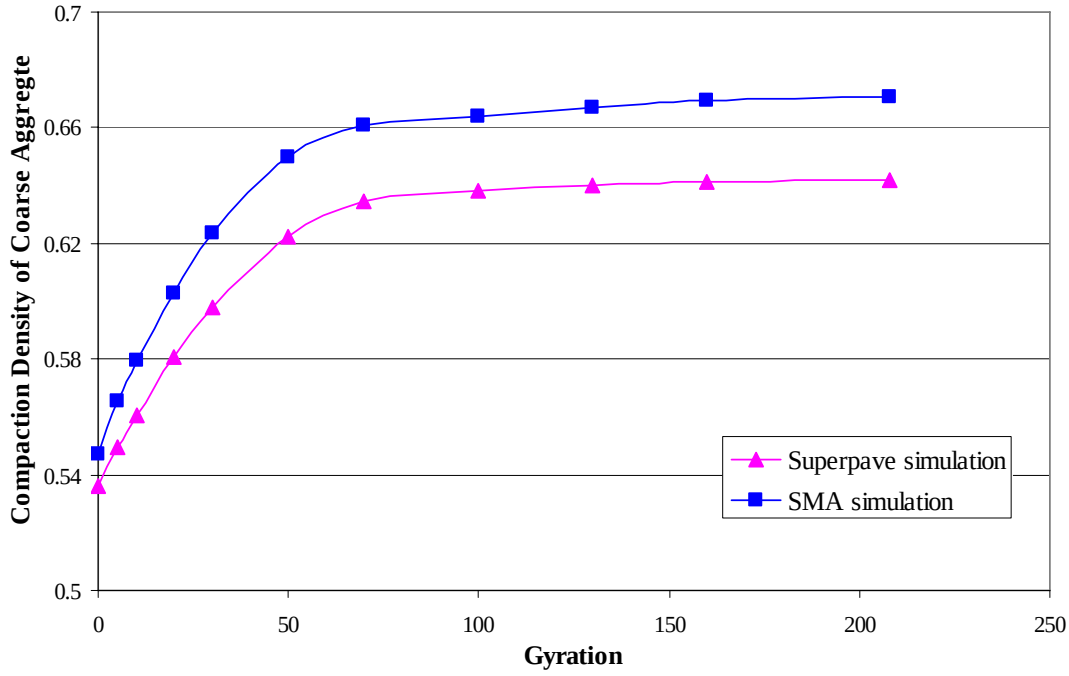

Figure 4.4 Compaction Curves of Coarse Aggregates

Table 4.1 DEM Air Voids Prediction

Proportion of composition	Coarse aggregate	Fine aggregate	Asphalt binder	Air voids
Superpave (volume %)	64.23	22.57	11.96	1.24
SMA (volume %)	67.13	16.78	14.04	2.05

4.5.2 Laboratory Test and Verification

Superpave gyratory compaction tests were conducted in the laboratory for SMA and Superpave mixture which were prepared according to above aggregate gradation and volume proportion. The SGC compactions were conducted by reference to AASHTO standard T312. In order to make the compaction test similar to DEM simulation, rounded aggregate (un-crushed gravels) were selected for coarse aggregates (Figure 4.5). The height of sample was recorded during compaction process to calculate air voids compaction curve. The air voids curves of the SGC compaction test and the air voids curves predicted through above mentioned method are shown in Figure 4.7. From the Figure 4.7, it can be seen that the air void curves of simulations are pretty close to that of laboratory test and the final air voids of simulations are a little lower than that of laboratory test. The low air voids of simulation probably have two reasons. The first reason is the assumption of using spherical particles to model coarse aggregates. Although rounded gravels were chosen for laboratory testing, they still have some angularity and should be more difficult to compact than pure spherical particles due to the interlock effect. The second reason could be the assumption of ideal filling of asphalt cement in the voids between coarse aggregates. Fine aggregates and asphalt binder will

inevitably have some influence on the packing of coarse aggregates during asphalt mixture compaction.

Figure 4.5 Coarse aggregate selection

Figure 4.6 Laboratory SGC compaction test

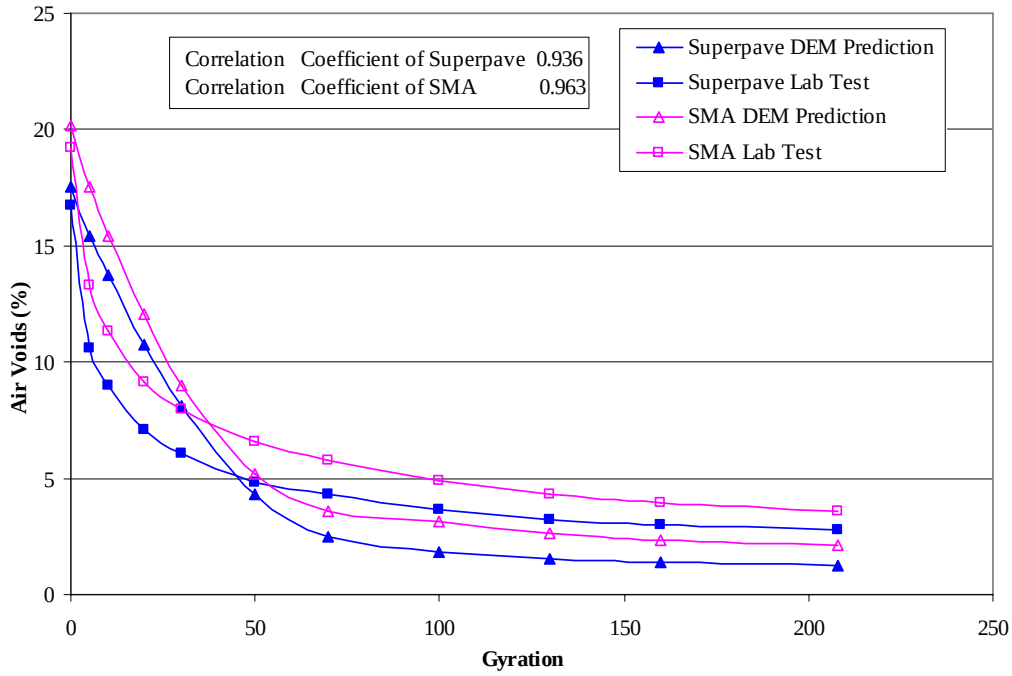

Figure 4.7 DEM prediction and Lab test

4.5.3 Effect of Minimum Simulated Particle Size

As mentioned above, due to the limitation of computer processing capability, it is common to only simulate aggregates bigger than a certain particular size in DEM simulation. The above DEM SGC compaction simulation only simulated the aggregates larger than 2.36 mm. In order to study the effect of minimum simulated particle size on the DEM compaction results, four different aggregate size conditions were simulated and the difference between DEM simulation and lab test results were studied:

Condition I: aggregates bigger than 9.5 mm (simulate 9.5-25mm aggregates);

Condition II: aggregates bigger than 4.75 mm (simulate 4.75-25mm aggregates);

Condition III: aggregates bigger than 2.36 mm (simulate 2.36-25mm aggregates);

Condition IV: aggregates bigger than 1.18 mm (simulate 1.18-25mm aggregates).

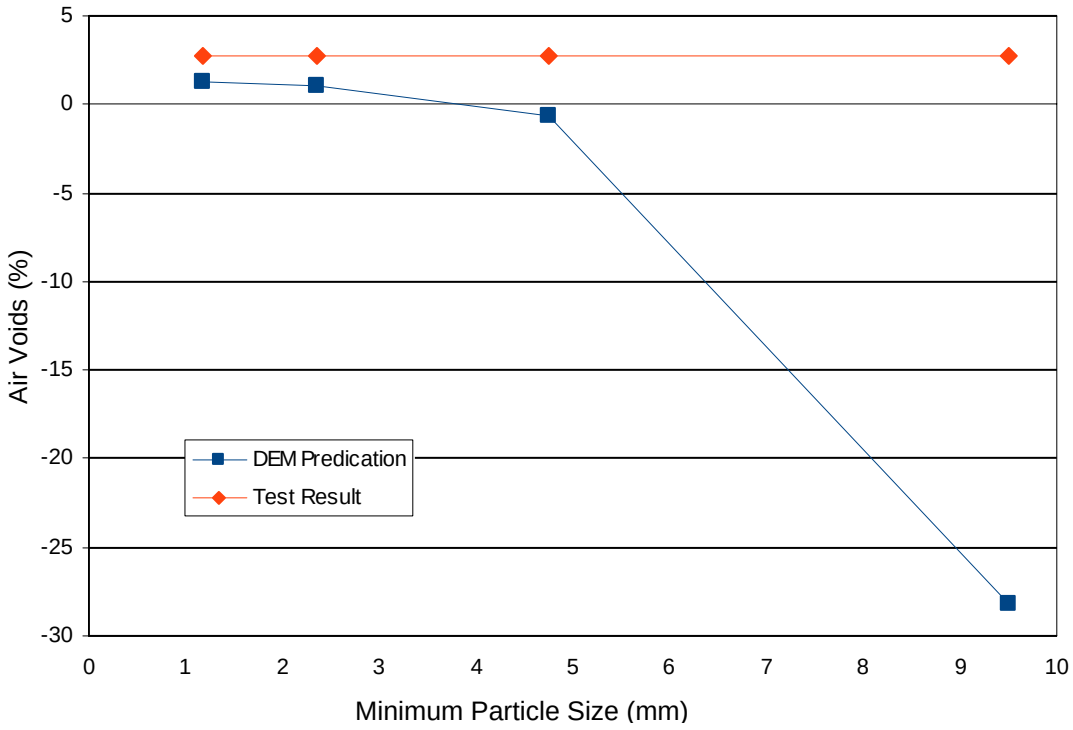

Figure 4.8 DEM simulation results of Superpave

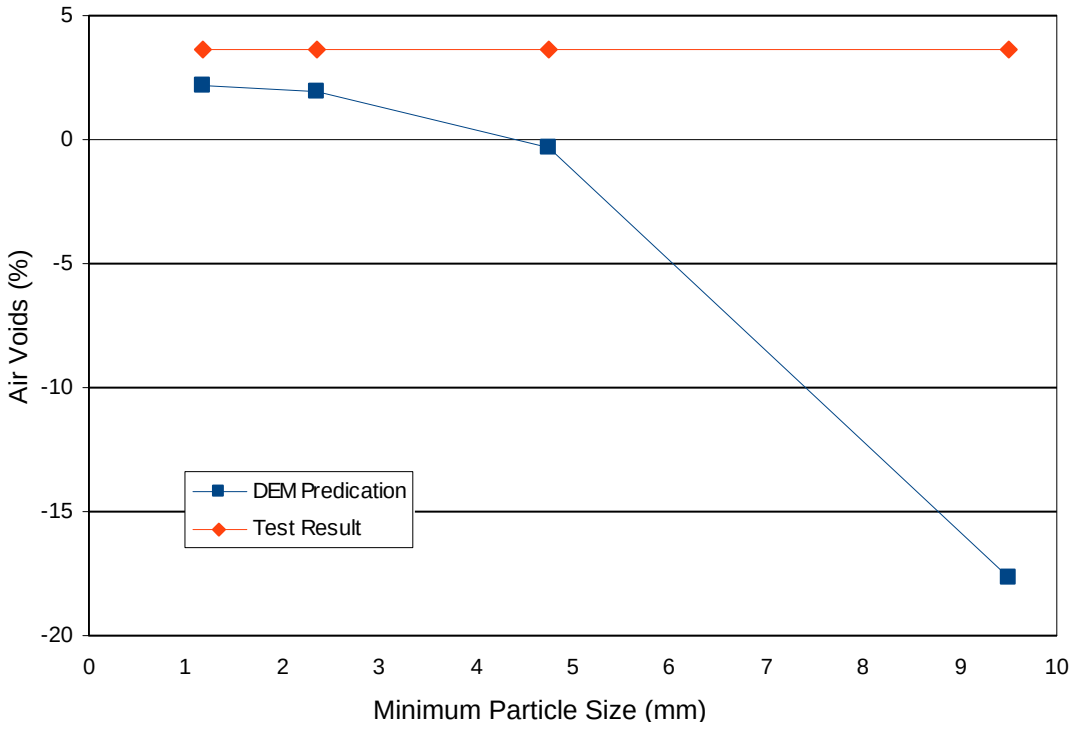

Figure 4.9 DEM simulation results of SMA

Figure 4.8 and 4.9 present the DEM simulation results of the two different gradations

(Superpave and SMA shown in Figure 4.3) for different minimum particle sizes used in DEM simulation. From these two figures, it can be seen that the simulation results get closer to the test result when small minimum aggregate size were used in DEM compaction simulation. When only aggregates bigger than 9.5 mm were simulated, there have great errors between the DEM prediction air voids and laboratory test results. The errors were significantly reduced by considering more small aggregates in asphalt mixture compaction during DEM simulation. From the figures, it can be seen that a good DEM simulation result can be obtained by simulating aggregates bigger than 2.36mm (Condition III) and 1.18mm (Condition IV). However, the DEM simulation of Condition IV involves more particles than Condition III and thus results in much more calculating amounts and longer calculating time. In addition, usually smaller particle size requires smaller time step during DEM simulation, thus increases the calculating time in another way. Compared with Condition III, Condition IV may have slightly better accuracy in prediction results, but takes much longer time during DEM simulation, which is inefficient especially when a large number of DEM calculation are needed. Condition III provides very close DEM prediction results as Condition IV and requires less calculation time, which was selected for the DEM simulation in this study.

4.5.4 Effect of Aspect Ratio of Coarse Aggregates

Simple spherical particles were used in the above DEM simulation. Due to the limitations of spheres, the effects of different aggregate shapes could not be reflected in such kind of simulation. However, aggregate shape is an important factor in asphalt mixture design and has a significant influence during compaction process of asphalt

mixture. Clump technique is a common method to model irregular shaped particles in DEM simulation. A clump is made of a group of spheres and behaves as a rigid body. The contact forces only exist between clumps and the contacts internal to the clump are skipped during the calculation to save computer time (Itasca, 2004). In this study, two simple non-spherical shape particles were generated by using clump technique to model the elongated particles in length-width ratio 2:1 and 3:1 (Figure 4.10).

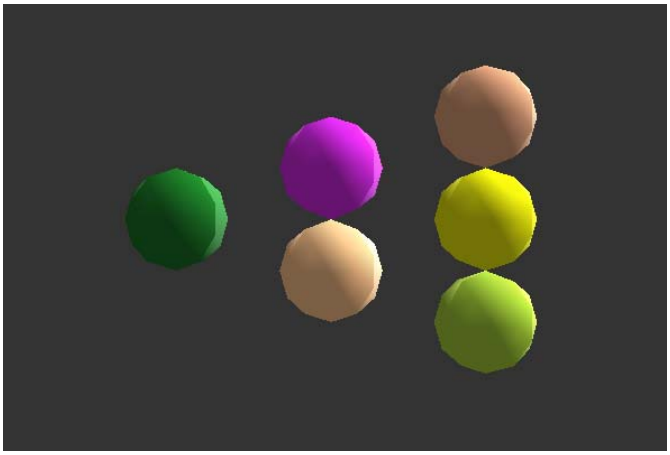

Figure 4.10 DEM Clumps technique

Two more DEM model, one model with all particles in length-width ratio 2:1 and another with all particles in length-width ratio 3:1, were established. The equivalent grain size ($D_e = \sqrt[3]{6V/\pi}$) was used as clump particle size when generating particles according to the aggregate gradation. The Superpave aggregate gradation was selected here, and the simulation results are shown in Figure 4.11. From Figure 4.11, it can be seen that the length-width ratio significantly affects the compaction process. The air voids of the mixture with length-width ratio 3:1 elongated aggregate is much higher than that of other two types of asphalt mixture. Although these non-spherical shapes still can not represent the real shape of all aggregates in asphalt mixture, the calculating results demonstrate that

clump sensitively reflect the effect of aggregate shapes on asphalt mixture compaction in DEM simulation and could be an effective technique for modeling irregular shape aggregates in asphalt mixture compaction DEM simulation.

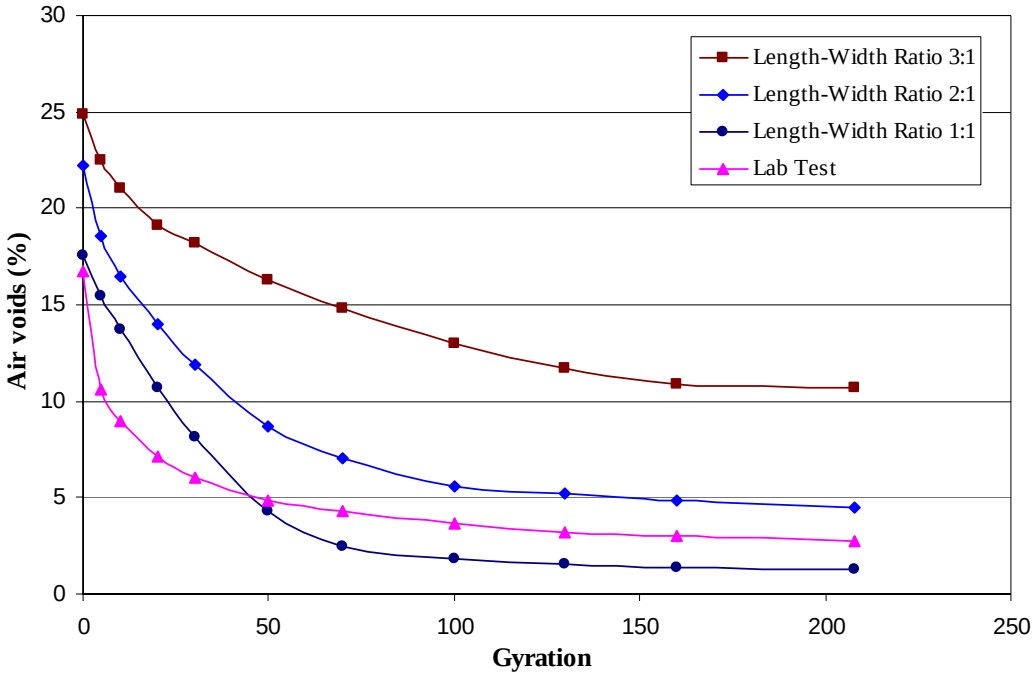

Figure 4.11 DEM Clump Simulation Results

4.5.5 Effect of Gyration Angle

Gyration angle is an important parameter of the SGC and can greatly affect the compaction effort and the final compaction. Butcher used Servopac Gyratory Compactor to study the effect of gyration angle on asphalt mixture compaction (Butcher, 1998). In order to study the effect of gyration angle on asphalt mixture compaction by DEM, a similar DEM simulation was conducted according to the materials' parameters from Butcher's paper. The AC40 asphalt mixture and 4 angles were simulated here. Butcher's results are illustrated in Figure 4.12 and DEM prediction results are exhibited in Figure 4.13. Both figures exhibit the same trend, which indicate that the compaction progress of

mixture increase with the increase of gyration angle. The effect of the gyration angle does not seem to be so significant when the angle is greater than 2 degrees. At the same gyrations, the packing density at 0.25 degree was much lower than that at 1, 2, 3 degrees, which means a low gyration angle can not effectively impart enough mechanical energy to compact specimen and thus result in poor compaction quality of asphalt mixture.

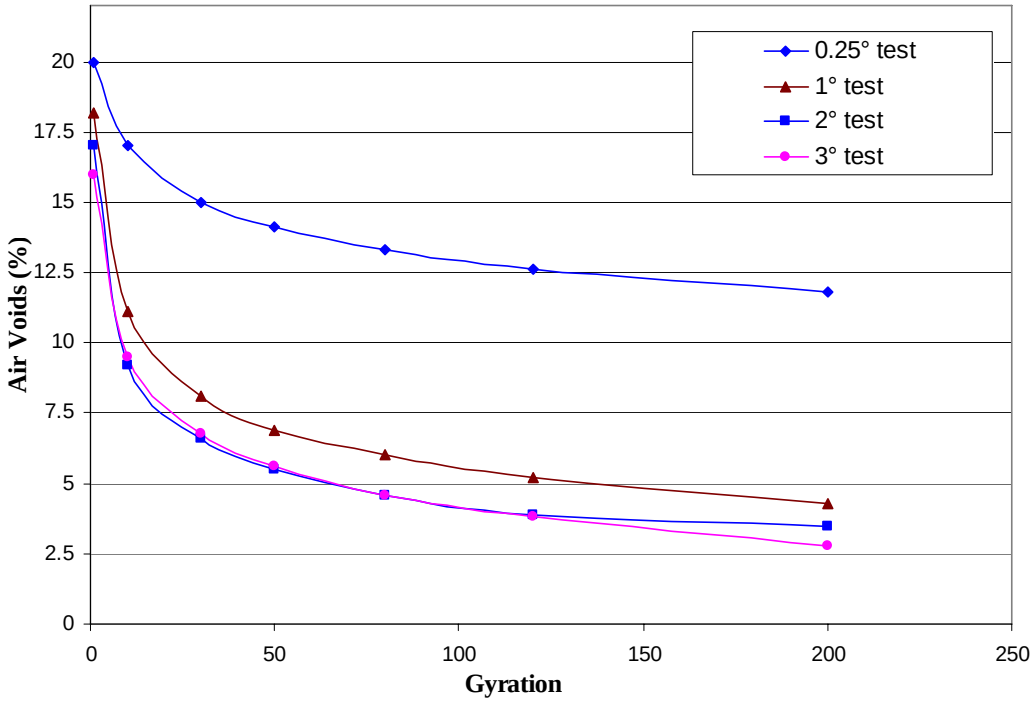

Figure 4.12 Butcher's test results

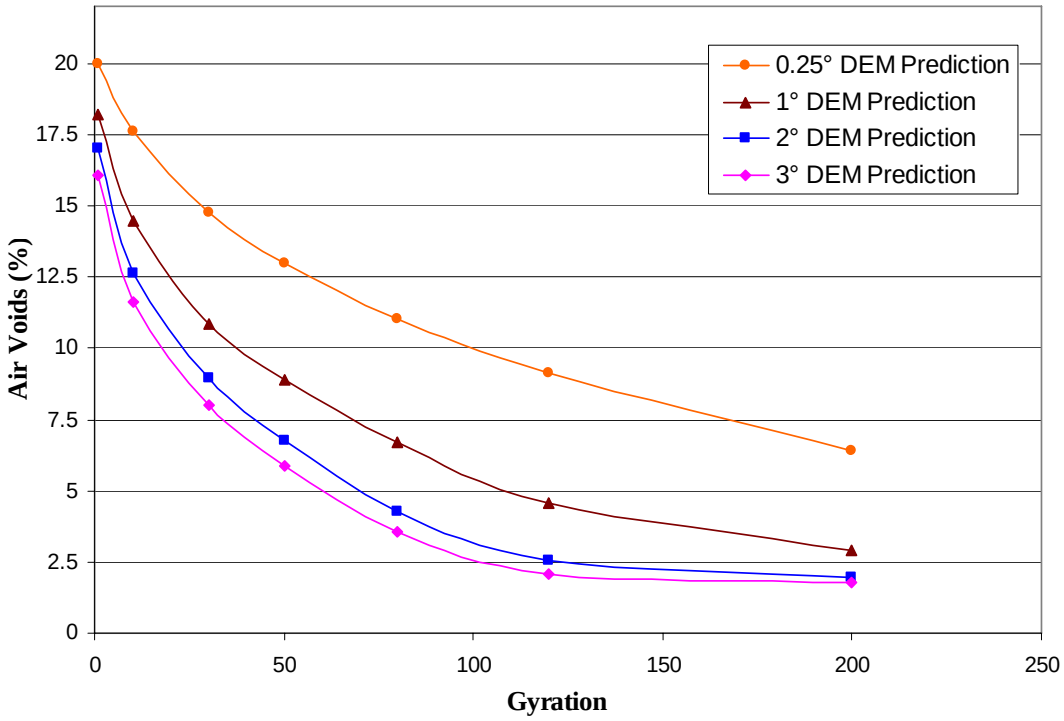

Figure 4.13 DEM Prediction results

4.5.6 Effect of Burger's Parameters

Asphalt mixture is a viscoelasatic material and highly sensitive to temperature. Asphalt mixtures become softer with the increase in temperature. In order to consider the temperature effect, the contact law parameters should be changed. In this study, DEM simulations were simulated at three temperatures (110°, 130°, 150°). The input parameters of different temperatures can be obtained by using above mentioned regression method and the Burger's Model Parameter at different temperatures are represented in Table 4.2. Figure 4.14 is the packing curves at different temperatures. From Figure 4.14, it can be seen that asphalt mixture is easier to be compacted at high temperature. Compared with high temperature, the compaction process is relatively slow and the final air voids is higher under a lower temperature. The DEM prediction results

consist with common sense, which demonstrates that DEM has the capability to study the effect of temperature and could be an effective tool for the analyses of asphalt mixtures compaction in different temperature conditions.

Table 4.2 Burger's Model Parameter at different temperatures

Temperature	E_1 (MPa)	η_1 (MPa·s)	E_2 (MPa)	η_2 (MPa·s)
110°	53.227	1085.284	24.711	5.496
130°	30.006	1031.328	20.505	4.233
150°	19.960	1030.856	19.255	3.717

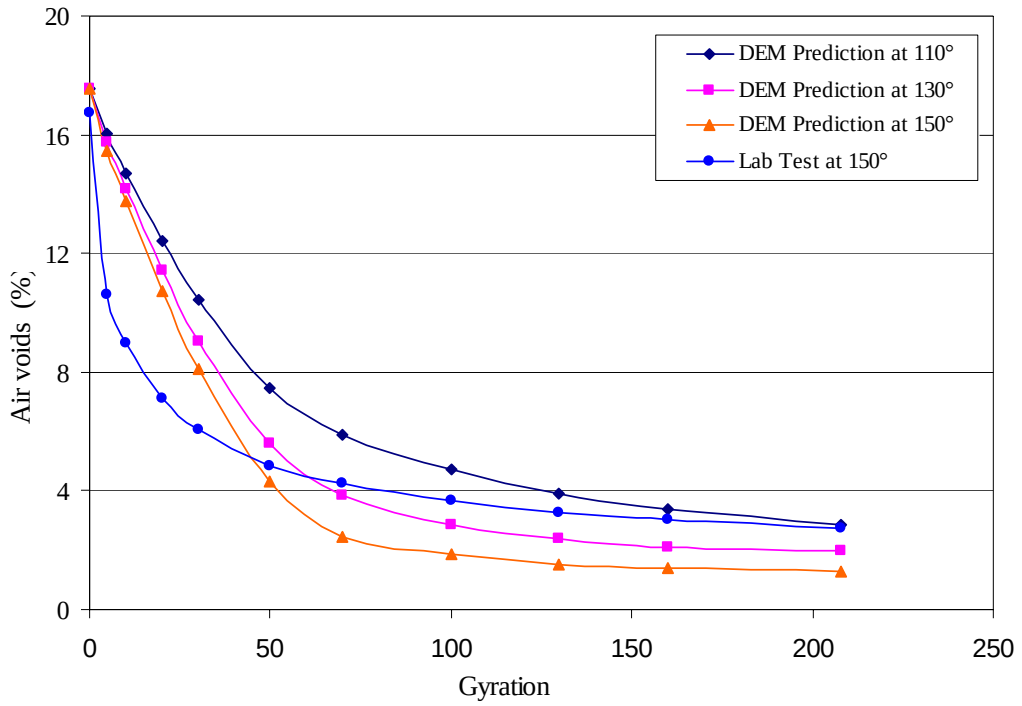

Figure 4.14 Effects of Temperatures

4.5.7 Effect of Gyration

Gyration is an important compaction parameter in SGC compaction and can significantly affect mixture compaction process. Figure 4.15 shows the DEM simulation result of SMA mixture compaction with and without gyration. It is evident that the

mixture can obtain better compaction with gyration. In the early compaction stage, there is no significant difference between these two compaction molds at the time when mixture is still loose and easy to be compacted. However, the mixture is hard to be further compacted without the contribution of gyration. Figure 4.16 presents the motion trace of particle during the compaction process, which reflects the effect of gyration from another point of view. This figure indicates that a particle compacted with gyration has more movement in both horizontal and vertical directions, whereas particle compacted without gyration almost only moves along vertical direction and has a relatively small movement in horizontal direction. The gyratory compaction effort is a multi-directional applied stress that encourages aggregate to seek the optimal moving route during compaction. The movement of aggregates in more directions is helpful to the slippage and filling of aggregates and thus can result in better mixture compaction.

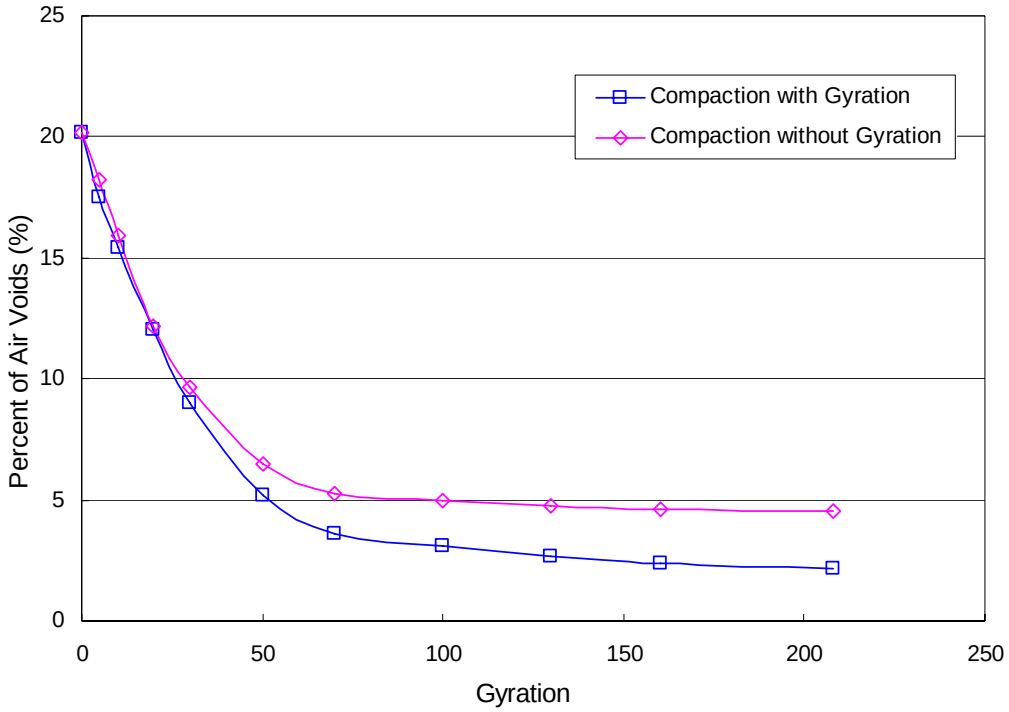

Figure 4.15 Compaction with and without Gyration

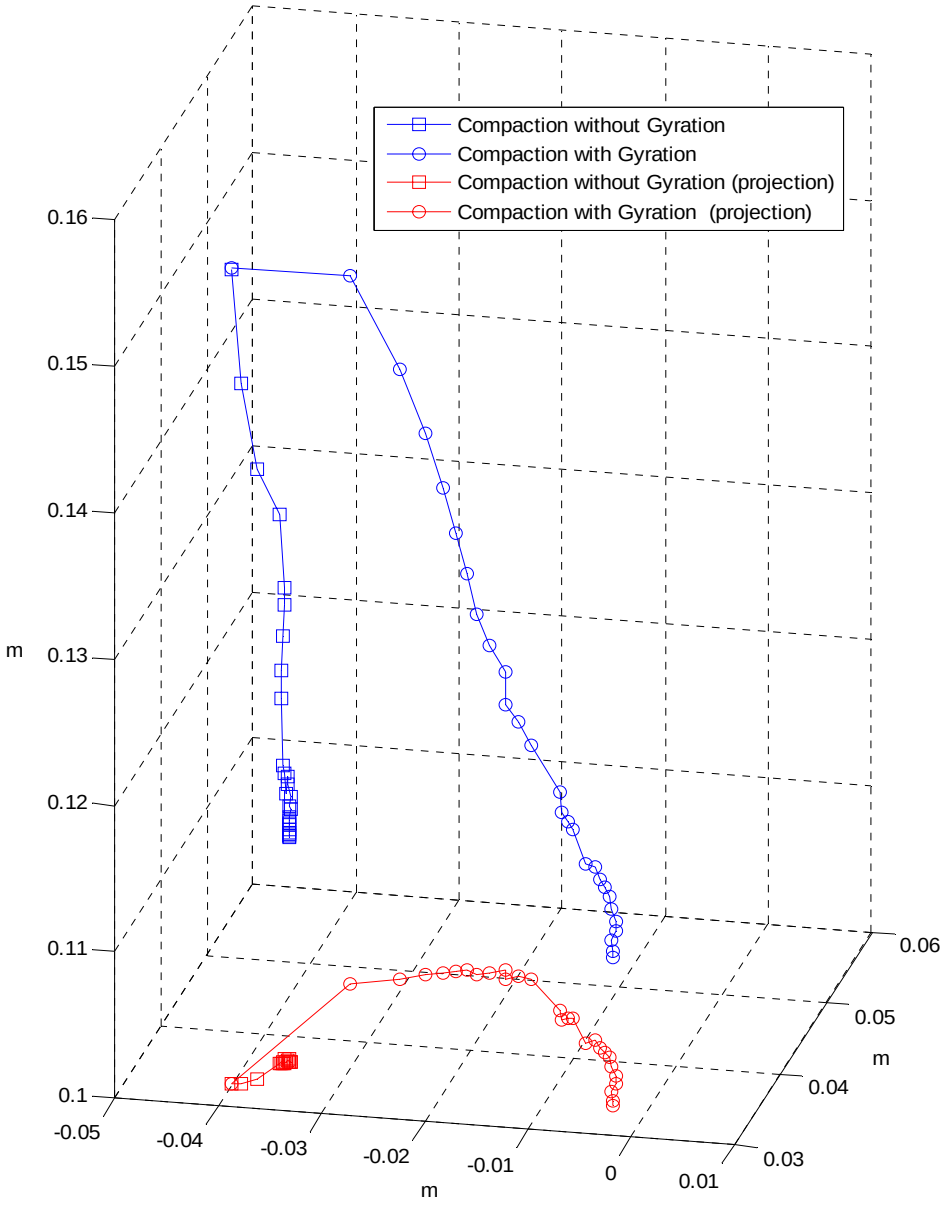

Figure 4.16 Motion trace of particles

CHAPTER 5 DEM SIMULATION OF ASPHALT VIBRATION COMPACTION

5.1 Introduction

This chapter presents the DEM simulation results of asphalt mixture vibratory compaction by using open source DEM code. The asphalt mixture vibratory compaction tests at different conditions were also conducted in lab. The prediction accuracy of the DEM models in predicting the air voids was evaluated through the comparison between the DEM predicted results and the laboratory measured test data. The air voids compaction process was studied and the effect of vibration force and vibration speed on asphalt mixture compaction was investigated.

5.2 Asphalt Mixture Vibratory Compaction Method

Depending on the requirement of laboratory test, asphalt mixture specimens can be cylindrical, trapezoidal, or rectangular in shape and compaction can be achieved through impact, kneading, or vibration. The asphalt vibratory compactor (AVC) can compact asphalt mixture specimens at a similar amplitude, frequency and relative mass as applied by a construction vibratory roller on the road, and is a common compaction method to make asphalt mixture specimens for both cylinder and rectangular in shape for laboratory tests (Collins *et al.*, 2003). For example, asphalt mixture specimens compacted by asphalt vibratory compactor are widely used in the Asphalt Pavement Analyzer (APA) to

evaluate susceptibility to permanent deformation (rutting), fatigue cracking, and moisture damage of hot asphalt mixture.

The asphalt vibratory compactor, as shown in Figure 5.1, consists of the following four basic components (Collins *et al.*, 2003):

(1) Vibrating compaction assembly

The vibrating compaction assembly is the most important part in the asphalt vibratory compactor and is composed of the following components:

- Pneumatic actuator which drives the vibrating assembly and provides the compressive force necessary for compacting loose asphalt mixture;
- Vibrating assembly consisting of two high efficiency vibrators bolted to the base plate;
- Compaction head attached to the vibrating assembly base plate (a rectangular head for 125 mm by 300 mm beam specimens and a circular head for 150 mm diameter cylindrical specimens;
- Specimen supporting base, with a recessed area positioned directly below the compaction head for the beam mold or the cylinder mold to fit into during the compaction operation.

(2) Specimen mold

Two types of specimen molds are made of rigid steel material for compaction of the beam specimen and the cylindrical specimens.

(3) Specimen extruding assembly

Specimen extruding assembly is for extruding the specimen from the specimen mold immediately after compaction.

(4) Operation control system

The operation control system is used to perform the specimen compaction and extrusion operations, which includes pressure regulator, pressure gauge, control unit and control circuit box.

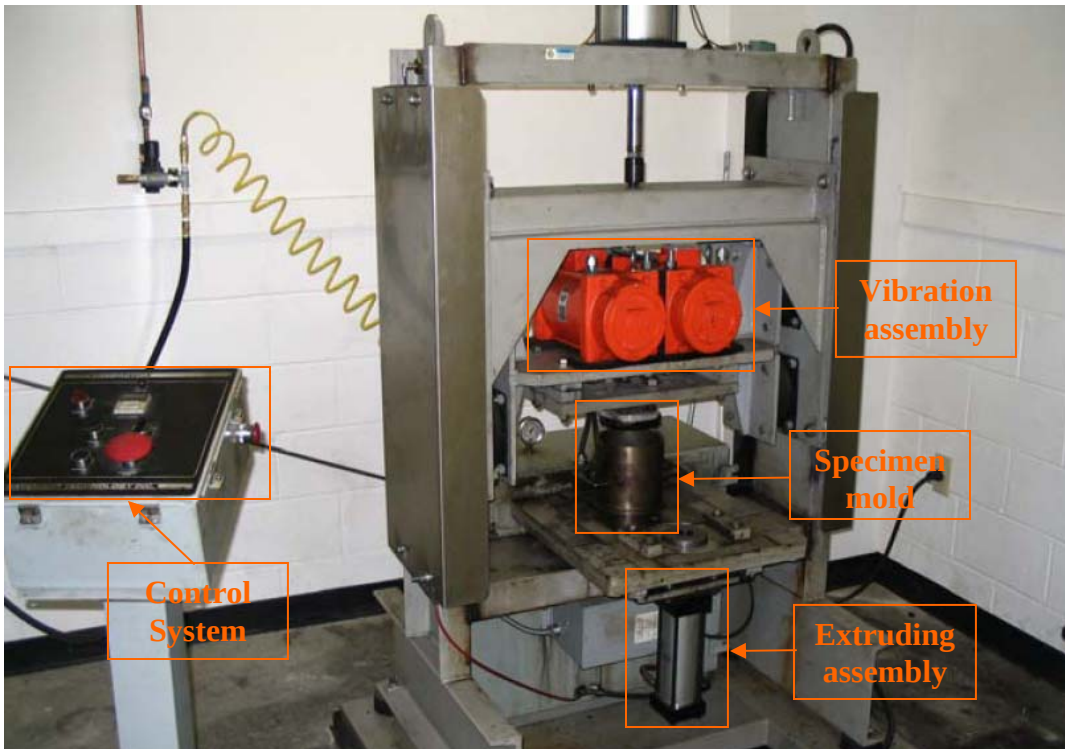

Figure 5.1 Asphalt Vibratory Compactor (AVC)

Prior to compacting asphalt mixture samples, the compaction head of the asphalt vibratory compactor needs to be calibrated to produce a sample at pre-determined height by adjusting the position of compaction plate. Both the pre-arranged loose mix and compaction mold are placed in an oven at compaction temperature for required time. In vibration compaction, the pre-determined weight of loose asphalt mixture is poured into the cylindrical or rectangular preheated steel mold, and then the mold is transferred to the supporting base of the Asphalt Vibratory Compactor and fit into the recessed area. The

volume of the mix (in grams) should be determined from target final density, theoretical maximum specific gravity of the mix and the mold volume. The electronic control units of asphalt vibratory compactor allow to set a testing time and to control the specimen height. Once the compaction starts, the compaction head moves downward and the vibrating actions will be activated automatically when compaction head reaches the top of the steel mold. Under the static compression force and the dynamic vibrating actions, the loose asphalt mixture is consolidated and compacted in specimen mold according to pre-setting times or heights. After the asphalt mixture sample is compacted, the vibrating compaction assembly will automatically retract and asphalt mixture samples are extracted with the help of an air cylinder.

The static compaction force is controlled by the compaction pressure and the counter balance pressure. The compactor head comes down at the system pressure (Ex. 90psi). When the compaction head reaches the top of the steel mold and the compaction motors start, the counter balance valve opens and puts balance pressure to the compaction head upward (Ex. 30psi). So 90psi down with 30psi up pressure would translate into a static pressure of 60psi (413.64 kPa). The vibrating action is produced by two vibrators attached on the compaction head. Each compactor can provide a minimum of 100 lb and a maximum of 1600 lb vibration force, which results in a minimum 23.7 kPa and maximum 358 kPa pressure for two compactors. During the compaction process, the compactor stops automatically at two type conditions, time control and height control. When either one of these conditions is satisfied, the compactor stop automatically. In order to study the effect of different factors on asphalt mixture vibration compaction, the time control termination methods was used here and the control height was set at a low

value (Ex. 1 inch) by adjusting compaction head. The compaction time can be adjusted from the cycle time counter on the control unit and specimen height was measured after asphalt mixture compaction.

Hurley and Prowell (2006) presented three reasons of using asphalt vibratory compactor when producing asphalt mixture specimens. The first reason is the Superpave gyratory compactor is insensitive to temperature changes. A second reason is that it is easier to produce samples for the Asphalt Pavement Analyzer (APA) with the vibratory compactor than with a Marshall hammer (the Marshall hammer is known to be sensitive to compaction temperature). The third reason is that the vibratory compactor applies a vertical load, frequency, and amplitude that is comparable to those found in a typical vibratory roadway compactor. According to Jackson and Owenby's report, volumetric properties were observed to be relatively uniform throughout the vibratory compacted specimens and the compaction process using the AVC is similar to the compaction process using a vibratory compactor in the field (Jackson and Owenby, 1998). Tarefder and Zaman (2002) pointed out SGC has a tendency to compact mixes in excess of what can be achieved with conventional paving equipment in the field. The bulk density values of the AVC compacted cylindrical specimens are similar to those of field compacted specimens. However, some researchers found it is difficult to reach the high level of density (like 97%) with asphalt vibratory compactor (Cooley & Kandhal, 1999). Bennert *et al.*, (2003) reported that the vibratory compactor has difficulty compacting 19mm coarse pills due to the confinement of larger aggregates within the small mold.

5.3 Vibration Compaction DEM Simulation Process

As mentioned above, the asphalt mixture is compacted under a combination effect of static force and dynamic vibration force. The dynamic vibration action is produced by rotating eccentric weights inside the vibrator and the default rotational speed is 3600 Vibrations Per Minute (VPM). According to the calculation results of static force and dynamic vibration force, the input compaction force can be presented as shown in Figure 5.2, which is also used as the force function of the compaction plate in DEM vibration compaction simulation. It should be noted that, since an explicit time stepping algorithm is employed in DEM simulation, the values of compaction force is constant in each specific time step and the value of compaction force at different time step will be calculated according to the force function.

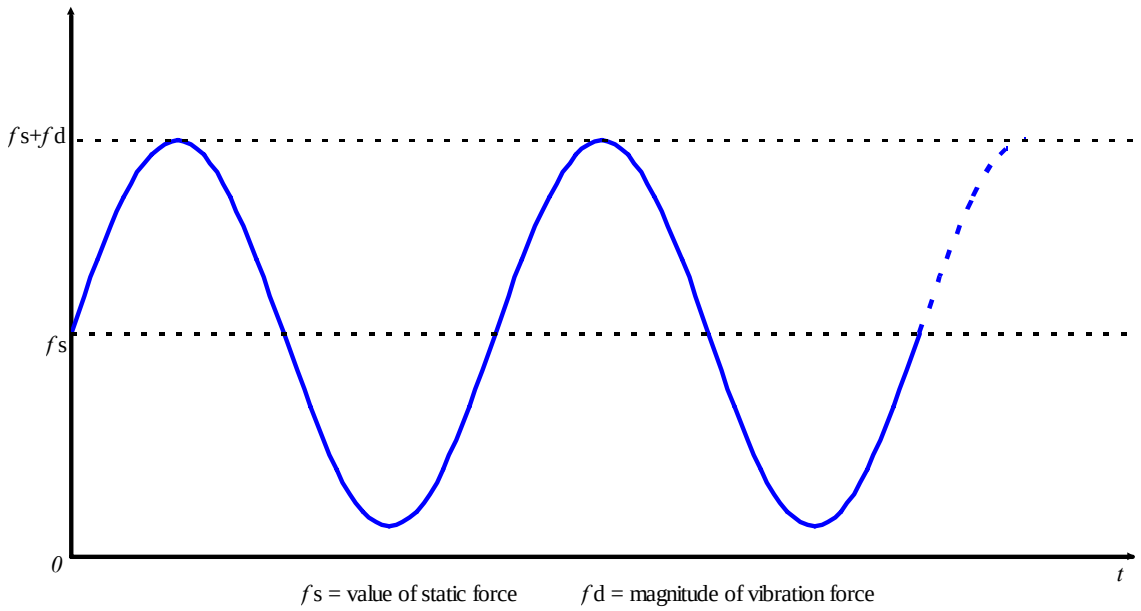

Figure 5.2 Force Function of Compaction Plate

The DEM simulation of asphalt mixture vibration compaction can be basically divided into two steps. The first step is the packing of particles in specimen mold under gravity force and the second step is the vibration compaction of particles under a combination effect of dynamic vibration force and static force.

The procedures of the DEM simulation process is summarized as follows:

- Generate open top compaction mold according to mold dimensions;
- Calculate particle numbers of each particle size according to gradation curve;
- Randomly generate particles in specific space within compaction mold;
- Packing of spheres under gravity force until stable inside the mold;
- Generate vibration plates and set vibration force function of vibration plate;
- Particles compaction under the action of vibration compaction plate.
- Record the position of compaction plate and particles;
- Calculate air void of asphalt mixture according to output data.

5.4 DEM Simulation Results

5.4.1 Compaction with Different Duration Time

A SMA mixture with the gradation as shown in Figure 4.3 was simulated here and verification laboratory vibratory compaction tests were conducted. Figure 5.3 shows the DEM simulation results and laboratory test results for asphalt mixture vibration compaction with different compaction duration times. It is apparent that the air voids decrease with time increase in both DEM simulation and laboratory test and the compaction gaining become slower with the time increase. From the figure, it also can be

observed that the DEM simulation results are smaller than that of laboratory test results, which probably due to the less interlock effect between spherical particles in DEM compaction simulation. Less interlock between particles mean less resistance during the asphalt mixture compaction process, so the asphalt mixture can be better compacted and have relatively low air voids in DEM simulation.

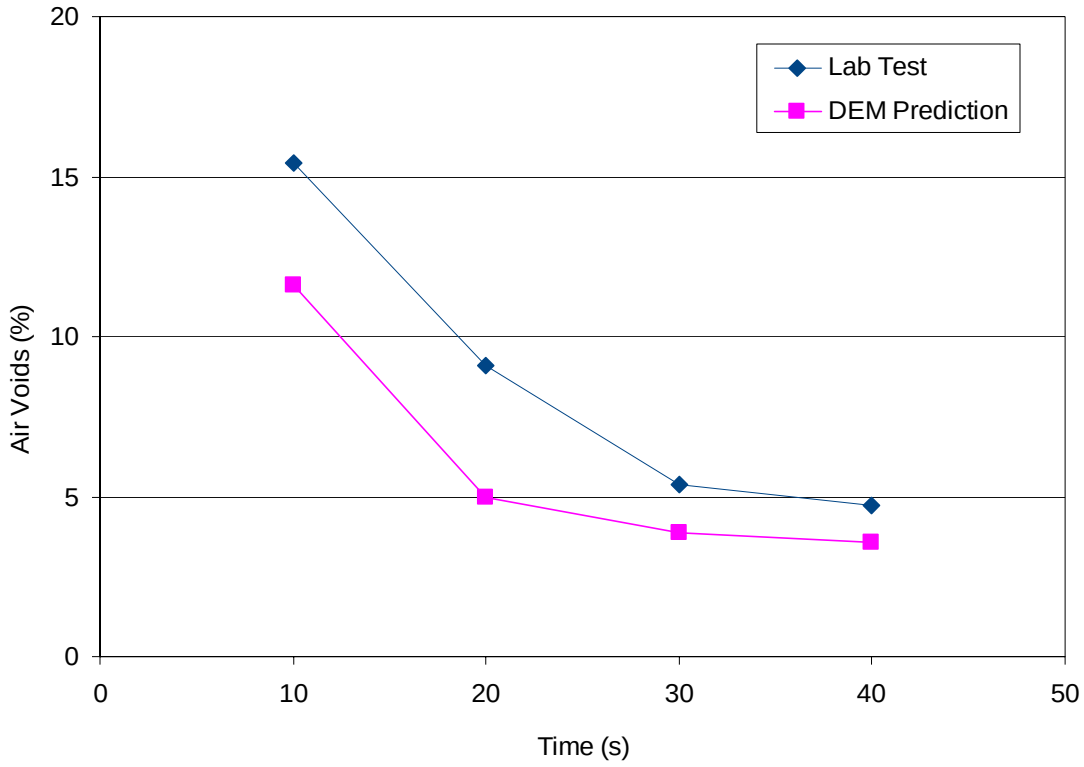

Figure 5.3 Air Voids vs. Compaction time

5.4.2 Effect of Vibration Force

Vibration force is an important factor which can significantly affect asphalt mixture vibration compaction process. The vibration force of vibrators attached on the compaction head is adjustable by changing the eccentric settings (Figure 5.4). The vibrators have six levels of eccentric setting which will produce different amplitudes of

vibration force. The vibration forces of different settings can be found from the VIBCO vibrator manual and are presented in Table 5.1. Since the vibration force of setting 5 and 6 are pretty close, only setting 1~5 were simulated here. The DEM simulation and laboratory test results of asphalt mixture compaction under different vibration forces are shown in Figure 5.5. As seen in Figure 5.5, DEM simulation and laboratory test results follow the same development trend in compaction process. From the figure, it can be seen that the air voids decrease with the increase of vibration force and the decrease rate becomes slower at high vibration force level. The simulation results indicate that high vibration force is required to make low air voids asphalt mixture specimen using vibration compaction method. Since the vibratory compaction effort is a one-dimensional stress to compact asphalt mixture and it is difficult to reach the high level of density (Cooley & Kandhal, 1999), the vibration force is vitally important to asphalt mixture compaction.

Figure 5.4 Setting of Vibration Force

Table 5.1 Vibration force at different setting

Setting number	1	2	3	4	5	6
Force (N)	222.5	2225	4227.5	5785	6675	7565

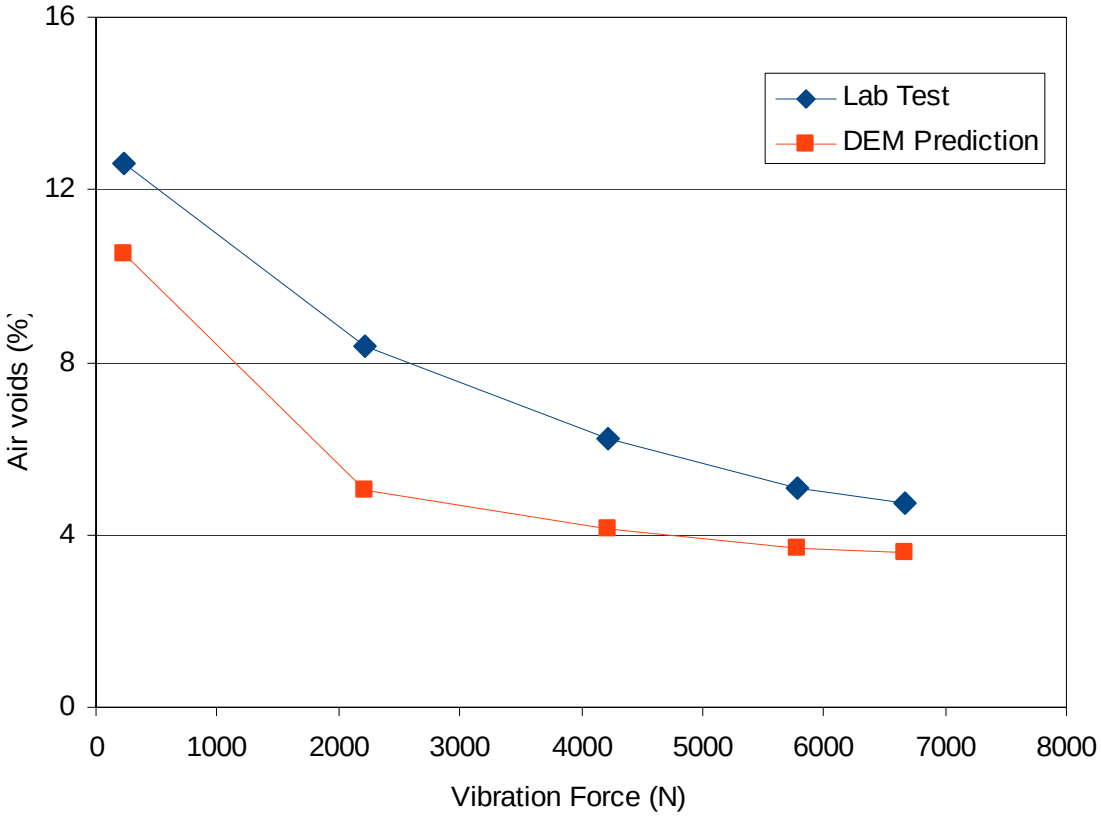

Figure 5.5 Vibration compaction of different vibration force

5.4.3 Effect of Vibration Speed

Vibration frequency is another factor which may significantly influence the asphalt mixture compaction process. However, due to the cost and actual considerations, most of laboratory asphalt mixture vibration compactors can not adjust vibration speed to study the effect of vibration frequency, which usually require the complete replacement of vibrators. In this study, the open source DEM code was employed to study the effect of

vibration frequency on the asphalt mixture compaction by simply setting the vibration speed value in DEM code, which greatly reduces the research cost without making expensive changes to asphalt mixture vibration compactor in lab. Figure 5.6 presents the DEM simulation results of vibratory compaction at different vibration speed. The original speed of vibrator is 3600 vpm and two more speeds are simulated here, which can be simply done by adjusting the force function of compaction plate during DEM simulation. As shown in figure 5.6, due to the vibration effect, high vibration speed was found to have low air voids and it seems harder to get desired density with the low vibration speed. From the figure, it also can be observed that the asphalt mixture can be compacted under the effect of high speed vibration action within relatively short time, which is helpful to obtain well compacted asphalt mixture.

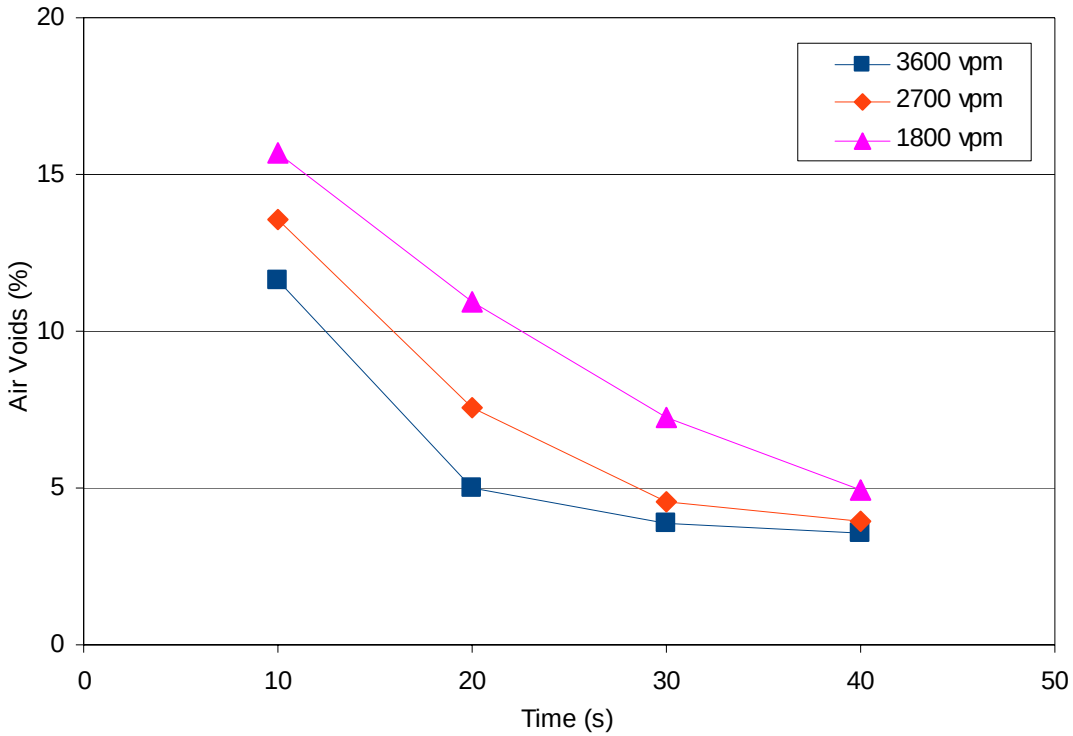

Figure 5.6 Vibration compaction of different vibration speed

CHAPTER 6 DEM SIMULATION OF APA LINEAR KNEADING COMPACTION

6.1 Introduction

This chapter presents the application of open source DEM code to simulate a self developed linear kneading HMA mixture compaction. The modified linear kneading compaction was based on Asphalt Pavement Analyzer (APA) machine which originally used to test rutting and fatigue behavior of asphalt mixture. The effect of compaction pressure, wheel speed and boundary condition on asphalt mixture compaction was studied and the predicted air voids obtained from DEM simulation was compared to the laboratory measured test results.

6.2 Linear Kneading Compaction Method

Currently, Asphalt Vibratory Compactor is the most common used method of compacting beam asphalt mixture specimens. However, some researchers have used linear kneading compactor (LKC) for beams specimens, which can achieve the desired density without fracturing aggregates and is more adaptable for producing a larger variety of sizes and shapes. For example, linear kneading compactor is a standard compaction method of making beam specimens in the Colorado Department of Transportation and the specification of this Standard Method was established in 2009 (CDOT, 2009).

In linear kneading compaction (as seen in Figure 6.1), the pre-heated mold is filled with a pre-determined weight of loose hot mix calculated from the target final density, theoretical maximum specific gravity of the mix and the mold volume. A series of closely fitting rectangular compacting plates are placed in a vertical row across the plant mix. A steel roller successively applies force to the top of the compacting plates while the mold moves back and forth on a sliding table. The steel roller transmits a rolling action force to the plant mix through the steel plates, one plate at a time. So a linear compression wave is produced in the mix by the bottom edges of the plates as the roller pushes down on each plate. This compacting motion continues until the height of the sample of plant mix is reduced to the height calculated to yield the predetermined voids and density.

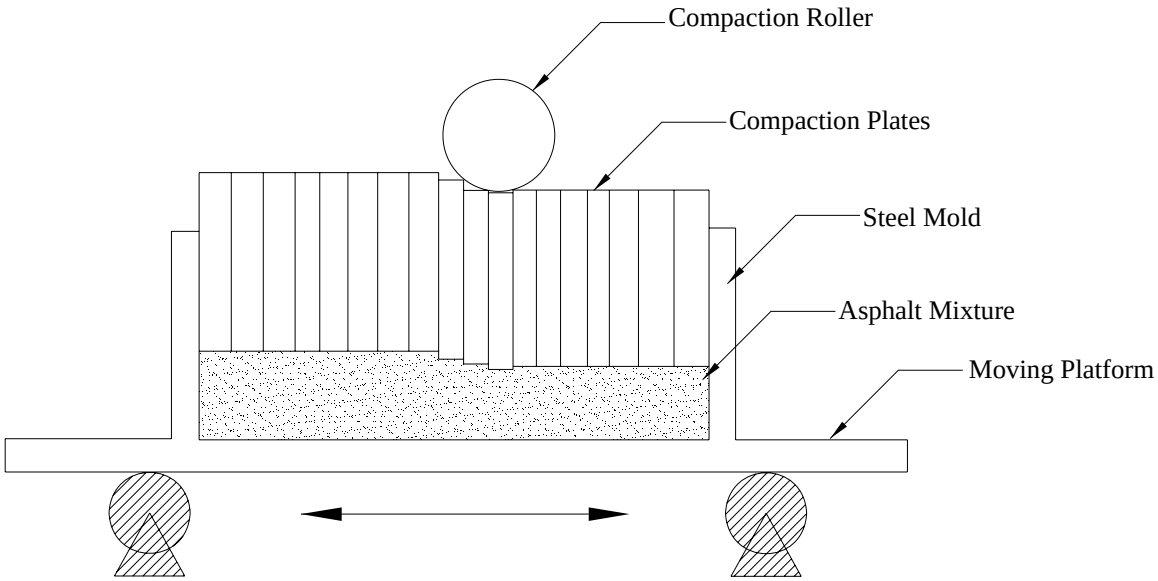

Figure 6.1 Schematic diagram of linear kneading compaction

After comparison of test results from laboratory and field Compacted Samples, Stevenson and Aschenbrener (1994) pointed out that kneading action allows the mixture

to be compacted without fracturing the aggregates and is probably very similar to a steel wheel roller. Masad *et al* (1999) used DIP to quantify the internal structure parameters of specimens compacted using Superpave gyratory compactor and linear kneading compactor and found out that LKC specimens had more contacts than the SGC specimens. The high contact number means better aggregate structure and may result in higher resistance to permanent deformation and higher shear strength (Khosla, 2002). Four types asphalt mixture compaction methods (gyratory compactor, Marshall hammer, ELF linear kneading compactor and the gyratory compactor) were used by Button to evaluate the probability of producing specimens similar to pavement cores (Button *et al.*, 1994). Laboratory-fabricated specimens from each compaction device were tested for mechanical properties such as indirect tensile resilient modulus, indirect tensile strength, strain at failure, and compressive creep. The test results indicated that there was not a great deal of difference between the various compactors

6.3 APA Linear Kneading Compaction

Although linear kneading compaction has been used by many researchers to make beam specimens, the cost of linear kneading compactor is pretty high. According to the information collected from internet, the price of linear kneading compactor is around $60,000~$90,000, which makes it unavailable for many research organizations. In this study, a modified kneading compaction was conducted on Asphalt Pavement Analyzer (APA) machine and simulated using discrete element method. In the modified test, the Asphalt Pavement Analyzer machine, originally used to test rutting and fatigue behavior of asphalt mixture (Figure 6.2), was used to compact hot mixed asphalt mixture. The

original test mold of the APA machine was modified into steel boxes at different dimensions (length 305 mm, height 75 mm, three different width 50, 100, 200 mm). Compared with traditional linear kneading compaction, the Asphalt Pavement Analyzer machine not only provides an adjustable moving load condition which is more similar and close to real field pavement compaction, but also automatic data collection which is useful to collect deformation information during compaction and helpful to understand the compaction process. With advantages of controllable load conditions and automatic data collection, the Asphalt Pavement Analyzer machine can be extend to do some researches more than asphalt mixture test rutting and fatigue analysis. For example, Han *et al.* (2008) used Asphalt Pavement Analyzer machine to evaluate geosynthetic-soil confinement. In his proposed test, a geosynthetic sheet is placed within a base course to form a reinforced base in modified test mold, which is subjected to APA wheel loading. The measured rut depth with the number of cycles of wheel loading was then used to evaluate the geosynthetic-soil confinement.

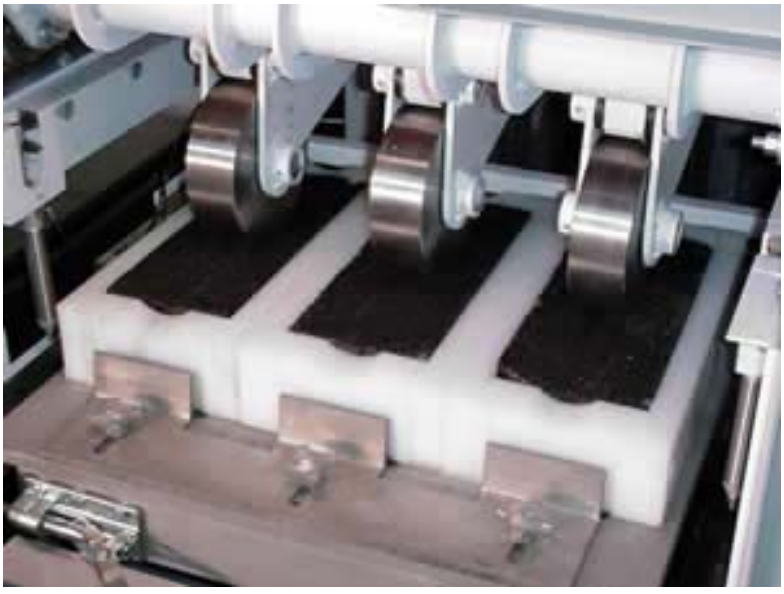

Figure 6.2 APA rutting test

Similar to traditional linear kneading compactor, in this APA linear kneading compaction (as shown in Figure 6.3), a pre-determined weight of hot mix is placed in an self designed open top steel mold and a series of vertically aligned steel plates (width 3/4 inch) are positioned on top of the hot mix, and then a hydraulically-loaded APA steel roller moves on the vertically moveable steel plates and produces a rolling action force to the underneath mixture through the steel plates. The mixture is then compacted with kneading and compressing effect under APA moving roller. The maximum load provided by the APA machine is 265 lb and the load can be adjusted to study the compaction with different compaction effort. The speed of the APA wheel is also adjustable and the position of the APA wheel can be recorded automatically during compaction process. The modified APA linear kneading compaction is in a force control compaction condition and the moving APA load is closer to the real field compaction pattern.

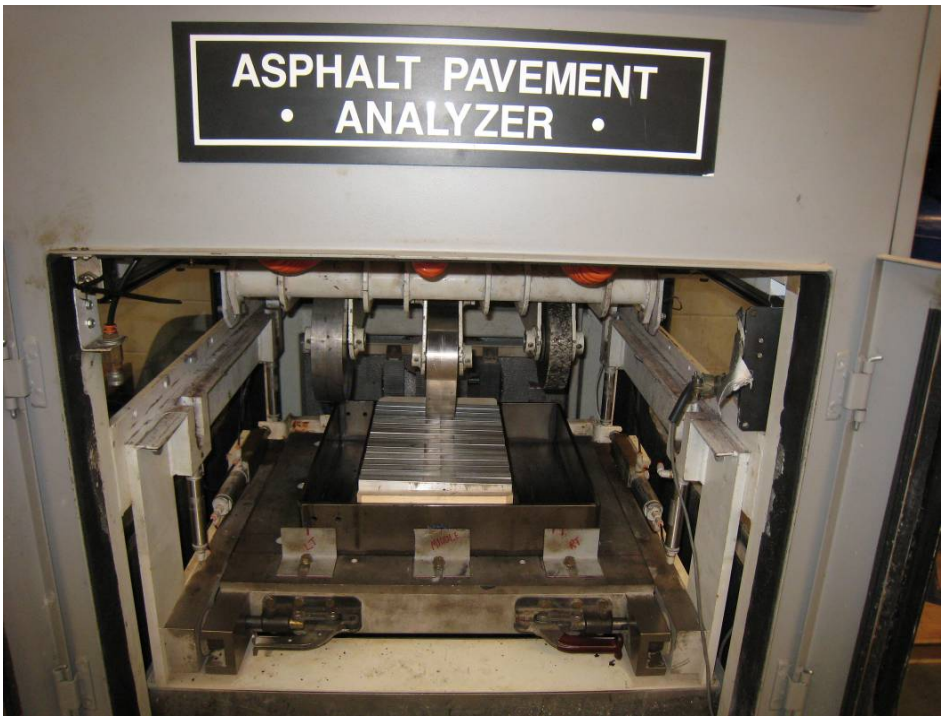

Figure 6.3 Modified APA linear kneading compactor

Figure 6.4 Asphalt mixture compacted with APA linear kneading compactor

6.4 DEM Simulation Process

In DEM simulation of APA linear kneading compaction, the kneading action force can be simulated by setting the load function of each plate (Figure 6.5). Take half compaction cycle as example, when the compactor begins to compact the asphalt mixture and wheel move on plate 1, the plate 1 applies a force equal to pre-setting APA wheel load on the underneath particles, while the forces of other plates are set to zero. When the wheel moves forward, plate 2 applies a force on underneath particles and other plates apply zero force. In the same way, the compaction force will gradually be applied by each plate in specific time based on the APA load and speed (Figure 6.6).

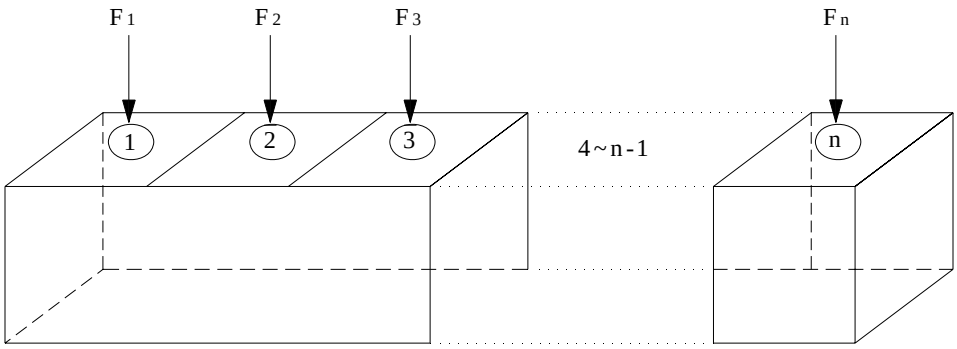

Figure 6.5 schematic diagram of kneading action force

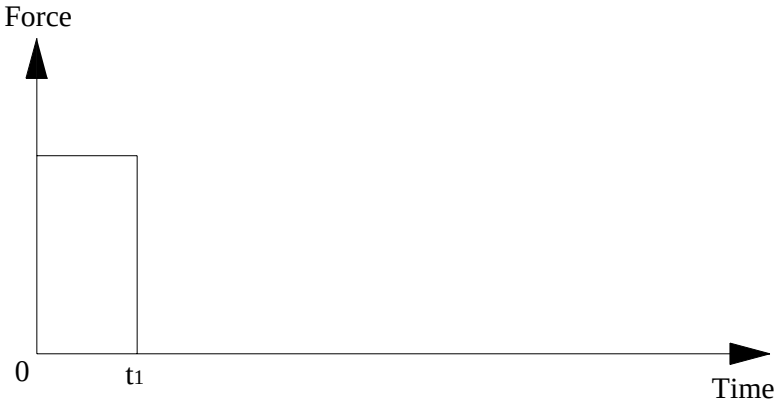

Figure 6.6a Force applied by Plate 1 (F_1)

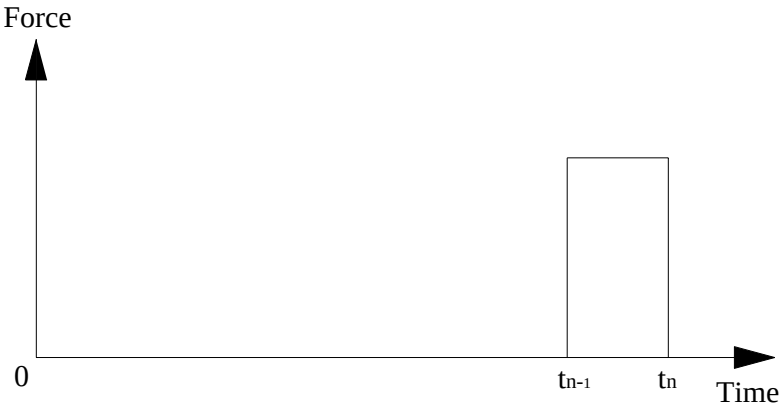

Figure 6.6b Force applied by Plate n (Fn)

Figure 6.6 Force applied by Plates

The DEM simulation of APA linear kneading compaction can be basically divided into two steps. The first step is the packing of particles under gravity force and the second step is the compaction under kneading action force. The procedures of the DEM simulation process is summarized as follows:

- Generate open top compaction box according to mold dimensions;
- Calculate particle numbers of each particle size according to gradation curve;
- Randomly generate particles in specific space;
- Packing of particles under gravity force until it is stable inside the mold;
- Generate compression plates and set compaction force function of each plates with above mentioned method;
- Particles compaction under the action of a series of compaction plates.
- Record the position of all compression plates and spheres at the end of each compaction cycle;
- Calculate air void of asphalt mixture in each cycle.

6.5 DEM Simulation Results

6.5.1 Compaction Process of APA Linear Kneading Compaction

A SMA mixture with the gradation shown in Figure 4.3 was simulated here and verification laboratory compaction tests were conducted. Figure 6.7 shows the air voids compaction process of APA linear kneading compaction for both DEM simulation and laboratory test at speed 30 (1 second/circle) and pressure 600 kPa. From the figure, it can be seen that DEM simulation results and laboratory test results have the same

development trend in air voids compaction process and the DEM predicted value is also close to the laboratory test results.

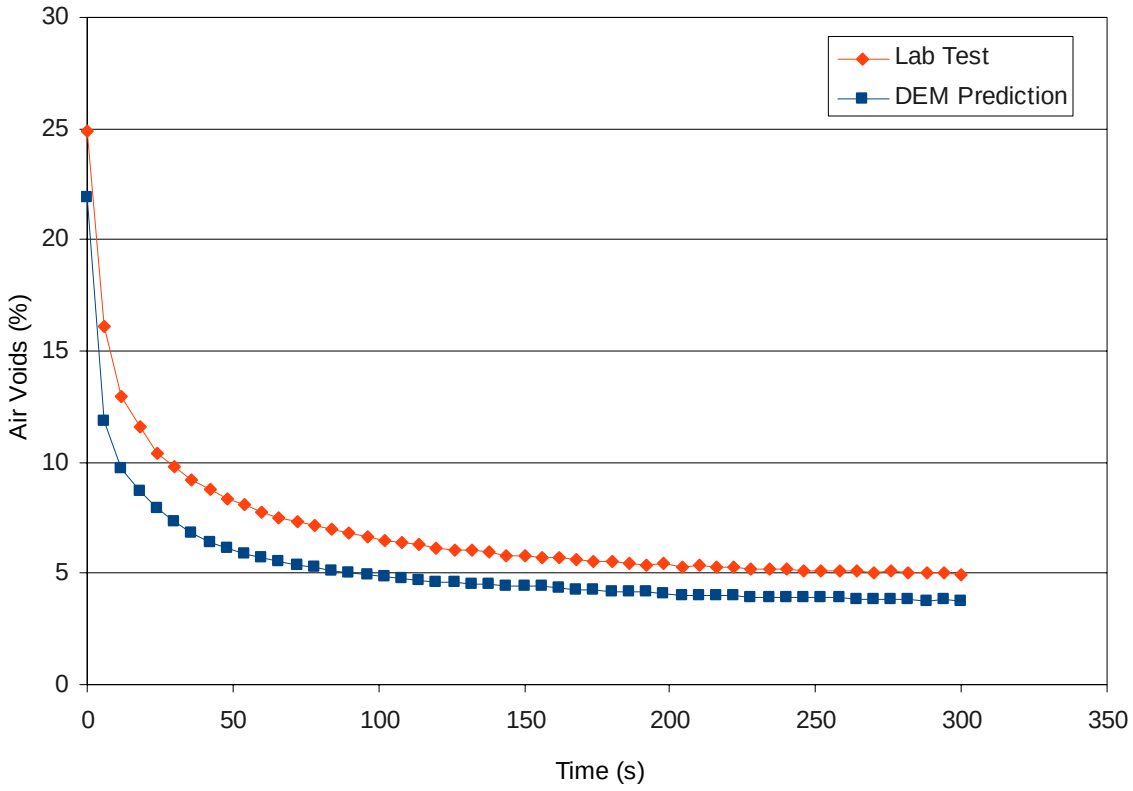

Figure 6.7 Compaction process of APA kneading compaction

6.5.2 Effect of Compaction Pressure

The compaction pressure between the steel plates and underneath asphalt mixture can be adjusted by setting different APA machine wheel load. Figure 6.8 presents the DEM simulation results and lab test results of different compaction pressure in 100 mm width mold at wheel speed 30 (1 second/cycle). It is apparent that the air voids decrease with the increase of compaction pressure in both DEM simulation and lab test. The air voids of DEM simulation decrease quicker than that of lab test in beginning stage and slower later. This may be because of the effect of interlock between aggregates in laboratory

compaction tests. However the interlock effect is not so strong in DEM compaction simulation due to the spherical assumption of aggregate. When the compaction pressures were low, the asphalt mixtures can not be well compacted in both lab test and DEM simulation, so both results show high voids in the beginning stage. With the increase of compaction force, although both lab test and DEM simulation have the same compaction pressure absolute increment, the asphalt mixture can be better compacted in DEM simulation due to less interlock effect between round particles, so the DEM prediction air voids decrease faster than lab test results. With the continuous increase of compaction pressure, there is no space in mixture which can be further compacted in DEM simulation, so the DEM prediction air voids decrease slower than that of lab test, and both air voids in high compaction pressure are low and close to each other.

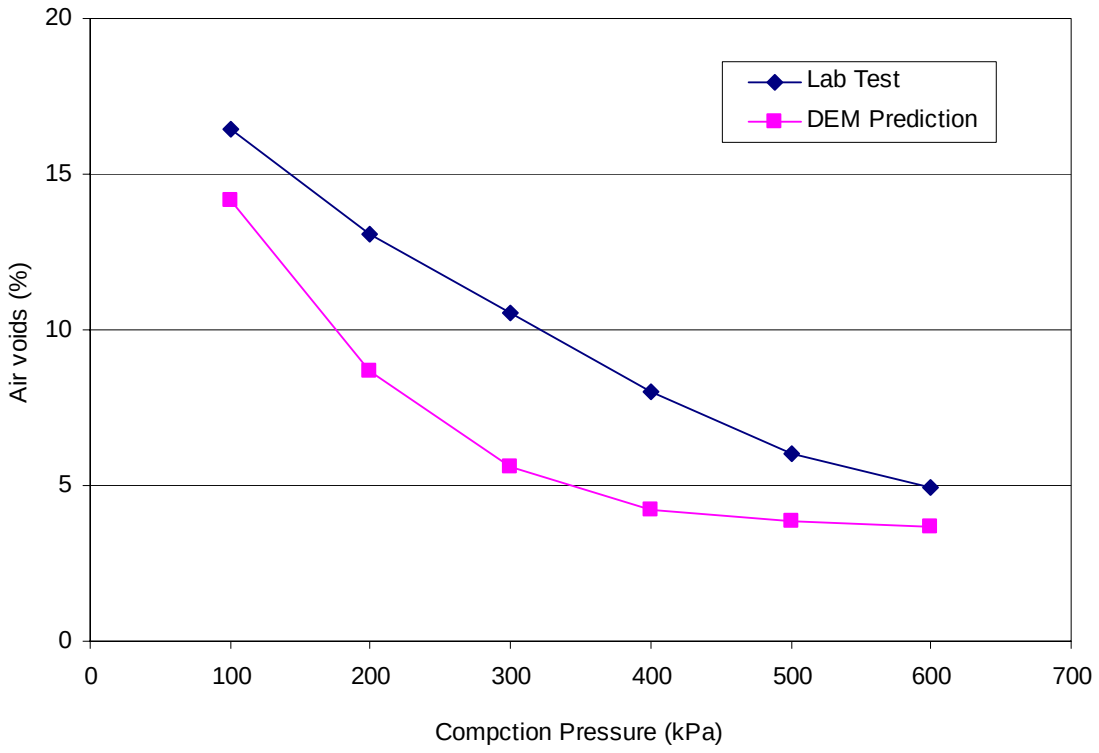

Figure 6.8 Air Voids vs. Compaction pressure

6.5.3 Effect of Wheel Speed

The wheel speed is adjustable in APA machine and thus the adjustable wheel speed can be used to study the effect of kneading frequency on asphalt mixture compaction. The period for each wheel speed can be found in APA manual and was shown in Table 6.1.

Table 6.1 APA wheel speed

APA wheel speed	10	20	30	40	50
Period (Second/Cycle)	3	1.5	1	0.75	0.6

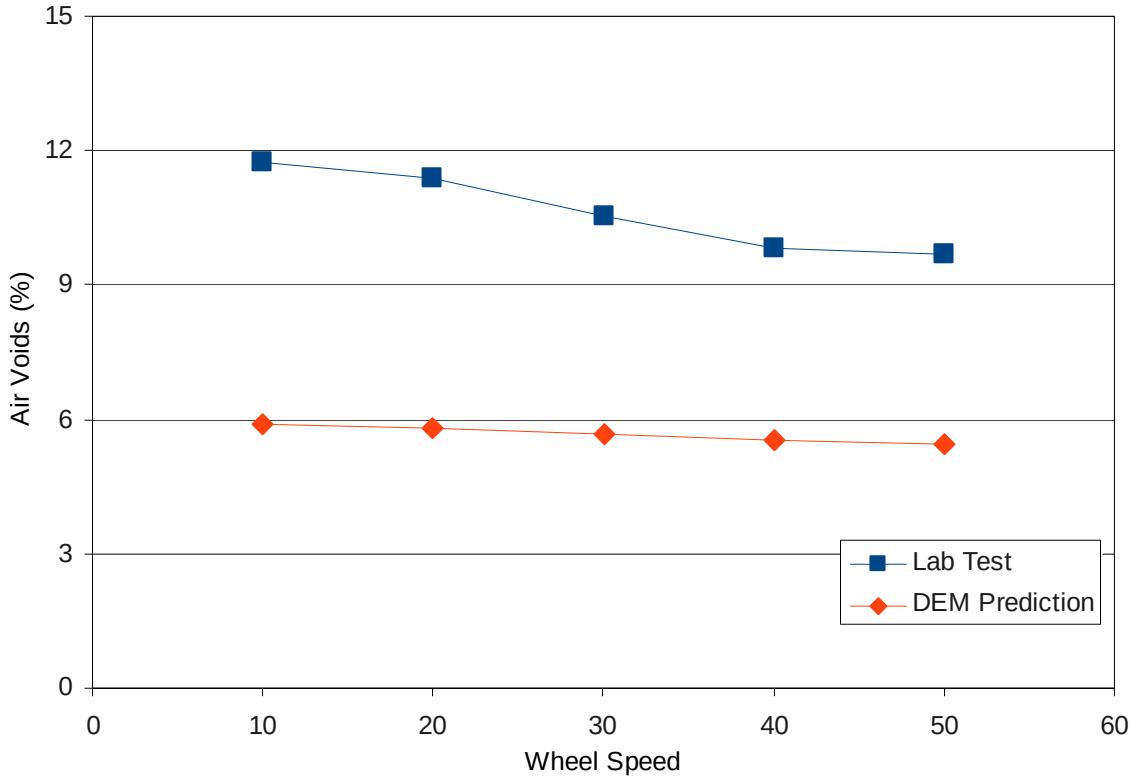

Figure 6.9 Air voids vs. wheel speed

The DEM simulation and laboratory test results in 100 mm width mold are shown in Figure 6.9. Since high compaction pressure usually causes pretty low air voids, it may be difficult to tell the difference of compaction at different speed, so compaction pressure

300 kPa was used here. From the figure, it can be seen that the air voids are highly affected by wheel speed in laboratory compaction test. The high wheel speed means more kneading times at a given time during compaction and thus results in lower air voids. The air voids of DEM simulation also decrease with the increase of wheel speed, but the difference caused by wheel speed is not so significant as that in laboratory compaction tests, which may also because of above mentioned less interlock between particles in DEM simulation.

6.5.4 Effect of Boundary Condition

In this APA linear kneading test, the self designed steel mold has three different widths (50, 100, 200mm) which can be used to study the effect of boundary condition on asphalt mixture compaction. Since the maximum load provided by APA machine is 265 lb (1178 N), the compaction pressure simulated here is 200 kPa and the wheel speed is setting at 30 (1 second/cycle). Figure 6.10 presents the DEM simulation and lab test results. From the figure, it can be seen that mold width has certain influence on asphalt mixture compaction in both DEM simulation and laboratory tests. The wide mold has less boundary constraint and has low air voids.

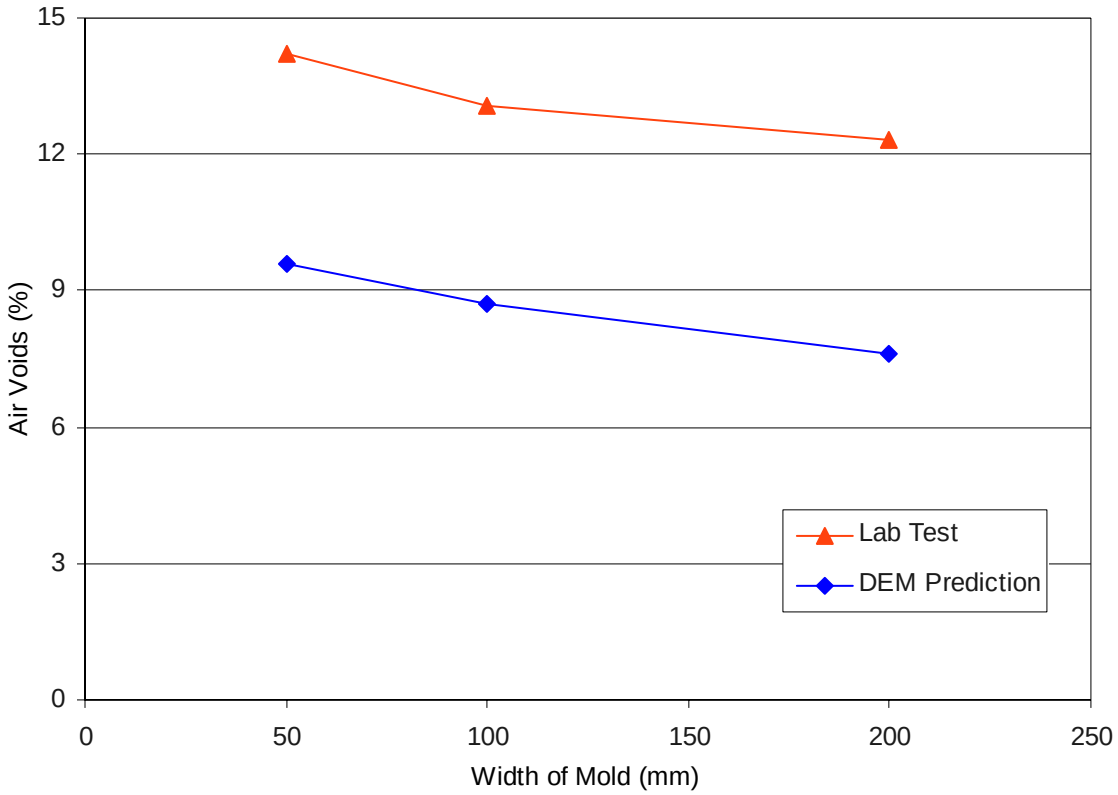

Figure 6.10 Effect of boundary condition

CHAPTER 7 AIR VOIDS DISTRIBUTION ANALYSIS USING DEM

7.1 Introduction

Heterogeneous air voids distribution is a common phenomenon in asphalt mixture and can greatly affect the behavior of asphalt mixture. The air void distribution is related with several factors such as compaction effort, method of compaction, aggregate gradation etc. In this study, an open source discrete element method (DEM) code was used to simulate the compaction of hot-mix asphalt (HMA) and the DEM virtual digital specimens were further post processed to investigate the effect of compaction factors on air voids distribution. The compaction process of gyratory compaction and vibration compaction were simulated, and the effect of aggregate gradation, specimen height, mold size, mold shape and compaction method on air voids inhomogeneous distribution were studied.

7.2 Air Voids Distribution and Research Method

Hot-mix asphalt (HMA) is a multi-phase composite material that consists of asphalt binder, coarse aggregate, fine aggregate, mineral filler, and other additives. The asphalt mixture behavior is highly related with the volumetric fraction and space distribution of these components. Air void is probably the most important volumetric property of asphalt

mixture and highly influences its stability and durability. Low air voids usually cause rutting of asphalt mixture due to plastic flow and high air voids can result in premature cracking or raveling due to moistures and oxidation (Roberts *et al.,* 1996). Although the amount of air voids in asphalt mixture greatly affects the behavior of asphalt mixture, asphalt mixture specimens with the same total volume of air voids may show distinct mechanical behavior because of the air voids distribution. However, due to the limitation of laboratory techniques, researchers usually use average volume of air voids to design and evaluate asphalt mixture.

In recent years, in order to capture internal structure of asphalt mixture and study the effect of air voids distribution on asphalt mixture behavior, non-destructive digital image analysis techniques, especially X-ray computed tomography technology, have been used by researches and have yielded some useful results. As early as 1999, Masad *et al.* used an x-ray computed tomography system along with image analysis techniques to quantify the structure of air voids within asphalt mixture. He analyzed the distribution of air void size and number of air voids with depth by processing horizontal x-ray tomography image of asphalt concrete specimen and studied the effect of several factors, like number of gyrations, compaction method and aggregate gradation. He found a “bathtub” vertical air void distribution pattern in gyratory compacted specimens based on the images captured using the X-ray tomography (Figure 7.1).

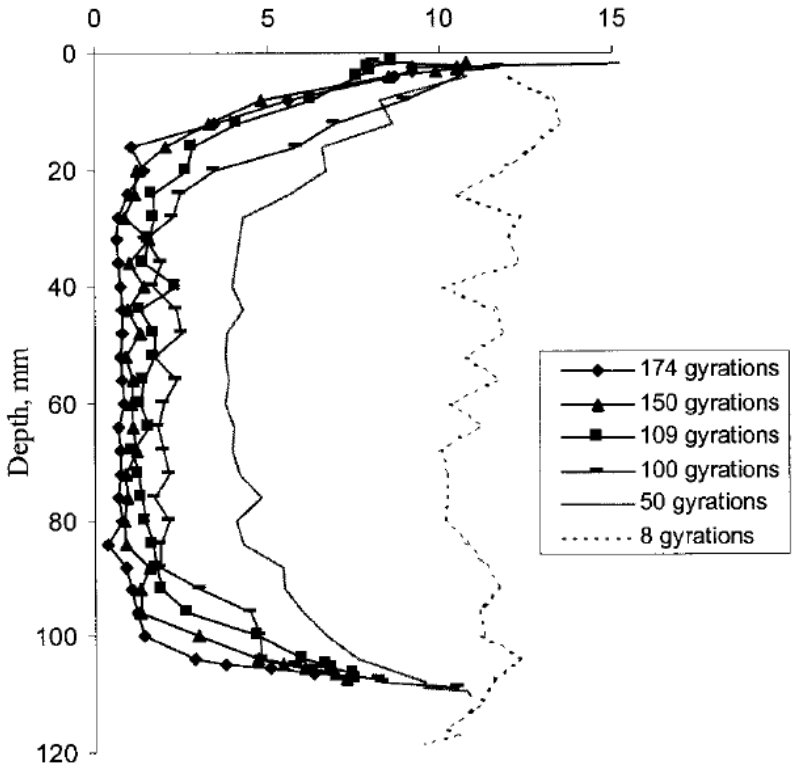

Figure 7.1 Vertical Voids distribution in Gyratory Specimens (Masad, 1999)

Masad *et al.* (2002) studied vertical air voids distribution in gyratory compacted specimen, linear kneading compacted specimen and field core based on the images captured using the X-ray tomography，and found different air voids distribution pattern in these asphalt mixture specimens. Muraya (2007) studied the air voids distribution of three different types of asphalt mixture (porous asphalt concrete, stone mastic asphalt concrete and the dense asphalt concrete) with a more complicated coring pattern in post processing stage of X-ray images and got different vertical air voids distribution pattern at different rays within asphalt mixture specimen. The air voids distribution in lateral direction was also studied. Thyagarajan *et al.* (2010) employed X-ray computed tomography to characterize the lateral air void distribution within asphalt mixture specimens prepared with different gyratory compactors and the test results clearly shows

the non-uniformity in the lateral air void distribution within HMA specimens. He found that air void content increases at an exponential rate as the distance from the specimen core increases towards the circumference and regions close to mold boundary have the highest air void content (Figure 7.2).

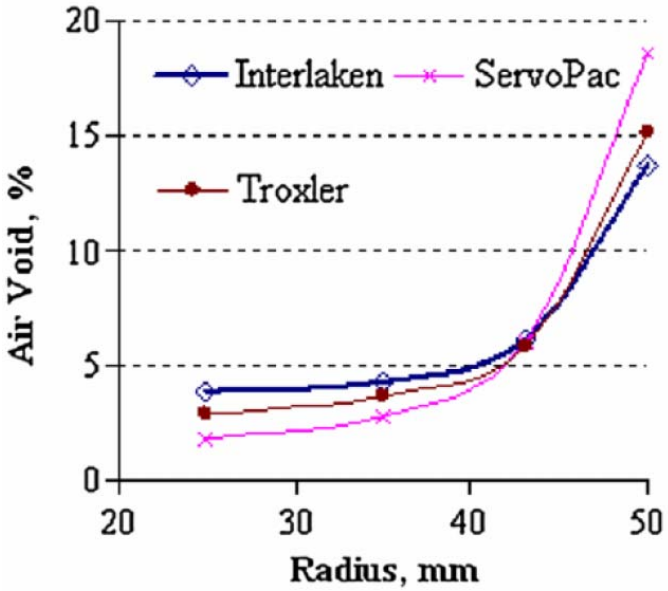

Figure 7.2 Lateral Voids distribution in Gyratory Specimens (Thyagarajan, 2010)

Besides the air voids distribution pattern in asphalt mixture, the inhomogeneous degree of air voids distribution had also been studied. Dubois studied the internal structure of gyratory and roller compacted specimens by means of gamma-ray measurements and used Standard deviation to evaluate the influence of both specimen dimensions and the coring direction on compaction homogeneity. Thyagarajana *et al.* (2010) investigated both vertical and lateral air voids distribution in asphalt specimen by analyzing successive X-ray images. He developed vertical heterogeneity index and lateral heterogeneity index to describe the level of heterogeneity of the air void distribution within the specimen in the vertical and lateral directions, and evaluate the effect of

compaction factor on heterogeneity of asphalt mixture, like compaction method, specimen preparation and height.

7.3 Air Voids Distribution Analysis by using DEM

Discrete Element Method (DEM) is a discontinuum analysis approach which can simulate the deformation process of joint systems or discrete particles assembly under quasi-static and dynamic conditions and gain further insight into the interaction among discrete particles. Hot mix asphalt mixture compaction actually is aggregates packing process and the slippages occur between aggregates during compaction, which makes asphalt mixture compaction a potential research object of discrete element method. This paper attempts to use open source DEM code to simulate asphalt mixture compaction and virtual digital specimens can be obtained by output of the simulation data. Then, the air voids distribution can be investigated by processing the virtual digital specimen. With the help of DEM simulation, the effect of compaction factors (like compaction method, compaction boundary) on air voids distribution can be investigated.

7.3.1 Heterogeneity of Air Voids Distribution

As mentioned above, the asphalt mixture specimens with the same total volume of air voids may have distinct mechanical behavior due to heterogeneous air voids distribution. During asphalt mixture compaction DEM simulation, the virtual digital compaction specimens can be obtained by outputting geometric data of aggregate particles at specific time steps. With appropriate post-processing of these digital specimens, the air voids distribution within the digital specimen can be investigated. In

order to study the air voids distribution in vertical and lateral direction, the virtual digital specimen will be divided into ten layers in vertical direction and six equal regions having the same cross-sectional area in lateral direction. The virtual cutting and coring pattern of digital specimen are shown in Figure 7.3 and the post-processed digital specimens are shown in Figure 7.4.

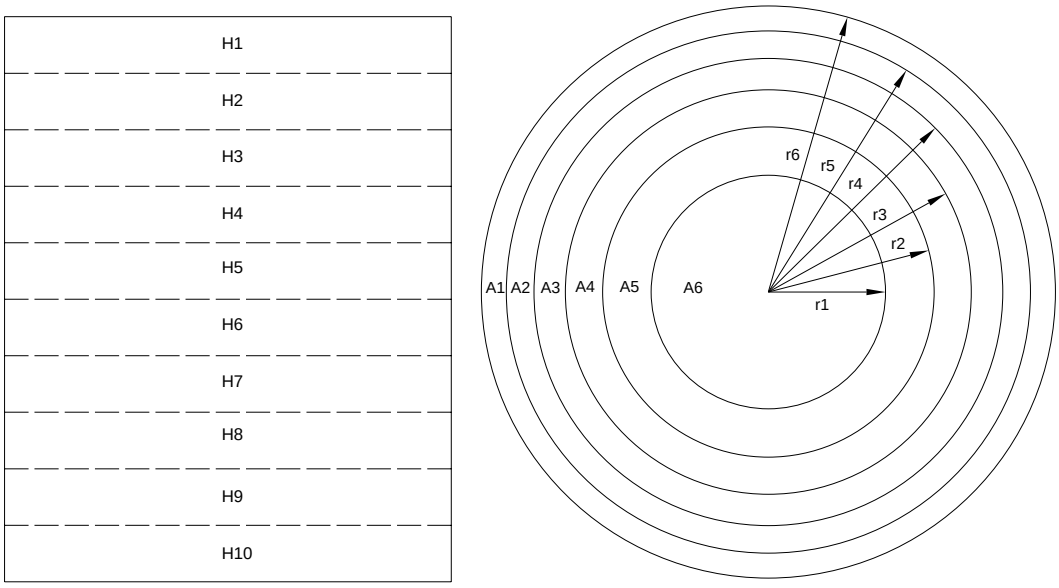

Figure 7.3 Virtual cutting and coring pattern of digital specimen

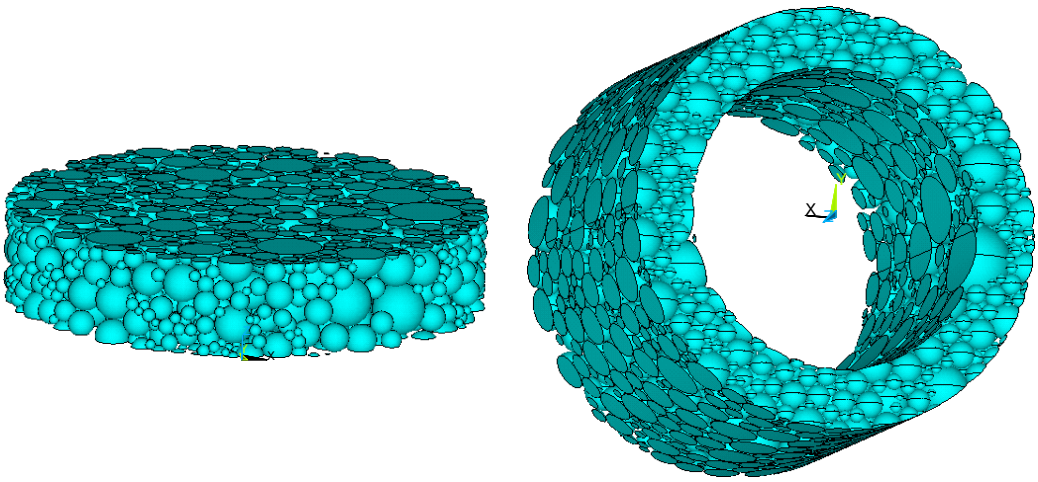

Figure 7.4 Post-processing of DEM digital specimen

Figure 7.5 presents the DEM prediction results of vertical air voids distribution within gyratory compacted specimen. From the figure, it can be seen that the air voids decrease as the number of gyrations increase and a “bathtub” vertical air voids distribution can be found, which is consistent with other researchers’ X-ray test results as shown in figure 7.1 (Masad, 1999; Tashman, 2002). Figure 7.6 shows the DEM prediction results of lateral air voids distribution within gyratory compacted specimen. In Figure 7.6, obvious non-uniform lateral air voids distribution can be found and the air voids decrease from outer region to inner region. The air voids in region close to mold boundary are much higher than that of other regions. The lateral air voids distribution also has the same variation trend as Thyagarajana’s test results as shown in figure 7.2 (Thyagarajana, 2010).

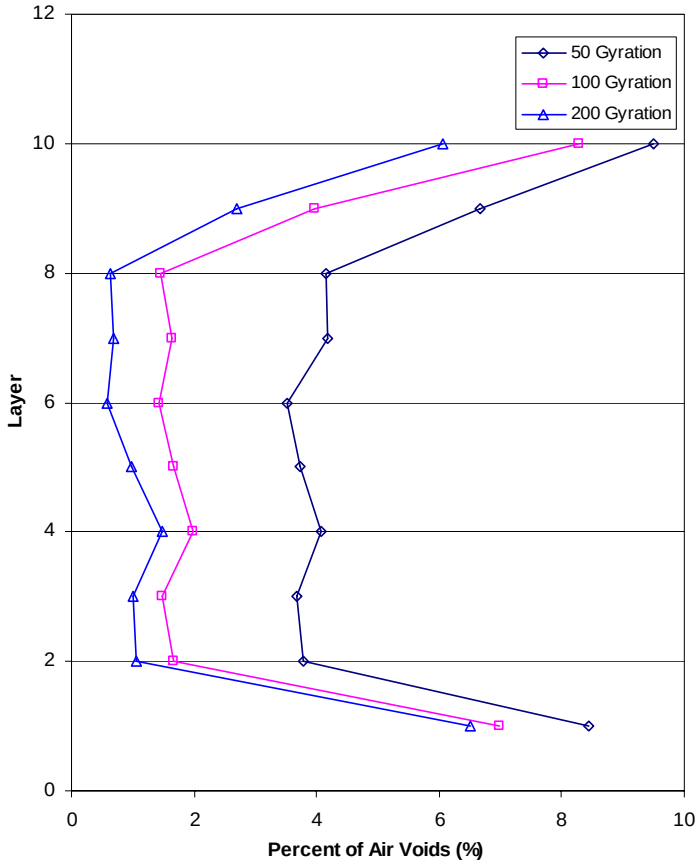

Figure 7.5 Air voids distribution in vertical direction

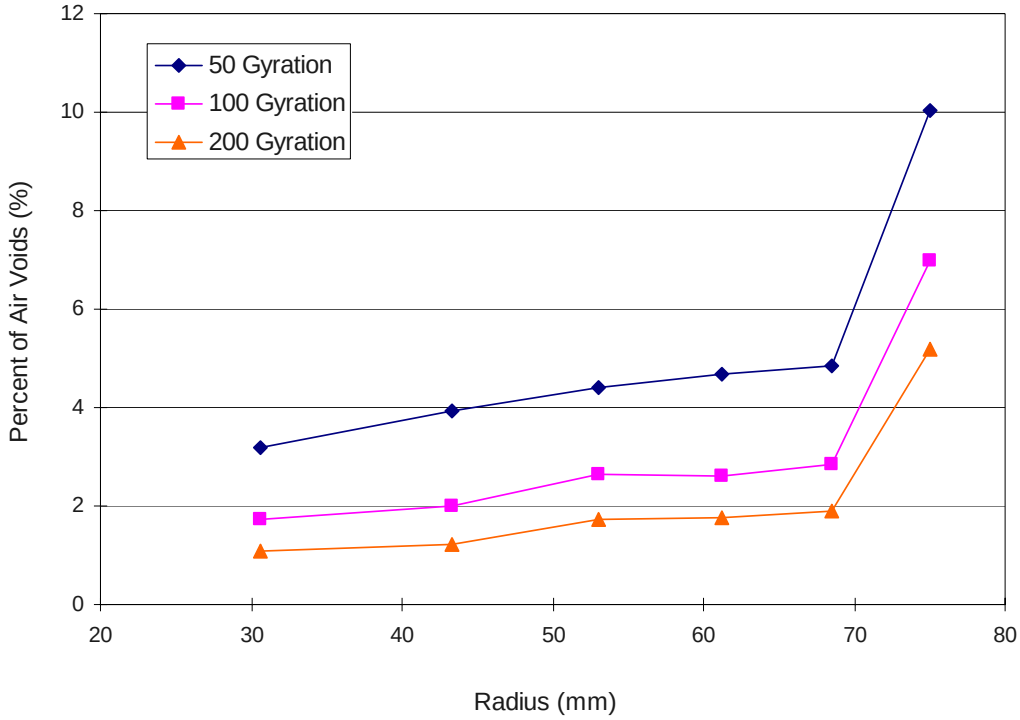

Figure 7.6 Air voids distribution in Lateral direction

Air void distribution is related with several factors such as compaction effort, method of compaction, aggregate gradation etc (Masad *et al.* 2002; Tashman *et al.* 2002). In order to quantitatively evaluate the effect of compaction methods, specimen height and specimen preparation on air void distribution, Thyagarajana *et al.* (2010) developed an index called heterogeneity index to describe the level of heterogeneity of the air void distribution within the specimen in the vertical and lateral directions. For better understanding the effect of compaction factors, all the test specimens in his research have the air voids around 7% and the heterogeneity index was defined as follow:

$$HI = \frac{1}{M}\sum_{i=1}^{M} abs\left(\frac{V_i - V_{Avg}}{V_{Avg}}\right) \tag{7.1}$$

Where M is the total number of vertical layers or lateral regions; V_i is the air void content in the ith layer or region and V_{Avg} is the overall average air void content of the specimen.

With the help of DEM simulation, the effect of these factors can be easily investigated by analyzing the virtual digital specimens at different compaction conditions. In this study, the effect of compaction method, aggregate gradation, specimen height, mold size and shape on air voids distribution were studied. The detailed DEM simulation plan is listed in Table 7.1 and three DEM digital specimens were generated for each compaction condition. From above DEM simulation results, it can be seen that the virtual digital specimen with any specific air voids can be obtained by taking the output of the simulation data at specific time steps. In this study, the heterogeneity index developed by Thyagarajana was used to study the effect of compaction factors and all virtual digital specimens have air voids around 5%.

Table 7.1 DEM simulation plan for air voids distribution analysis

Specimen number	Compaction method	Aggregate gradation	Height (mm)	Mold size (mm)	Mold shape
1-1,2,3	SGC	CA=0.7	160	150	cylinder
2-1,2,3	SGC	CA=0.7	140	150	cylinder
3-1,2,3	SGC	CA=0.7	120	150	cylinder
4-1,2,3	SGC	CA=0.7	100	150	cylinder
5-1,2,3	SGC	CA=0.7	120	175	cylinder
6-1,2,3	SGC	CA=0.7	120	125	cylinder
7-1,2,3	SGC	CA=0.7	120	100	cylinder
8-1,2,3	SGC	CA=0.1	120	150	cylinder
9-1,2,3	SGC	CA=0.3	120	125	cylinder
10-1,2,3	SGC	CA=1.0	120	100	Cylinder
11-1,2,3	Vibration	CA=0.7	120	150	cylinder
12-1,2,3	Vibration	CA=0.7	120	150	rectangular

- Specimen height (#1, 2, 3, 4; gyratory compaction)
- Aggregate gradation(#3, 8, 9, 10; gyratory compaction)

- Mold size (#3, 5, 6, 7; gyratory compaction)
- Mode shape (#11, 12; vibration compactor)
- Compaction method (#3, 11.)

7.3.2 Effect of Aggregate Gradation

Many researchers have proposed various ways to improve the performance of asphalt mixture through optimizing aggregate gradation and structure (Roque et al, 1997; Brigisson et al, 2001; Kim *et al.*, 2006, 2009; Vavrik *et al.*, 2001, 2002). Among the many ways, the Bailey method has been getting more and more attention and been successfully used in the selection of proper aggregate gradation. The Bailey method is an aggregate grading valuation and design method which is based on plane circle mode and was originally developed by Robert Bailey from the Illinois Department of Transpiration in the early 1980s. The Bailey Method has been proved to be a practical approach to select and adjust aggregate gradation in hot-mix asphalt (HMA) design and has been successfully applied to coarse-graded, fine-graded, and SMA Mixture all over the world (Vavrik *et al.*, 2001, 2002; Peng *et al.*, 2005; Khalid, 2006).

In the Bailey method, aggregates are divided into three portions (Coarse Aggregate, Coarse Portion of Fine Aggregate, and Fine Portion of Fine Aggregate) by a primary control sieve and a secondary control sieve. With the proportion relation between the divisions, three ratios are defined: Coarse Aggregate Ratio (CA Ratio), Fine Aggregate Coarse Ratio (FA_c Ratio), and Fine Aggregate Fine Ratio (FA_f Ratio). The CA ratio is the ratio of the fine part (interceptors) to the coarse part (pluggers) of the overall coarse aggregates and has significant effect on asphalt mixture volumetric properties and compactability. Vavrik (2002) pointed out that an increase in the CA Ratio will cause a

corresponding increase in the air voids and the segregation potential increases with the decrease of CA ratio.

In this study, CA ratio was used to select the coarse aggregate and then the relationship between aggregate gradation and heterogeneity of the air voids can be established through CA ratio and heterogeneity index. Four mixtures with different CA ratios (0.1, 0.4, 0.7, and 1.0) were simulated and the gradations are presented in Figure 7.7.

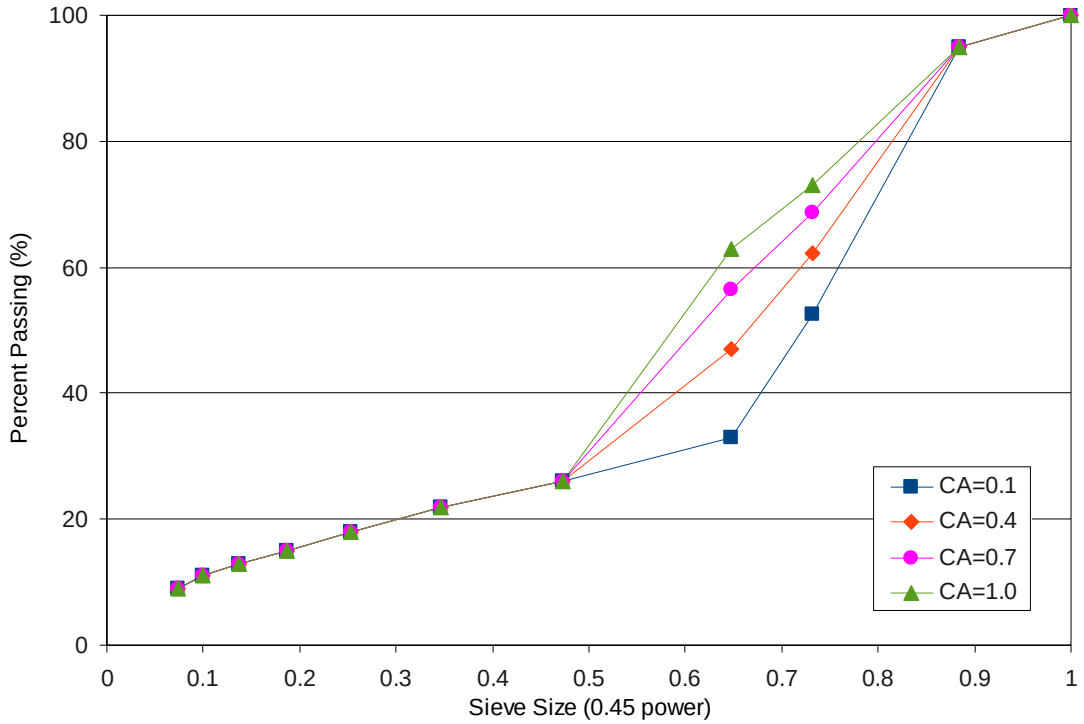

Figure 7.7 Aggregate gradation (maximum size 25 mm)

Figure 7.8 and 7.9 are the scatter plots of the vertical and lateral heterogeneity index with different CA ratios and Table 7.2 is the correlation analysis results of CA ratios. From the analysis results, it can be seen that CA ratio has strong and negative correlations with vertical heterogeneity index, which means CA ratio has considerable influence on vertical air voids distribution and the high CA ratio gradation has more uniform air voids

distribution. However, the CA ratio appears to have little effect on lateral air voids distribution.

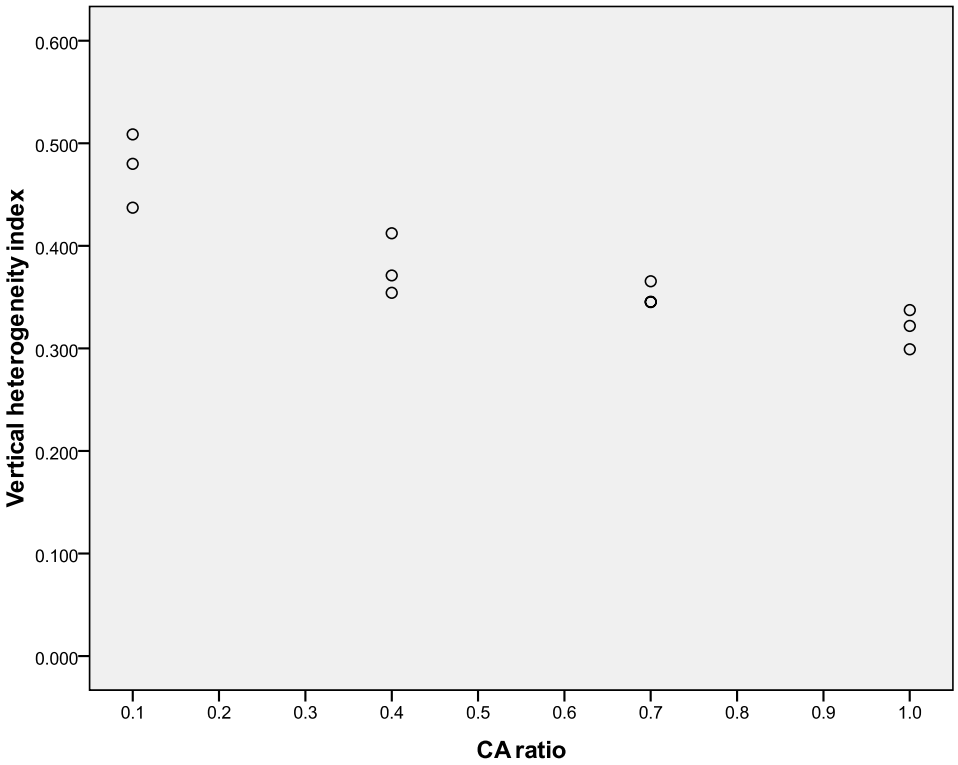

Figure 7.8 Effect of CA ratios on vertical heterogeneity index

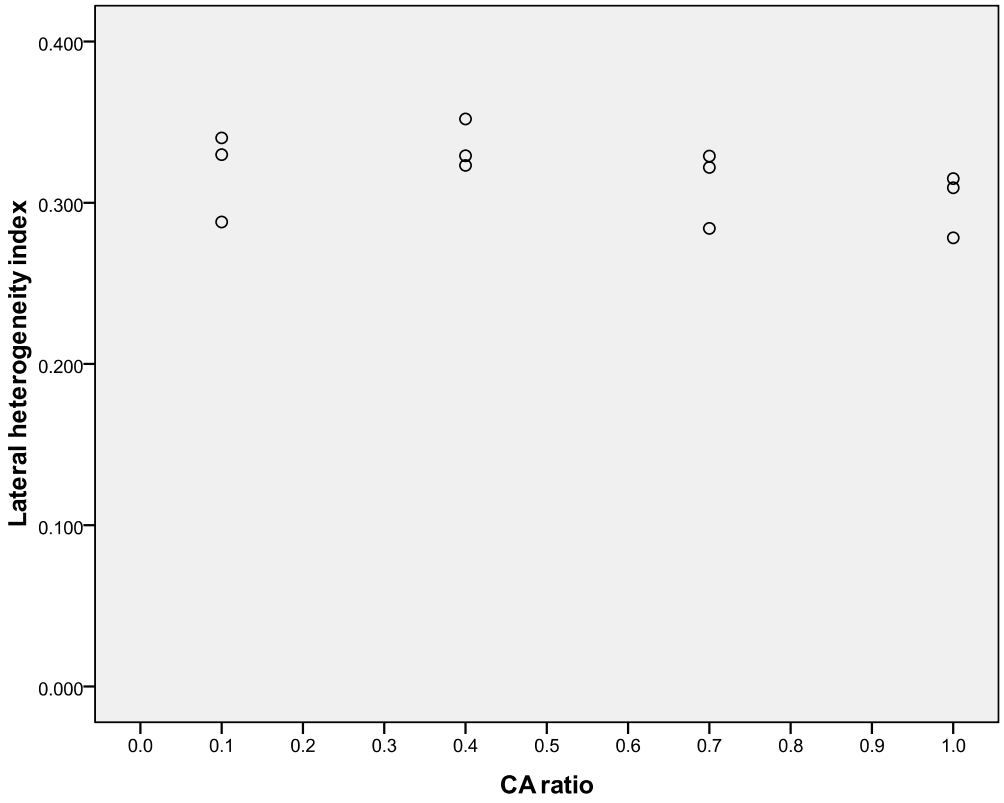

Figure 7.9 Effect of CA ratios on lateral heterogeneity index

Table 7.2 Correlation analysis of CA ratio

Correlations

		CA ratio	Vertical heterogeneity index	Lateral heterogeneity index
CA ratio	Pearson Correlation	1	-.894**	-.402
	Sig. (2-tailed)		.000	.196
	Sum of Squares and Cross-products	1.350	-.223	-.035
	Covariance	.123	-.020	-.003
	N	12	12	12

**. Correlation is significant at the 0.01 level (2-tailed).

7.3.3 Effect of Specimen Height

The geometry of the specimen also affects the air void distribution in HMA specimens (Thyagarajana, 2010). The vertical and lateral heterogeneity index of digital specimens with different heights is presented in Figure 7.10 and 7.11. The Correlation analysis results are shown in Table 7.3. From correlation analysis results, a strong and positive correlation was found between vertical heterogeneity index and specimen height. From Figure 7.10, it is pretty clear that the vertical heterogeneity index increases with the increase of specimen height, which is similar as Thyagarajana's research results. In Figure 7.11, it seems that the lateral heterogeneity index decreases slightly with the specimen height. However the correlation analysis results shows there is no statistically significant correlation between lateral heterogeneity index and specimen height. The effect of specimen height on lateral air voids distribution in this study is not so significant, consistent with Thyagarajana's results.

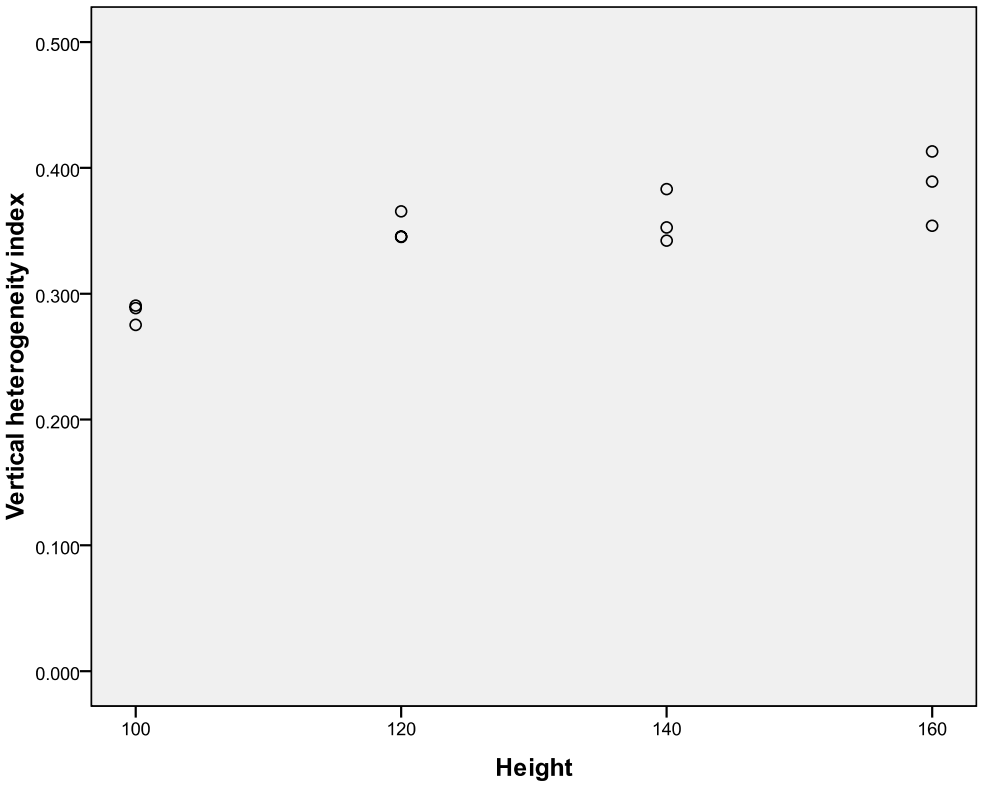

Figure 7.10 Effect of specimen height on vertical heterogeneity index

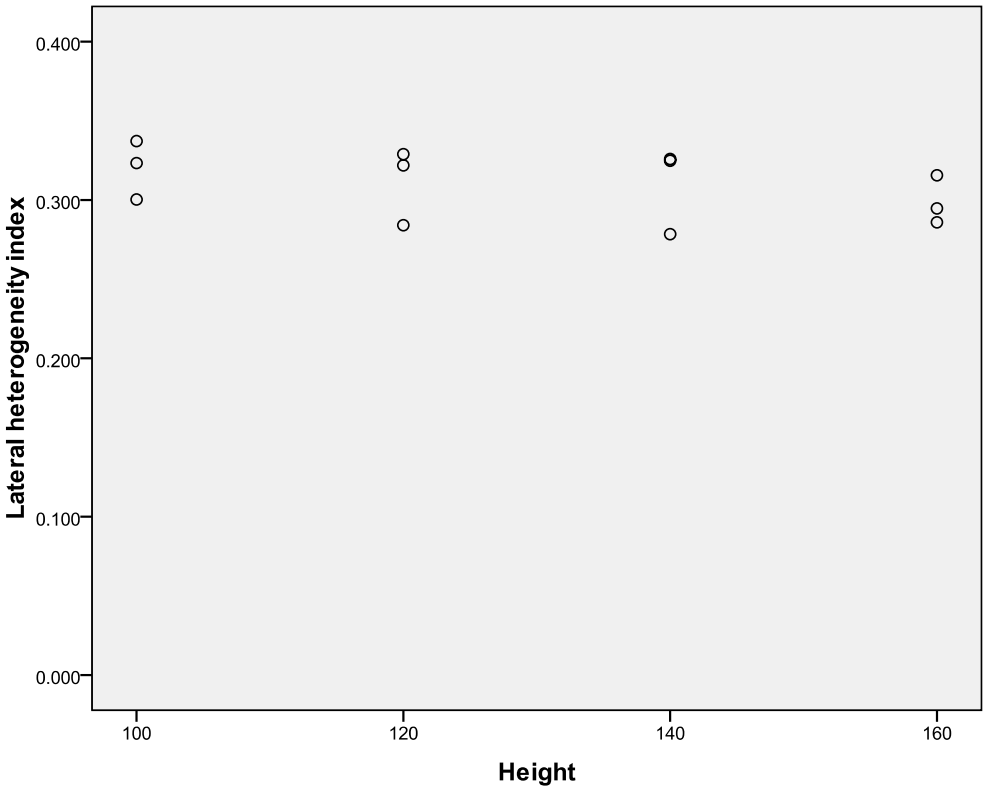

Figure 7.11 Effect of specimen height on lateral heterogeneity index

Table 7.3 Correlation analysis of specimen height

Correlations

		Height	Vertical heterogeneity index	Lateral heterogeneity index
Height	Pearson Correlation	1	.855**	-.384
	Sig. (2-tailed)		.000	.218
	Sum of Squares and Cross-products	6000.000	9.274	-1.996
	Covariance	545.455	.843	-.181
	N	12	12	12

**. Correlation is significant at the 0.01 level (2-tailed).

7.3.4 Effect of Mold Size

Due to the limitation of compaction device, most of previous research focused on the effect of compaction parameters related with compaction machine and seldom studied the effect of compaction mold. However, from above internal air voids distribution analysis, it can be seen that air voids could be affected by mold boundaries. In order to study the edge effect on air voids distribution, compaction molds with four different diameters were simulated. Figure 7.12 and 7.13 show the post-processing results of virtual digital specimen compacted within different size molds (Diameter=100, 125, 150, 175 mm) and Table 7.4 presents the correlation analysis results of mold size. Figure 7.12 and 7.13 clearly shows edge effect on air voids distribution. It can be seen that both vertical and lateral heterogeneity index decrease with the mold size and the edge effect is significant on lateral air voids distribution, which means the big mold size can make more uniform air voids distribution asphalt specimen in both vertical and lateral direction. The

correlation analysis results also show strong correlation between mold diameter and both vertical and lateral air voids distribution.

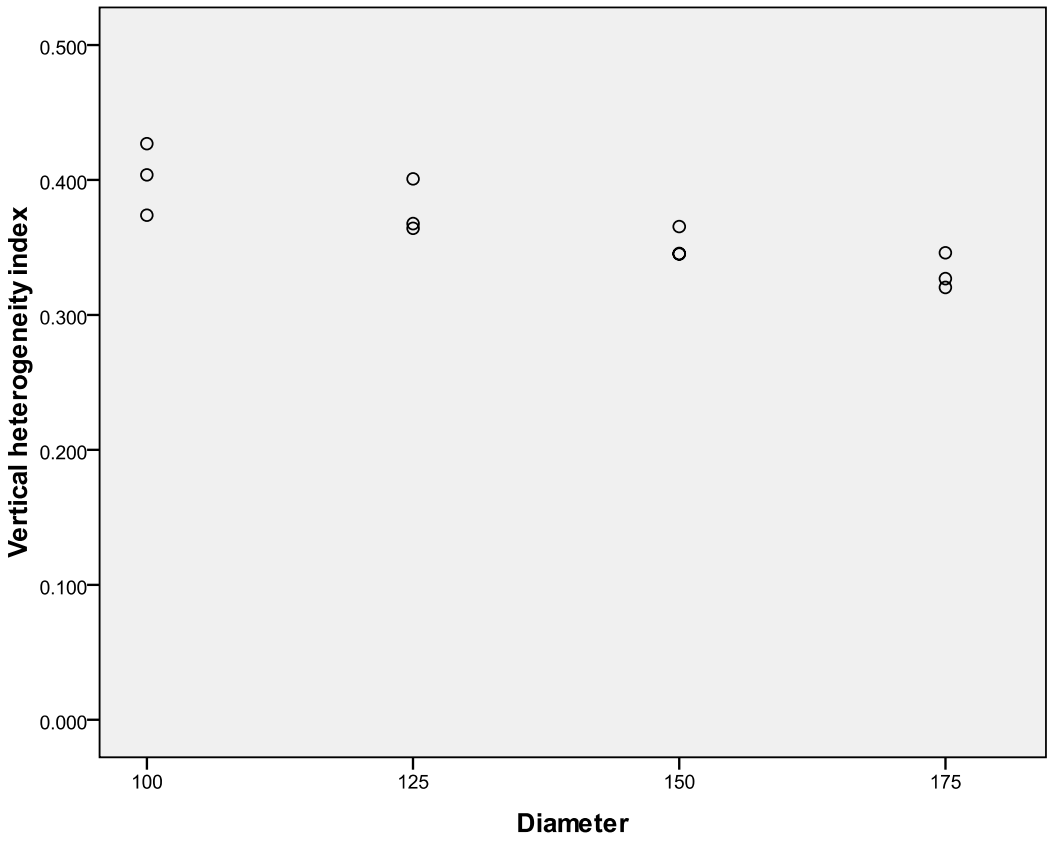

Figure 7.12 Effect of mold size on vertical heterogeneity index

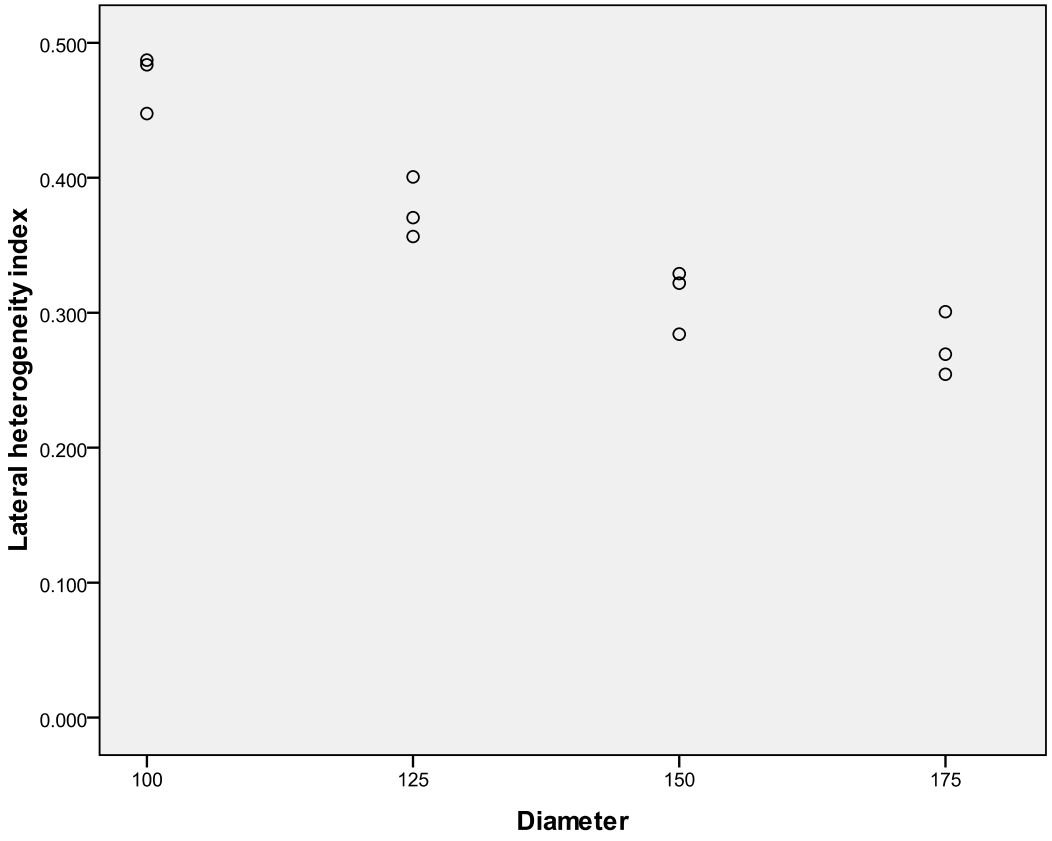

Figure 7.13 Effect of mold size on lateral heterogeneity index

Table 7.4 Correlation analysis of mold size

Correlations

		Diameter	Vertical heterogeneity index	Lateral heterogeneity index
Diameter	Pearson Correlation	1	-.863**	-.950**
	Sig. (2-tailed)		.000	.000
	Sum of Squares and Cross-products	9375.000	-8.879	-24.681
	Covariance	852.273	-.807	-2.244
	N	12	12	12

**. Correlation is significant at the 0.01 level (2-tailed).

7.3.5 Effect of Mold Shape

From above DEM simulation results, it can be seen that compaction mold size has a significant effect on air voids distribution. The mold shape also has edge effect on asphalt mixture compaction and air voids distribution. Vibration compaction is one common asphalt mixture compaction method for making both cylinder asphalt specimen and rectangular specimen. In this study, the vibration compactions with two different mold shapes were simulated using DEM code. The tetragonal compaction mold and cylinder compaction mold have equal cross-sectional area in vibration compaction DEM simulation. In DEM simulation, only flat surface walls are available and curved surface walls should be made by combining several flat surface walls. In this study, the tetragonal and cylindrical containers were formed by combining 4 and 32 plates respectively. Figure 7.14 and 7.15 are the scatter plots of the vertical and lateral heterogeneity index with different mold shape and Table 7.5 presents the correlation analysis results. From Figure 7.14 and 7.15, it can be seen that the vertical heterogeneity index of digital specimen compacted in tetragonal mold is higher that in cylinder mold, but the effect is not very significant. However, the lateral heterogeneity index of digital specimen compacted in tetragonal mold is much higher than that in cylinder compaction mold. The correlation analysis results show that the lateral heterogeneity index is strongly correlated with mold shape and the correlation between vertical index and mold shape didn’t satisfy the level of significance equal to 0.01. The uneven lateral air voids distribution within specimen compacted in tetragonal mold may be due to the existence of tetragonal corners which limit the movement of aggregates in lateral direction during compaction process. Under the influence of the corner, it is hard to achieve the required density in this area.

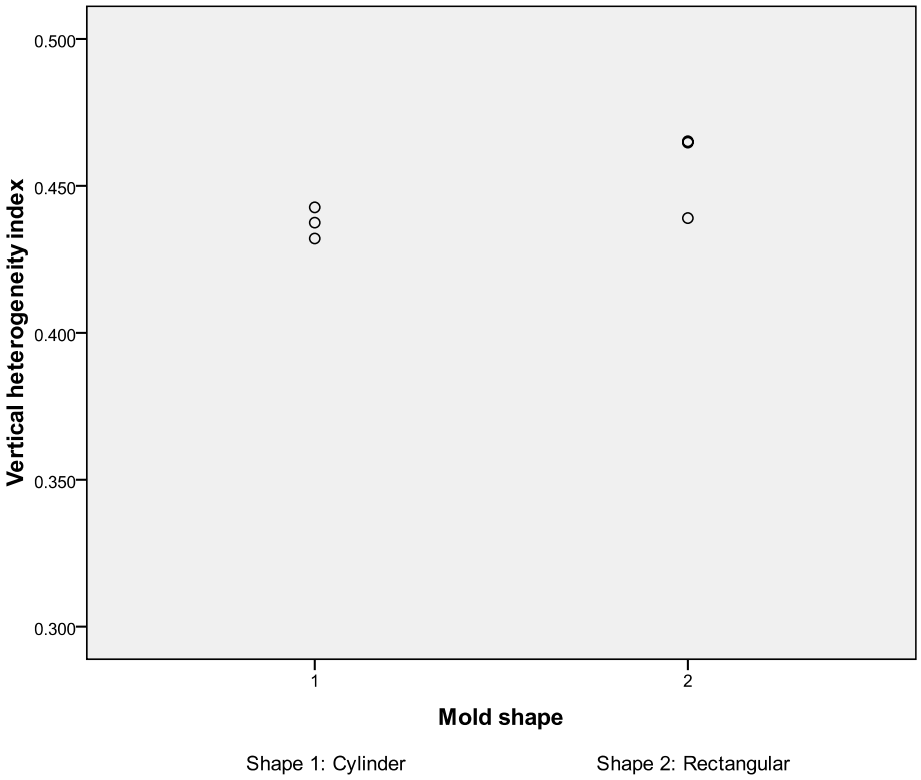

Figure 7.14 Effect of mold shape on vertical heterogeneity index

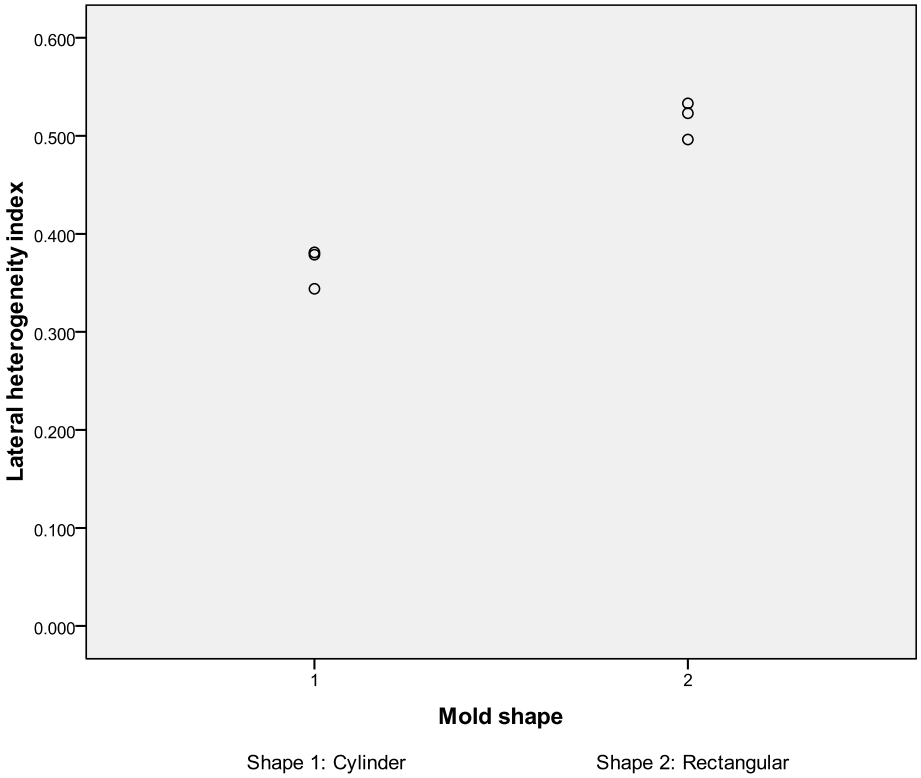

Figure 7.15 Effect of mold shape on lateral heterogeneity index

Table 7.5 Correlation analysis of mold shape

Correlations

		Mold shape	Vertical heterogeneity index	Lateral heterogeneity index
Mold shape	Pearson Correlation	1	.717	.977**
	Sig. (2-tailed)		.108	.001
	Sum of Squares and Cross-products	1.500	.028	.224
	Covariance	.300	.006	.045
	N	6	6	6

**. Correlation is significant at the 0.01 level (2-tailed).

7.3.6 Effect of Compaction Method

Gyratory compaction and vibration compaction are two commonly used compaction methods to make asphalt mixture specimens. Figure 7.16 and 7.17 shows the vertical and lateral heterogeneity index of cylindrical specimens compacted by gyratory and vibration compactor. Table 7.6 presents the correlation analysis results of compaction method. Form the figures, it can be observed that the gyratory compacted specimens have smaller vertical and lateral heterogeneity index than the vibration compacted specimen. The correlation analysis results also show that the correlation between compaction method and both vertical and lateral heterogeneity index are significant at the level of 0.01 and 0.05 respectively. The analysis results indicate that the gyratory compacted specimen has more homogenous air voids distribution than vibration compaction specimen in both vertical and lateral direction. Compared with vibration compaction, the aggregates have more movement in horizontal direction with the impact of gyration. The ability for

aggregates movement in more directions is helpful to the slippage and filling of aggregates and thus can result in better mixture compaction.

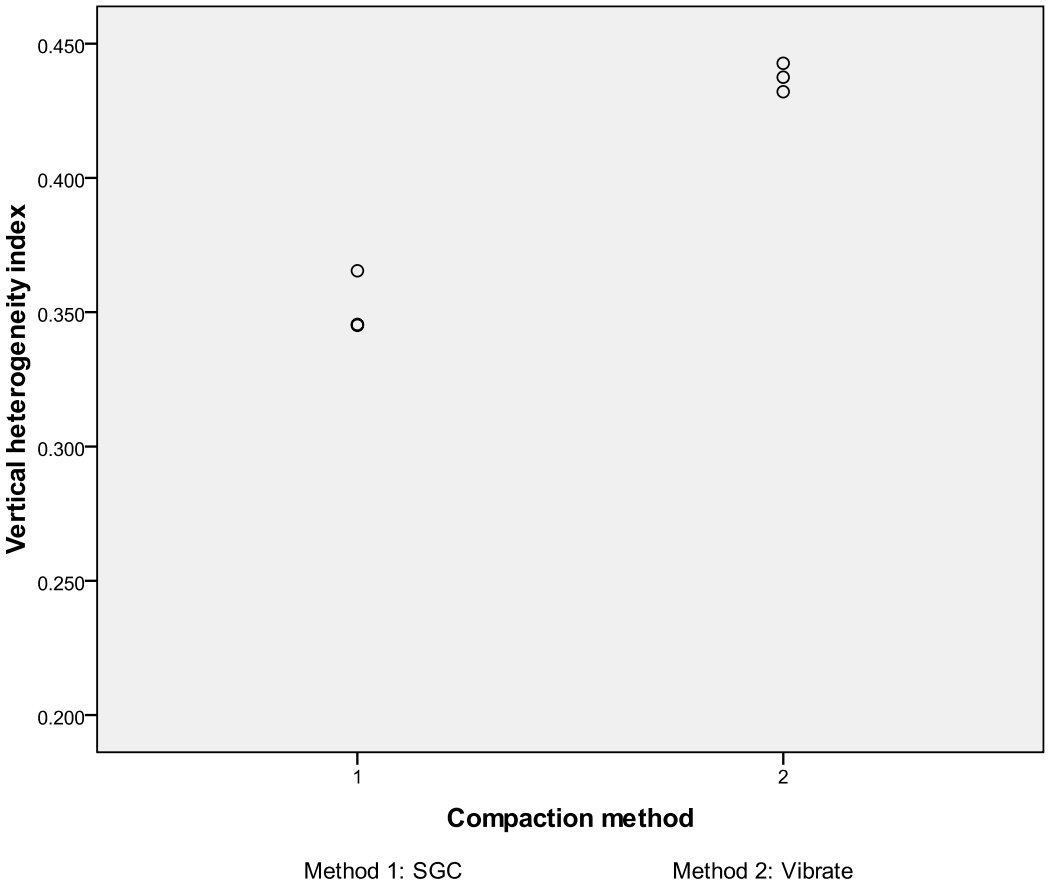

Figure 7.16 Effect of compaction method vertical heterogeneity index

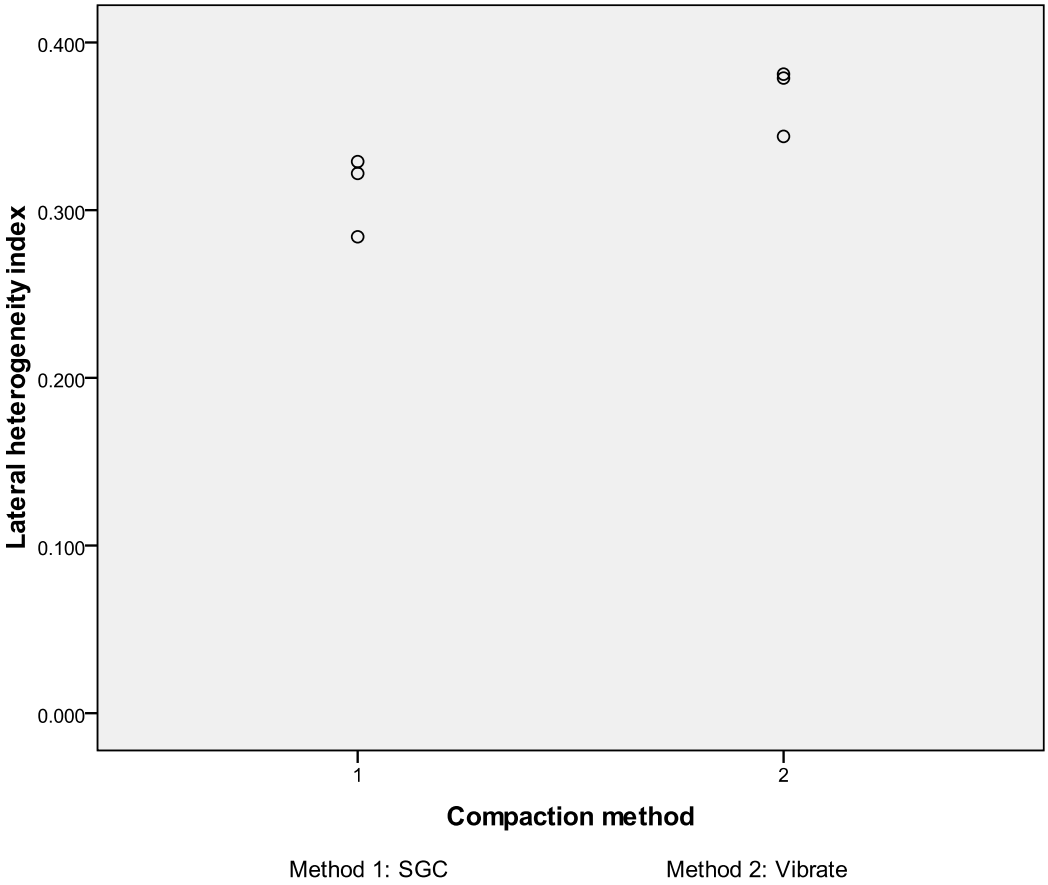

Figure 7.17 Effect of compaction method lateral heterogeneity index

Table 7.6 Correlation analysis of compaction method

Correlations

		Compaction method	Vertical heterogeneity index	Lateral heterogeneity index
Compaction method	Pearson Correlation	1	.985**	.837*
	Sig. (2-tailed)		.000	.038
	Sum of Squares and Cross-products	1.500	.128	.084
	Covariance	.300	.026	.017
	N	6	6	6

**. Correlation is significant at the 0.01 level (2-tailed).

*. Correlation is significant at the 0.05 level (2-tailed).

CHAPTER 8 SUMMARY, CONCLUSIONS AND RECOMMENDATIONS

8.1 Summary

The primary objective of this study was to simulate asphalt compaction process by using discrete element method and investigate the heterogeneous air voids distribution with the help of DEM simulation. By completing this study, an open source DEM code, YADE, was modified and implemented with the C++ programming language for the DEM simulation of asphalt mixture compaction.

A viscoelastic contact model was developed in DEM code and verified through comparing with well established analytical solutions. The input parameters of the new developed contact model were obtained through nonlinear regression analysis of dynamic modulus test results. Two commonly used compaction methods (Superpave gyratory compaction and asphalt vibratory compaction) and one self developed APA linear kneading compaction were simulated using DEM code YADE and the DEM compaction model were verified through the comparison between the DEM predicted results and the laboratory measured test data. The air voids distribution within asphalt specimen was analyzed by post processing virtual DEM compaction digital specimen and the level of heterogeneity of the air void distribution within the specimen in the vertical and lateral directions was studied. The DEM simulation results have a good agreement with laboratory test results, which demonstrates that DEM can be used to simulate asphalt

mixture compaction under different loading conditions and is a potentially helpful tool for asphalt mixture compaction analysis.

8.2 Conclusions

Conclusions obtained from this study are presented in four parts: (1) DEM simulation of Superpave gyratory compaction; (2) DEM simulation of asphalt vibratory compaction; (3) DEM simulation of APA linear kneading compaction; and (4) DEM analysis of air voids distribution.

8.2.1 DEM Simulation of Superpave Gyratory Compaction

A 3D DEM simulation has been carried out to study compaction process of Superpave gyration compactor. A sensitivity analysis and comparisons of DEM simulations to laboratory experiments and published results indicated highly agreeable results or trends. Based on the DEM simulation results, the following conclusions can be found. Although some findings in this DEM simulation are well known, they have also been reflected through DEM simulation:

- With inherent advantages in granular materials analysis, the discrete element method can be used to examine the effect of aggregate gradation, shape, the properties of asphalt mixture and the parameter of compaction machine. The simulation results in this paper were in a good agreement with the experimental data and previous research results, which demonstrates that the DEM simulation could be a potentially helpful tool for asphalt mix design by reducing the number of physical compaction in the laboratory.

- Based on the study of minimum particle size, the finer the size of aggregate used in the DEM simulation, the better the simulation results. The errors were significantly reduced by considering more fine aggregates. Compared with minimum particle size 1.36 mm, a good DEM simulation result also can be obtained by simulating aggregates bigger than 2.36 mm for the mixture used in this study, which greatly reduces the computational complexity in DEM simulation.
- Aggregate gradation is an important factor in asphalt mixture compaction. DEM simulation in this paper successfully predicted compaction curves of two asphalt mixture (Superpave and SMA) with reasonable accuracies.
- The aggregate shape plays an important role in asphalt mixture compaction. DEM simulation results show that the air voids increase significantly with the aspect ratio of elongation, which agrees with common knowledge.
- Gyration angle can significantly affect asphalt mixture compaction. The packing density increased with the gyration angle and asphalt mixture became more difficult for compaction when the gyration angle was set too low.
- The Burger's model parameters can reflect the effect of temperature on mixture compaction. In the DEM simulation, asphalt mixture would be compacted faster at higher temperature than at lower temperature, which agrees with common knowledge.
- The motion trace indicates that aggregates compacted without gyration have less movement in horizontal directions, which is unfavorable for slippage and filling of aggregates and thus leads to hard mixture compaction.

8.2.2 DEM Simulation of Asphalt Vibratory Compaction

In this section, the asphalt vibratory compaction was simulated using DEM code and the asphalt mixture vibratory compaction tests at different conditions were also conducted in the lab. The air voids compaction process was studied and the effect of vibration force and vibration speed on asphalt mixture compaction was investigated. Based on the DEM simulation results, the following conclusions can be found or confirmed:

- Both DEM simulation and laboratory test results exhibit the same development trend in air voids compaction process and the compaction gaining become slower with the time increase. DEM simulation results are smaller than that of laboratory test results, which is probably due to the less interlock effect between particles in DEM simulation.
- For the vibration compaction at different vibration force, both DEM simulation and laboratory test results have the same trend, the air voids decrease with the increase of vibration force, which demonstrate that DEM can be used to study asphalt mixture compaction under different compaction effort.
- The DEM simulation results show that vibration speed can significantly influence the compaction results and low vibration speed is harder to compact asphalt mixture to desired density with limited time.

8.2.3 DEM Simulation of APA Linear Kneading Compaction

In this section, the open source code, YADE, was applied to study asphalt mixture compaction by using modified APA linear kneading compactor. The effect of compaction pressure, wheel speed and boundary condition on asphalt mixture compaction was

studied and the predicted air voids obtained from DEM simulation were compared to the laboratory measured test results. Based on the DEM simulation results, the following conclusions can be found or confirmed:

- DEM simulation results and laboratory test results have the same development trend in air voids compaction process and the DEM predicted value is also close to the laboratory test results.
- By adjusting APA wheel load, the compaction pressure between steel plates and mixture can be studied. The air voids of DEM simulation decrease quicker than that of lab test in beginning stage and slower later. This difference may be because of different interlock effect of aggregates in lab test and DEM simulation.
- The kneading frequency has certain influence on asphalt mixture compaction and high kneading speed results in better asphalt mixture compaction due to the kneading effect.
- Both DEM simulation and test results show that compaction boundary condition can greatly affect asphalt mixture compaction results. The DEM results show that DEM simulation can be used to predict mixture compaction under different boundary conditions, which means DEM has potential to investigate mixture compaction under field boundary conditions with enough processing power of computer.

8.2.4 DEM Analysis of Air Voids Distribution

In this section, the air voids distribution within an asphalt specimen was analyzed by post processing virtual DEM compaction digital specimen and the level of heterogeneity

of the air void distribution within the specimen in the vertical and lateral directions was studied. Based on the DEM simulation results, the following conclusions can be drawn:

- From the DEM digital specimen post-processing results, it can be seen that a "bathtub" vertical air voids distribution can be found in gyratory compacted specimens and the air voids in the region close to the mold boundary are much higher than that of other regions due to the edge effect.
- CA ratio has considerable influence on vertical air voids distribution and the gradation with high CA ratio has more uniform air voids distribution, and the effect of CA ratio on lateral air voids distribution is not statistically significant.
- According to the DEM post-processing and correlation analysis results, the asphalt mixture height has significantly effect on the vertical air void distribution. The high asphalt specimen resulted in more uneven air voids distribution in the vertical direction and more even air voids distribution in the lateral direction.
- From the DEM simulation results, it can be seen that both the vertical and lateral heterogeneity index decrease with the mold size and the edge effect is pretty significant on lateral air voids distribution.
- The mold shape also has an edge effect on asphalt mixture compaction and air voids distribution. The asphalt mixture compacted in cylinder mold has more even air voids distribution in lateral direction than that in tetragonal mold.
- The compaction methods have obvious effect on air voids distribution in both vertical and lateral distribution. The gyratory compacted specimen has more homogenous air voids distribution than vibration compaction specimen.

8.3 Recommendation

This study focuses on the application of discrete element method on asphalt mixture compaction and the air voids distribution within asphalt mixture compaction using open source DEM code. The laboratory compaction tests were conducted to verify the DEM simulation results. This study provides a new way to study asphalt mixture compaction through internal microscopic view and also gives a direction for future DEM research of asphalt mixture compaction. Some recommendations are provided here for further research work:

- Due to the limitation of computer processing capability, it is still difficult to simulate all the aggregate particles in asphalt mixture compaction (tens of millions of small particles have to be considered in asphalt mixture). In this study, after studying the effect of minimum simulated particle size on the compaction results, it found that the prediction errors were reduced by considering more fine aggregates in DEM simulation. Nowadays, the DEM analyses have been limited to about 10^5 particles. The minimum size of aggregates simulated in this study is 2.36 mm, which still has certain influence on the prediction results of air voids during DEM simulation. Although Cundall (2001) has suggested that 10^{11} particles could be available within 20 years, currently, the most direct and apparent solution is the use of parallel processing, which will allow analyses of 10^6 or even 10^9 particles, depending on 2D or 3D.
- As seen from the previous chapters, spherical particles were used in most of the DEM simulations in this study, which makes the contact condition simple and

greatly eases the calculation difficulty. However, aggregate shape is an important factor in asphalt mixture design and has a significant influence during compaction process of asphalt mixture. The X-ray computed tomography technology is non-destructive digital image analysis techniques and has been used by researchers to characterize the geometrical property of aggregates (Masad, 2002). Clump technique is a common method to model irregular shaped particles in DEM simulation. With the combination of X-ray computed tomography technology and Clump technique, the shape of aggregates can be better simulated and DEM simulation of asphalt mixture compaction could come closer to describing the reality of asphalt mixture compaction. However, the use of clump technique will further increase the number of particles in DEM simulation, since one aggregate may consist of several spherical particles.

REFERENCES

Abbas, A. (2004) “Simulation of the micromechanical behavior of asphalt mixture using the discrete element method”, PhD Dissertation of Washington State University

Abbas, A. *et al.* (2007) “Micromechanical modeling of the viscoelastic behavior of asphalt mixture using the discrete-element method”, International Journal of Geomechanics, v7, n2, 131-139

Abe,S., Place, D. Mora, p. (2004) “A parallel implementation of the lattice solid model for the simulation of rock mechanics and earthquake dynamics”, Pure Appl Geophys, Vol. 161, pp. 2265–2277.

Hand, A.J. *et al.* (2001) “Gradation Effects on Hot-Mix Asphalt Performance”, Transportation Research Record: Journal of the Transportation Research Board, Volume 1767, pp.152-157

Adhikari, S. and You, Z., “3D discrete element models of the hollow cylindrical asphalt concrete specimens subject to the internal pressure”, International Journal of Pavement Engineering, Volume 11, Issue 5 October 2010 , pp. 429 – 439

Aparicio, N. D. and Cocks, A.C.F. (1995) On the representation of random packings of spheres for sintering simulations, Acta Metallurgica et Materialia, Volume 43, Issue 10, Pages 3873-3884

Belheine, N. *et al.* (2009) “Numerical Simulation of Drained Triaxial Test Using 3D Discrete Element Modeling”, Computers and Geotechnics, Volume 36, Issues 1-2, pp. 320-331

Bennert, T. *et al.* (2001) “Evaluation of a Rutting/Fatigue Cracking Device”, Final report, NJDOT Research Project Manager

Bhandaria, A. and Han, J. (2010) “Investigation of geotextile–soil interaction under a cyclic vertical load using the discrete element method”, Geotextiles and Geomembranes, Volume 28, Issue 1, Pages 33-43

Birgisson, B.; and Ruth, B.E. (2001) “Development of tentative guidelines for the selection of aggregate gradations for hot-mix asphalt”, ASTM STP 1412, ASTM, West Conshohocken, Pa., PP. 110–127

Brian D. Aho, William R. Vavrik, Samuel H. Carpenter. (2001) “Effect of Flat and Elongated Coarse Aggregate on Field Compaction of Hot-Mix Asphalt”, Journal of the Transportation Research Board, Volume 1761, Pages 26-31

Brown, E.R. (1990) “Density of Asphalt Concrete-How Much is Needed?”, Paper presented at 69th Annual Meeting of the Transportation Research Board, Washington, DC.

Butcher M. (1998) “Determining gyratory compaction characteristics using servopac gyratory compactor”, Transportation Research Board, No. 1630, pp. 89-97

Buttlar,W. G., and You, Z. (2001) “Discrete element modeling of asphalt concrete: A micro-fabric approach”, Journal of the Transportation Board, National Research Council, Washington, D.C., No. 1757, Geomaterials, pp. 111–118

Button and Little (1992), Evaluation of Laboratory Compaction Devices and Their Ability to Duplicate Field Compaction, Strategic Highway Research Program Report.

Camborde, F. *et al.* (2000) “Numerical study of rock and concrete behaviour by discrete element modelling, Computers and Geotechnics”, Volume 27, Issue 4, Pages 225-247

Chen, F. *et al.* (2007) “Prediction/Verification of Particle Motion in One Dimension with the Discrete-Element Method”, International Journal of Geomechanics, ASCE, Volume 7, Issue 5, 344-352

Chen, J. *et al.* (2005) “Influence of coarse aggregate shape on the strength of asphalt concrete mixture”, Journal of the eastern asia society for transportation studies, vol. 6, Pages 1062 - 1075

Collin, J.G., Kinney, T.C. and Fu, X. (1996) “Full scale highway load test of flexible pavement systems with geogrid reinforced base courses”, Geosynthetics International, Vol.3, No. 4, pp. 537-549

Collins, R. *et al.* (2003) “User’s guide of Asphalt Vibratory Compactor II”, Pavement Technology Inc. (PTI), pp. 6-7

Collop, A.C. *et al.* (2004) “Use of the Distinct Element Method to Model the Deformation Behavior of an Idealized Asphalt Mixture”, International Journal of Pavement Engineering, Vol. 5, Issue 1, pp. 1-7

Collop, A.C. *et al.* (2006) “Modelling dilation in an idealised asphalt mixture using discrete element modelling”, Granular Matter, Vol. 8, No. 3-4, pp. 175-184, 2006

Colorado Department of Transportation (CDOT), (2009) “Standard Method of Test for Linear Kneading Compaction of Bituminous Mixture”, Colorado Procedure–Laboratory 5116

Consuegra, A. (1989) “Comparative evaluation of laboratory compaction devices based on their ability to produce mixture with engineering properties similar to those produced in the field”, Transportation Research Record, n1228, p80-87

Cooley, L.A. and Kandhal, P.S. (1999) “Evaluation of Density Gradients in the APA Samples”, National Center for Asphalt Technology, Auburn University, Alabama

Cundall, P. A. (1971) “A computer model for simulating progressive large scale movements in blocky rock systems”, Symposium of the International Society for Rock Mechanics, France, II-8

Cundall, P. A. (2001). “A discontinuous future for numerical modeling in geomechanics?”, Proc. Inst. Civ. Engrs, Geotechnical Engineering 149, No. 1, pp. 41–47

Cundall, P.A., Strack O.D.L. (1979) “A discrete numerical model for granular assemblies”, Geotechnique, Vol. 29, No. 1, (1979), pp. 47-65

Dai, Q.and You, Z. (2007) “Prediction of Creep Stiffness of Asphalt Mixture with Micromechanical Finite-Element and Discrete-Element Models”, Journal of Engineering Mechanics, Vol. 133, No. 2

Fang, K.T. (1980) “The uniform design: application of number-theoretic methods in experimental design”, Acta Math. Appl. Sin. Vol. 3, Pages 363–372.

Fang, K.T. *et al.* (2000) “Uniform Design: Theory and Application”, Technometrics, Vol. 42, No. 3, pp. 237-248

Ferry, J. D. (1980) “Viscoelasticity properties of polymers”, 3rd Ed., Wiley, New York

Ford, M. C. (1988) “Pavement Densification Related to Asphalt Mix Characteristics”, Paper presented at the 1988 Annual Meeting of the Transportation Research Board, Washington, DC.

Giroud, J.P. and Han, J. (2004) “Design method for geogrid-reinforced unpaved roads–Part I: theoretical development”, ASCE Journal of Geotechnical and Geoenvironmental Engineering, Vol. 130, No. 8, pp. 776-786.

Haas, R., Walls, J., Carroll, R.G. (1988) “Geogrid reinforcement of granular bases in flexible pavements”, Transportation Research Record, Issue Number: 1188, p. 19-27

Haddock, J. *et al.* (1999) “Effect of Gradation on Asphalt Mixture Performance”, Transportation Research Record: Journal of the Transportation Research Board, Volume 1681, pp.59-68

Han, J., Zhang, Y.Z., Parsons, R.L. (2008) “Development of a performance-based laboratory test method for evaluating geosynthetic-soil confinement”, In: Paper Presented at the CD-Rom Publication, the 87th TRB Annual Meeting, January 13 to 17, Washington, DC.

Han, J., Zhang, Y.-Z., Parsons, R.L. (2008) “Development of a performance-based laboratory test method for evaluating geosynthetic-soil confinement”, In: Paper Presented at the CD-Rom Publication, the 87th TRB Annual Meeting, Washington, DC.

Harthong, B. *et al.* (2009) “Modeling of high-density compaction of granular materials by the Discrete Element Method”, International Journal of Solids and Structures, Volume 46, Issues 18-19, September 2009, Pages 3357-3364

Huang, B.H. *et al.* (2009) “Effects of coarse aggregate angularity and asphalt binder on laboratory measured permanent deformation properties of HMA”, International Journal of Pavement Engineering Vol. 10, No. 1, Pages 19–28

Huber, G. A. and G. H. Heiman. (1987) “Effect of Asphalt Concrete Parameter on Rutting Performance: A Field Investigation”, Association of Asphalt paving Technologists, Volume 56, pp. 33-61.

Hufenusa, R. *et al.* (2006) “Full-scale field tests on geosynthetic reinforced unpaved roads on soft subgrade”, Geotextiles and Geomembranes, Volume 24, Issue 1, Pages 21-37

Hurley, G. and Prowell, B. (2006) “Evaluation of Potential Processes for Use in Warm Asphalt Mixes”, Journal of the Association of Asphalt Paving Technologists, Vol. 75, pp. 41-85

Itasca Consulting Group. (2004) “PFC2D manual Ver.3.1”, Minneapolis

Jackson, N.M. and Owenby, E.A. (1998) “Evaluation of Laboratory Compaction of HMA”, Transportation Center, The University of Tennessee, Final Report

Jerier, J.F. *et al.* (2010) “Packing spherical discrete elements for large scale simulations, Computer Methods in Applied Mechanics and Engineering”, Volume 199, Issues 25-28, Pages 1668-1676

Jing, L. (2000) “Block system construction for three-dimensional discrete element models of fractured rocks”, International Journal of Rock Mechanics and Mining Sciences, Volume 37, Issue 4, 645-659

Jonathan, T.H. *et al.* (1992) “The effectiveness of geosynthetic reinforced embankments constructed over weak foundations”, Geotextiles and Geomembranes, Volume 11, Issue 2, Pages 133-150

Khalid, A.S. *et al.* (2006) “Compactability and performance of superpave mixture with aggregate structures designed using the Bailey method”, Asphalt Paving Technology:

Association of Asphalt Paving Technologists-Proceedings of the Technical Sessions, Vol. 75, pp. 91-132

Khosla, N.P. and Sadasivam, S. (2002) “Evaluation of the effects of mixture properties and compaction methods on the predicted performance of Superpave mixture”, final report FHWA/NC/2002-030, North Carolina State University

Kim, H. and Buttlar, W.G. (2005) “Micro mechanical fracture modeling of asphalt mixture using the discrete element method”, Geotechnical Special Publication, n 130-142, 209-223

Kim, H. *et al.* (2008) “Simulation of Fracture Behavior in Asphalt Concrete Using a Heterogeneous Cohesive Zone Discrete Element Model”, Journal of materials in civil engineering, Vol. 20, No. 8, pp. 552-563

Kim, S., Roque, R.; Birgisson, B.; Guarin, A. (2009) “Porosity of the Dominant Aggregate Size Range to Evaluate Coarse Aggregate Structure of Asphalt Mixture”, Journal of Materials in Civil Engineering, Vol. 21, No. 1, pp. 32–39

Kim, S.; Roque, R.; and Birgisson, B. (2006) “Identification and assessment of the dominant aggregate size range (DASR) of asphalt mixture”, Journal of the Association of Asphalt Paving Technologists, vol. 75, pp 789–814

Koneru, S. (2008) “A thermomechanical framework for modeling the compaction of asphalt mixes”, Mechanics of Materials, v 40, n 10, p 846-64

Konietzky, H., te Kamo, L., Groeger, T., Jenner, C. (2004) “Use of DEM to model the interlocking effect of geogrids under static and cyclic loading”, In: Paper Presented at the Numerical Modeling in Micromechanics via Particle Methods, Kyoto, Japan.

Kozicki, J. and Donze, F.V. (2008) “A new open-source software developed for numerical simulations using discrete modeling methods, Computer methods in applied mechanics and engineering, vol. 197, 4429-4443.

Kwon, J., Tutumluer, E., Konietzky, H. (2008) “Aggregate base residual stresses affecting geogrid reinforced flexible pavement response”, Journal International Journal of Pavement Engineering, Volume 9, Issue 4, pages 275 - 285

Kwon, J.; Tutumluer, E. and Kim, M. (2005) “Development of a mechanistic model for geosynthetic-reinforced flexible pavements”, Geosynth. Int., 12(6), 310–320

Leung, Y.W., Wang, Y. (2000) “Multiobjective Programming Using Uniform Design and Genetic Algorithm, IEEE transactions on systems, man, and cybernetics—part c: applications and reviews”, vol. 30, no. 3

Liang, Y.Z., Fang, K.T. and Xu, Q.S. (2001) “Uniform design and its applications in chemistry and chemical engineering”, Chemometrics and Intelligent Laboratory Systems, Volume 58, Issue 1, Pages 43-57

Linden, R.N. *et al.*. (1989) “Effect of Compaction on Asphalt Concrete Performance”, Transportation Research Record, volume 1217, Pages 20-28.

Liu, Q. and Cao, D. (2009) “Research on Material Composition and Performance of Porous Asphalt Pavement”, Journal of Materials in Civil Engineering, Vol. 21, No. 4, Pages 135-140

Liu, Y., Dai, Q. and You, Z. (2009) “Viscoelastic Model for Discrete Element Simulation of Asphalt Mixture”, Journal of Engineering Mechanics

Masad, E. and Button, J. (2004) “Implications of Experimental Measurements and Analyses of the Internal Structure of Hot-Mix Asphalt”, Transportation Research

Record: Journal of the Transportation Research Board, No. 1891, TRB, National Research Council, Washington, D.C., pp. 212–220.

Masad, E. *et al.* (1999) “Quantifying Laboratory Compaction Effects on the Internal Structure of Asphalt Concrete”, Transportation Research Record 1681, pp 179-185

Masad, E. *et al.* (2002) “Characterization of Air Void Distribution in Asphalt Mixes using X-ray Computed Tomography”, Journal of Materials in Civil Engineering, Vol. 14, No. 2, pp. 122-129

Matheson, A.J. (1974) “Computation of random packing of hard spheres”, Journal of Physics C: Solid State Physics, Volume 7, Number 15, pp. 2569-2576

McDowell, G.R. *et al.* (2006) “Discrete element modelling of geogrid-reinforced aggregates”, Proceedings of the Institution of Civil Engineers: Geotechnical Engineering, vol. 159, no. 1, pp. 35-48

Meegoda, J.N. and Chang, K.G. (1993) “Novel approach to develop a performance based test for rutting of asphalt concrete”, Pavement Innovations Theory to Practice, 126-140

Meegoda, J.N. and Chang, K.G. (1994) “Modeling viscoelastic behavior of Hot Mix Asphalt (HMA) using discrete element methods”, Proceedings of the Materials Engineering Conference, n804, 804-811

Moghaddas, F.N. and Small, J.C. (1996) “Effect of Geogrid Reinforcement in Model Track Tests on Pavements”, J. Transp. Engrg. Volume 122, Issue 6, pp. 468-474

Monismith, C. M. (1993) “Asphalt Concrete: An Extraordinary Material for Engineering Applications”, 13th Henry M. Shaw Lecture in Civil Engineering, Department of Civil Engineering, North Carolina State University, Raleigh, North Carolina

Muraya, P. M. (2007) “Homogeneous test specimens from gyratory compaction”, International Journal of Pavement Engineering, Vol. 8, No. 3, pp. 225–235

National Asphalt Pavement Association (NAPA, 2010), http://www.hotmix.org/index.php?option=com_content&task=view&id=14&Itemid=33

Pan, T., Tutumluer, E. and Carpenter, S.H. (2005) “Effect of Coarse Aggregate Morphologyon the Resilient Modulus of Hot-Mix Asphalt”, Transportation Research Record: Journal of the Transportation Research Board, No. 1929, pp. 1–9

Peng, B. *et al.* (2005) “Bailey Method for Aggregate Grading Design of SMA-16”, Journal of Highway and Transportation Research and Development, pp. 23-27

Perdomo, D., and Button, J. W. (1991). “Identifying and correcting rut susceptible asphalt mixture”, Transp. Res. Rec., Transportation Research Board, Washington, D.C.

Pirabarooban, S. *et al.* (2003) “Evaluation of Rutting Potential in Asphalt Mixes Using Finite Element Modeling”, presentation at 2003 Annual Conference of the Transportation Association

Popp, K. and Schiehlen, W. (2008) “Ground Vehicle Dynamics”, Berlin: Springer.

Renouf, M., Dubois, F. and Alart, P. (2006) “Numerical investigations of fault propagation and forced-fold using a non smooth discrete element method”, Rev. Eur. Method. Num., vol. 15, 549-570

Roberts, F.L. *et al.* (1996) “Hot mix asphalt materials, mixture design, and construction”, second edition, National Center for Asphalt Technology.

Rodrigo Delgadillo and Hussain U. Bahia. (2008) “Effects of Temperature and Pressure on Hot Mixed Asphalt Compaction: Field and Laboratory Study”, J. Mat. in Civ. Engrg. Volume 20, Issue 6, pp. 440-448

Roque, R.; Huang, S.; and Ruth, B.E. (1997) “Maximizing shear resistance of asphalt mixture by proper selection of aggregate gradation”, Proceedings of the 8th International Conference on Asphalt Pavements, Seattle, pp. 249–268

Rothwell, R. (2008) “Creating wealth with free software”, Free Software Magazine, http://www.freesoftwaremagazine.com/community_posts/creating_wealth_free_software

Rousseau, J. (2009) “Multidomain finite and discrete elements method for impact analysis of a concrete structure”, Engineering Structures, Volume 31, Issue 11, Pages 2735-2743

Rutgers, R., (1962) Packing of Spheres, Nature, Volume 193, Issue 4814, pp. 465-466.

Saad, B. Mitri, H. and Poorooshasb, H. (2005) “Three-Dimensional Dynamic Analysis of Flexible Conventional Pavement Foundation”, J. Transp. Engrg, Volume 131, Issue 6, pp. 460-469

Sadasivam, S. (2004) “Evaluation of the effects of compaction methods on the predicted performance of superpave mixture”, Doctoral dissertation, North Carolina State University

Saleeb, A. *et al.* (2005) “Numerical simulation techniques for HMA rutting under loaded wheel tester”, International Journal of Pavement Engineering, Volume 6, Number 1 , pp. 57-66(10)

Santucci, L.E., Allen, D.D. and Coats, R.L. (1985) “The Effects of Moisture and Compaction on the Quality of Asphalt Pavements”, Association of Asphalt Paving Technologists, Volume 54.

Scott, G D. (1960) “Packing of equal spheres”, Nature, 188:908-909.

Simpson, B. and Tatsuoka, F., Geotechnics: the next 60 years, (2008). Géotechnique 58, No. 5, 357–368

Stevenson, J.D. and Aschenbrener, T. (1994) “Comparison of Test Results from Laboratory and Field Compacted Samples”, Final Report, No. CDOT-DTD-R-94-3, Colorado Department of Transportation

Stevenson, J.D. and T. Aschenbrener (1994) “Comparison of Test Results from Laboratory and Field Compacted Samples”, Final Report No. CDOT-DTD-R-94-3, Colorado Department of Transportation

Sukumaran, B. *et al.* (2004) “Three dimensional finite element modeling of flexible pavements”, presented for the 2004 FAA worldwide airport technology transfer conference

Tarefder, R.A. and Zaman, M. (2002) “Evaluation of rutting potential of hot mix asphalt using the asphalt pavement analyzer”, Final Report, Oklahoma Department of Transportation

Tashman, L., *et al.* (2002) “X-Ray Tomography to Characterize Air Void Distribution in Superpave Gyratory-Compacted Specimens”, International Journal of Pavement Engineering, Volume 3, Issue 1, pages 19-28

Ter Huerne, H.L. *et al.* (2008) “Simulation of HMA compaction by using FEM”, International Journal of Pavement Engineering, Volume 9, Issue 3, pages 153 – 163

Thyagarajana, S. *et al.* (2010) “The heterogeneity and mechanical response of hot mix asphalt laboratory specimens”, International Journal of Pavement Engineering, Vol. 11, No. 2, pp. 107–121

Ting, J.M. *et al.* (1989) “Discrete Numerical Model for Soil Mechanics”, Journal of Geotechnical Engineering, Vol. 115, No. 3, 379-398

Tschoegl, N. W. (1989) “The phenomenological theory of linear viscoelastic behavior”, Springer, Berlin

Vavrik, W. R.; Huber, G..; Pine, W. J.; Carpenter, S.H.; Bailey, R. (2002) “Bailey Method for Gradation Selection in HMA Mixture Design”, Transportation Research E-Circular., E-C044

Vavrik, W. R.; Pine,W.J.; Carpenterv, S.H. (2002) “Aggregate Blending for Asphalt Mix Design: The Bailey Method”, Transportation Research Record 1789, Washington, D.C., pp. 146–153

Vavrik, W.R., Fries, R.J. and Carpenter, S.H. (1999) “Effect of Flat and Elongated Coarse Aggregate on Characteristics of Gyratory Compacted Samples”, Journal of the Transportation Research Board, Volume 1681, Pages 28-36

Vavrik, W.R.; Pine, W.J.; Huber, G.A.; Carpenter, S.H. and Bailey, R. (2001) “The Bailey Method of Gradation Evaluation: The Influence of Aggregate Gradation and Packing Characteristics on Voids in the Mineral Aggregate”, Journal of the Association of Asphalt Paving Technologists, Vol. 70, pp. 132–175

Wang, C., Tannant, D.D., Lilly, P.A. (2003) “Numerical analysis of the stability of heavily jointed rock slopes using PFC2D”, International Journal of Rock Mechanics and Mining Sciences, vol. 40, no. 3, pp. 415-424

Wang, L.B. *et al.* (2007) “Fundamental mechanics of asphalt compaction through FEM and DEM modeling”, Geotechnical Special Publication, n176, pp. 45-63

Wang, Y. *et al.* (2006) “Implementation of particle-scale rotation in the 3-D lattice solid model”, Pure Appl Geophys, Vol. 163, Pages 1769–1785.

Wei, Z. *et al.* (1993) “Uniform design: A new approach of designing fermentation media”, Biotechnol Tech , Volume 7, Number 5, p379-384

Xie, Y.S. and Zhao, Y.S. (2009) “Numerical simulation of the top coal caving process using the discrete element method”, International Journal of Rock Mechanics and Mining Sciences, v46, n6, 983-991

Yao, M. and Anandarajah, A. (2003) “Three-dimensional discrete element method of analysis of clays”, Journal of Engineering Mechanics, v129, n6, 585-596

You, Z. and Buttlar, W.G. (2004) “Discrete element modeling to predict the modulus of asphalt concrete mixture”, Journal of Materials in Civil Engineering, v16, n2, 140-146

You, Z. and Buttlar, W.G. (2005) “Application of Discrete Element Modeling Techniques to Predict the Complex Modulus of Asphalt-Aggregate Hollow Cylinders Subjected to Internal Pressure”, No. 1929, TRB, National Research Council, Washington, D.C., pp. 218-226

You, Z. and Buttlar, W.G. (2006) “Micromechanical Modeling Approach to Predict Compressive Dynamic Moduli of Asphalt Mixture Using the Distinct Element Method”, No. 1970, TRB, National Research Council, Washington, D.C., pp. 73–83

You, Z. *et al.* (2010) “Air void effect on an idealized asphalt mixture using two-dimensional and three-dimensional discrete element modeling approach”, International Journal of Pavement Engineering, Volume 11, Issue 5, pages 381-391

Zaghloul, S. and SWhite, T.D. (1993) “Use of a three-dimensional, dynamic finite element program for analysis of flexible pavement”, Transportation Research Record, Issue 1388, p. 60-69

Zheng, J.L. (2008) “ANSYS research on vibratory compacting process of hot asphalt mixture pavement”, Engineering Mechanics, v 25, n 10, p 200-206, October 2008

Ziauddin A. K. *et al.* (1998) “Comparative study of asphalt concrete laboratory compaction methods to simulate field compaction”, Construction and Building Materials, Volume 12, Issues 6-7, Pages 373-384

Zube, E. (1962) “Compaction Studies of Asphalt Concrete Pavement as Related to the Water Permeability Test”, 41st Annual Meeting of the Highway Research Board, Washington, DC.

APPENDICES

Appendices-A1 Hpp File of Burgers' Model in YADE Code

```
#ifndef Burgers_CONTACT_LAWNew_HPP
#define Burgers_CONTACT_LAWNew_HPP

#include<yade/core/InteractionSolver.hpp>
#include<yade/core/PhysicalAction.hpp>

#include <set>
#include <boost/tuple/tuple.hpp>

class PhysicalAction;

class BurgersContactLawNew : public InteractionSolver
{

      private :
            shared_ptr<PhysicalAction> actionForce;
            shared_ptr<PhysicalAction> actionMomentum;
            int actionForceIndex;
            int actionMomentumIndex;

      public :

            Real  BurEmn;// burger's E parameters for maxwell in normal
direction
            Real  BurEkn;// burger's E parameters for kelvin in normal
direction
            Real  BurEms;
            Real  BurEks;
            Real  BurDmn;// burger's Dashpot parameters for maxwell in
normal direction
            Real  BurDkn;// burger's Dashpot parameters for kelvin in
normal direction
            Real  BurDms;
            Real  BurDks;
            Real  BurPoi;// burger's Poisson ratio
                int sdecGroupMask;
            bool momentRotationLaw;
            BurgersContactLawNew();
            void action(MetaBody*);

      protected :
            void registerAttributes();
      NEEDS_BEX("Force","Momentum");
      REGISTER_CLASS_NAME(BurgersContactLawNew);
      REGISTER_BASE_CLASS_NAME(InteractionSolver);
};

REGISTER_SERIALIZABLE(BurgersContactLawNew,false);

#endif // Burgers_CONTACT_LAWNew_HPP
```

Appendices-A2 Cpp File of Burgers' Model in YADE Code

```
#include"BurgersContactLawNew.hpp"
#include<yade/pkg-dem/BodyMacroParameters.hpp>
#include<yade/pkg-dem/SpheresContactGeometry.hpp>
#include<yade/pkg-dem/SDECLinkGeometry.hpp>
#include<yade/pkg-dem/ElasticContactInteraction.hpp>
#include<yade/pkg-dem/SDECLinkPhysics.hpp>
#include<yade/core/Omega.hpp>
#include<yade/core/MetaBody.hpp>
#include<yade/pkg-common/Force.hpp>
#include<yade/pkg-common/Momentum.hpp>
#include<yade/core/PhysicalAction.hpp>

BurgersContactLawNew::BurgersContactLawNew() : InteractionSolver() ,
actionForce(new Force) , actionMomentum(new Momentum)
{
      sdecGroupMask=1;
      momentRotationLaw = true;
      actionForceIndex = actionForce->getClassIndex();
      actionMomentumIndex = actionMomentum->getClassIndex();
}


void BurgersContactLawNew::registerAttributes()
{
      InteractionSolver::registerAttributes();
      REGISTER_ATTRIBUTE(sdecGroupMask);
      REGISTER_ATTRIBUTE(momentRotationLaw);
      REGISTER_ATTRIBUTE(BurEmn);
      REGISTER_ATTRIBUTE(BurEkn);
      REGISTER_ATTRIBUTE(BurEms);
      REGISTER_ATTRIBUTE(BurEks);
      REGISTER_ATTRIBUTE(BurDmn);
      REGISTER_ATTRIBUTE(BurDkn);
      REGISTER_ATTRIBUTE(BurDms);
      REGISTER_ATTRIBUTE(BurDks);
      REGISTER_ATTRIBUTE(BurPoi);
}


void BurgersContactLawNew::action(MetaBody* ncb)
{
      shared_ptr<BodyContainer>& bodies = ncb->bodies;
      Real dt = Omega::instance().getTimeStep();

      InteractionContainer::iterator ii    = ncb->transientInteractions-
>begin();
      InteractionContainer::iterator iiEnd = ncb->transientInteractions-
>end();
      for(  ; ii!=iiEnd ; ++ii )
      {
            if ((*ii)->isReal)
```

```
            {
                  const shared_ptr<Interaction>& contact = *ii;
                  int id1 = contact->getId1();
                  int id2 = contact->getId2();

                  if( !( (*bodies)[id1]->getGroupMask() &
(*bodies)[id2]->getGroupMask() & sdecGroupMask) ) continue;

                  SpheresContactGeometry*    currentContactGeometry=
YADE_CAST<SpheresContactGeometry*>(contact->interactionGeometry.get());
                  ElasticContactInteraction* currentContactPhysics =
YADE_CAST<ElasticContactInteraction*> (contact-
>interactionPhysics.get());
                 if((!currentContactGeometry)||(!currentContactPhysics))
continue;

                  BodyMacroParameters* de1                          =
YADE_CAST<BodyMacroParameters*>((*bodies)[id1]-
>physicalParameters.get());
                  BodyMacroParameters* de2                          =
YADE_CAST<BodyMacroParameters*>((*bodies)[id2]-
>physicalParameters.get());

                  bool isDynamic1 = (*bodies)[id1]->isDynamic;
                  bool isDynamic2 = (*bodies)[id2]->isDynamic;

                  Real Da     = currentContactGeometry->radius1;
                  Real Db     = currentContactGeometry->radius2;

                  Vector3r& shearForce          = currentContactPhysics-
>shearForce;
                  Vector3r& normalForce         = currentContactPhysics-
>normalForce;
                  Vector3r& ukkn                = currentContactPhysics-
>ukkn;
                  Vector3r& shearForceT1        = currentContactPhysics-
>shearForceT1;
                  Vector3r& normalForceT1       = currentContactPhysics-
>normalForceT1;
                  Vector3r& ukks                = currentContactPhysics-
>ukks;
                  int& Ite                = currentContactPhysics->Ite;

                  Real    Dinit = Da+Db;
                    Real      knk = BurEkn*Dinit;
                    Real      cnk = BurDkn*Dinit;
                    Real      knm = BurEmn*Dinit;
                    Real      cnm = BurDmn*Dinit;
                    Real      ksk = BurEks*Dinit/(2.0+2.0*BurPoi);
                    Real      csk = BurDks*Dinit/(2.0+2.0*BurPoi);
                    Real      ksm = BurEms*Dinit/(2.0+2.0*BurPoi);
                    Real      csm = BurDms*Dinit/(2.0+2.0*BurPoi);

                  Real un=currentContactGeometry->penetrationDepth;
                  Real burnA=1.0+knk*dt/(2.0*cnk);
```

```
                Real burnB=1.0-knk*dt/(2.0*cnk);
                Real burnC=dt/(2.0*cnk*burnA)+1.0/knm+dt/(2.0*cnm);
                Real burnD=dt/(2.0*cnk*burnA)-1.0/knm+dt/(2.0*cnm);
                Real bursA=1.0+ksk*dt/(2.0*csk);
                Real bursB=1.0-ksk*dt/(2.0*csk);
                Real bursC=dt/(2.0*csk*bursA)+1.0/ksm+dt/(2.0*csm);
                Real bursD=dt/(2.0*csk*bursA)-1.0/ksm+dt/(2.0*csm);

                if (contact->isNew)
                      {   ukkn=Vector3r(0,0,0);
                          ukks=Vector3r(0,0,0);
                          shearForce=Vector3r(0,0,0);
                          normalForce=knm*std::max(un,(Real)
0)*currentContactGeometry->normal;
                       }

                Vector3r axis;
                Real angle;
                axis = currentContactPhysics-
>prevNormal.Cross(currentContactGeometry->normal);
                shearForce -= shearForce.Cross(axis);
                Vector3r summaryAngularVelocity(0,0,0);
                if (isDynamic1) summaryAngularVelocity += de1-
>angularVelocity;
                if (isDynamic2) summaryAngularVelocity += de2-
>angularVelocity;
                angle = dt*0.5*currentContactGeometry-
>normal.Dot(summaryAngularVelocity);
                axis = angle*currentContactGeometry->normal;
                shearForce -= shearForce.Cross(axis);

                Vector3r x                  =
currentContactGeometry->contactPoint;
                Vector3r c1x                       = (x - de1-
>se3.position);
                Vector3r c2x                       = (x - de2-
>se3.position);
                      Vector3r _c1x_    = (isDynamic1) ?
currentContactGeometry->radius1*currentContactGeometry->normal : x -
de1->zeroPoint;
                      Vector3r _c2x_    = (isDynamic2) ? -
currentContactGeometry->radius2*currentContactGeometry->normal : x -
de2->zeroPoint;
                Vector3r relativeVelocity          = (de2-
>velocity+de2->angularVelocity.Cross(_c2x_))-(de1->velocity+de1-
>angularVelocity.Cross(_c1x_));
                      Vector3r normalVelocity =
std::abs(currentContactGeometry-
>normal.Dot(relativeVelocity))*currentContactGeometry->normal;
                      Vector3r shearVelocity             =
relativeVelocity-normalVelocity;
                Vector3r shearDisplacement         = shearVelocity*dt;
                Vector3r normalDisplacement         =
normalVelocity*dt;
```

```
                        if (contact->isNew)
Ite=Omega::instance().getCurrentIteration();
                normalForceT1 = (normalDisplacement+ukkn*(1.0-
burnB/burnA)-normalForce*burnD)/burnC;
                ukkn =
(ukkn*burnB+(normalForceT1+normalForce)*dt/(2.0*cnk))/burnA;
                normalForce = normalForceT1;

                shearForceT1 = -1.0*(shearDisplacement+ukks*(1.0-
bursB/bursA)+bursD*shearForce)/bursC;
                ukks = (ukks*bursB-
(shearForceT1+shearForce)*dt/(2.0*csk))/bursA;
                shearForce = shearForceT1;

                Real maxFs = normalForce.SquaredLength() *
std::pow(currentContactPhysics->tangensOfFrictionAngle,2);
                if( shearForce.SquaredLength() > maxFs )
                {
                     maxFs = Mathr::Sqrt(maxFs) / shearForce.Length();
                      shearForce *= maxFs;
                }


                Vector3r f                    = normalForce +
shearForce;

                static_cast<Force*>   ( ncb->physicalActions-
>find( id1 , actionForceIndex).get() )->force    -= f;
                static_cast<Force*>   ( ncb->physicalActions-
>find( id2 , actionForceIndex ).get() )->force    += f;

                static_cast<Momentum*>( ncb->physicalActions-
>find( id1 , actionMomentumIndex ).get() )->momentum -= c1x.Cross(f);
                static_cast<Momentum*>( ncb->physicalActions-
>find( id2 , actionMomentumIndex ).get() )->momentum += c2x.Cross(f);

                currentContactPhysics->prevNormal =
currentContactGeometry->normal;
            }
      }
}

YADE_PLUGIN();
```

Appendices-B1 Hpp File of Rotation Plate Engine in YADE Code

```
#ifndef ROTATIONENGINE_HPP
#define ROTATIONENGINE_HPP

#include<yade/core/DeusExMachina.hpp>
#include <Wm3Vector3.h>
#include<yade/lib-base/yadeWm3.hpp>

class RotationEngine : public DeusExMachina
{
	public :
		RotationEngine();

		Real angularVelocity;
		Vector3r rotationAxis;
		bool rotateAroundZero;
		Vector3r zeroPoint;

		void applyCondition(MetaBody * );

	protected :
		void registerAttributes();
		void postProcessAttributes(bool deserializing);
	REGISTER_CLASS_NAME(RotationEngine);
	REGISTER_BASE_CLASS_NAME(DeusExMachina);
};

REGISTER_SERIALIZABLE(RotationEngine,false);

#endif // ROTATIONENGINE_HPP
```

Appendices-B2 Cpp File of Rotation Plate Engine in YADE Code

```
#include "RotationEngine.hpp"
#include<yade/pkg-common/RigidBodyParameters.hpp>
#include<yade/core/MetaBody.hpp>
#include<yade/lib-base/yadeWm3Extra.hpp>


RotationEngine::RotationEngine()
{
      rotateAroundZero = false;
      zeroPoint = Vector3r(0,0,0);
}


void RotationEngine::registerAttributes()
{
      DeusExMachina::registerAttributes();
      REGISTER_ATTRIBUTE(angularVelocity);
      REGISTER_ATTRIBUTE(rotationAxis);
      REGISTER_ATTRIBUTE(rotateAroundZero);
      REGISTER_ATTRIBUTE(zeroPoint);
}

void RotationEngine::postProcessAttributes(bool deserializing)
{
            if (!deserializing) return;
            rotationAxis.Normalize();
}

void RotationEngine::applyCondition(MetaBody *ncb)
{

      shared_ptr<BodyContainer> bodies = ncb->bodies;

      std::vector<int>::const_iterator ii = subscribedBodies.begin();
      std::vector<int>::const_iterator iiEnd = subscribedBodies.end();

      Real dt = Omega::instance().getTimeStep();
      // time = dt;

      Quaternionr q;
      q.FromAxisAngle(rotationAxis,angularVelocity*dt);

      Vector3r ax;
      Real an;

      for(;ii!=iiEnd;++ii)
      {
            RigidBodyParameters * rb =
static_cast<RigidBodyParameters*>((*bodies)[*ii]-
>physicalParameters.get());
```

```
            if(rotateAroundZero)
                  rb->se3.position  = q*(rb->se3.position-
zeroPoint)+zeroPoint; // for RotatingBox

            rb->se3.orientation     = q*rb->se3.orientation;
            rb->se3.orientation.Normalize();
            rb->se3.orientation.ToAxisAngle(ax,an);

            rb->angularVelocity     = rotationAxis*angularVelocity;
            rb->velocity            = Vector3r(0,0,0);
      }


}

YADE_PLUGIN();
```

Appendices-C1 Hpp File of Constant Pressure Engine in YADE

Code

```
#ifndef COMPRESSION_PLATE_HPP
#define COMPRESSION_PLATE_HPP

#include<yade/core/DeusExMachina.hpp>
#include <Wm3Vector3.h>
#include<yade/lib-base/yadeWm3.hpp>
#include <string>

#define TR {if (Omega::instance().getCurrentIteration()%100==0) TRACE; }
class PhysicalAction;
class MetaBody;
class PhysicalParameters;

class CompressionPlate : public DeusExMachina
{
      private :
            int ForceClassIndex;

        public :
                Real       stiffnessCompressionPlate;
              int        Plate_id, UpdateInterval;
                int        &CompressionPlate_id;
                Vector3r   normalCompressionPlate;
                Vector3r   previousTranslationCompressionPlate;
                Real       wallDamping;
                Real       sigma_iso;
              Real       depth;
              Real       width;
                Real       platedeg;
            std::string  outputFile;
                bool       CompressionPlate_activated;
                Real       max_vel;

            Real angularVelocity;
            Vector3r rotationAxis;
            bool rotateAroundZero;
            Vector3r zeroPoint;
                int        Ite;

                CompressionPlate();
            virtual ~CompressionPlate();

            virtual void applyCondition(MetaBody*);
            //! Regulate the stress applied on walls with flag
wall_XXX_activated = true
            void controlExternalStress(MetaBody* ncb, Vector3r
resultantForce, PhysicalParameters* p, Real wall_max_vel);
            void updateStiffness(MetaBody* ncb);
```

```
            DECLARE_LOGGER;

      protected :
            virtual void registerAttributes();
      NEEDS_BEX("Force");
      REGISTER_CLASS_NAME(CompressionPlate);
      REGISTER_BASE_CLASS_NAME(DeusExMachina);
};

REGISTER_SERIALIZABLE(CompressionPlate,false);

#endif // COMPRESSION_PLATE_HPP
```

Appendices-C2 Cpp file of Constant Pressure Engine in YADE

Code

```
#include"CompressionPlate.hpp"
#include<yade/pkg-common/InteractingSphere.hpp>
#include<yade/pkg-common/InteractingBox.hpp>
#include<yade/pkg-dem/SpheresContactGeometry.hpp>
#include<yade/pkg-dem/ElasticContactInteraction.hpp>
#include<yade/pkg-common/Force.hpp>
#include<yade/pkg-common/RigidBodyParameters.hpp>
#include<yade/pkg-common/ParticleParameters.hpp>

#include<yade/core/MetaBody.hpp>
#include<yade/pkg-common/Sphere.hpp>
#include<yade/extra/Shop.hpp>
#include<boost/lexical_cast.hpp>
#include <string>

CREATE_LOGGER(CompressionPlate);

CompressionPlate::CompressionPlate():CompressionPlate_id(Plate_id)
{
        shared_ptr<Force> tmpF(new Force);
        ForceClassIndex=tmpF->getClassIndex();

        stiffnessCompressionPlate = 0;
        Plate_id = 0;
        normalCompressionPlate = Vector3r::ZERO;
        previousTranslationCompressionPlate = Vector3r::ZERO;
        wallDamping = 0;
        sigma_iso = 0;
        depth = 0;
        width = 0;
        platedeg=0;
        CompressionPlate_activated = true;
        max_vel = 0.001;
        outputFile = "0D";
        rotateAroundZero = false;
        zeroPoint = Vector3r(0,0,0);
        UpdateInterval = 2000;
        Ite=90000000;
}

CompressionPlate::~CompressionPlate()
{
}

void CompressionPlate::registerAttributes()
{
      DeusExMachina::registerAttributes();
      REGISTER_ATTRIBUTE(stiffnessCompressionPlate);
```

```
	REGISTER_ATTRIBUTE(CompressionPlate_id);
	REGISTER_ATTRIBUTE(normalCompressionPlate);
	REGISTER_ATTRIBUTE(wallDamping);
	REGISTER_ATTRIBUTE(previousTranslationCompressionPlate);
	REGISTER_ATTRIBUTE(CompressionPlate_activated);
	REGISTER_ATTRIBUTE(max_vel);
	REGISTER_ATTRIBUTE(width);
	REGISTER_ATTRIBUTE(depth);
	REGISTER_ATTRIBUTE(sigma_iso);
	REGISTER_ATTRIBUTE(platedeg);
	REGISTER_ATTRIBUTE(outputFile);
	REGISTER_ATTRIBUTE(angularVelocity);
	REGISTER_ATTRIBUTE(rotationAxis);
	REGISTER_ATTRIBUTE(rotateAroundZero);
	REGISTER_ATTRIBUTE(zeroPoint);
	REGISTER_ATTRIBUTE(Ite);
}

void CompressionPlate::updateStiffness (MetaBody * ncb)
{
	stiffnessCompressionPlate = 0;
	InteractionContainer::iterator ii    = ncb->transientInteractions-
>begin();
	InteractionContainer::iterator iiEnd = ncb->transientInteractions-
>end();
	for(  ; ii!=iiEnd ; ++ii )
	{
		if ((*ii)->isReal)
		{
			const shared_ptr<Interaction>& contact = *ii;
			Real fn = (static_cast<ElasticContactInteraction*>
	(contact->interactionPhysics.get()))->normalForce.Length();

			if (fn!=0)
			{
				int id1 = contact->getId1(), id2 = contact-
>getId2();

					if ( Plate_id==id1 || Plate_id==id2 )
					{
						ElasticContactInteraction*
currentContactPhysics =

	static_cast<ElasticContactInteraction*> ( contact-
>interactionPhysics.get() );
						stiffnessCompressionPlate  +=
currentContactPhysics->kn;

					}
			}
		}
	}
}
```

```
void CompressionPlate::controlExternalStress(MetaBody* ncb, Vector3r
resultantForce, PhysicalParameters* p, Real wall_max_vel)
{
      Real
translation=normalCompressionPlate.Dot(static_cast<Force*>( ncb-
>physicalActions->find(Plate_id,ForceClassIndex).get() )->force -
resultantForce);
      Real dt = Omega::instance().getTimeStep();
      // time = dt;
      Quaternionr q;
      q.FromAxisAngle(rotationAxis,angularVelocity*dt);
      if (translation!=0)
      {

         if (stiffnessCompressionPlate!=0)
         {
           if (Ite>Omega::instance().getCurrentIteration())
Ite=Omega::instance().getCurrentIteration();
                  translation /= stiffnessCompressionPlate;
                  translation = std::min( std::abs(translation),
wall_max_vel*Omega::instance().getTimeStep() ) *
Mathr::Sign(translation);
         }
         else
            translation = wall_max_vel *
Mathr::Sign(translation)*Omega::instance().getTimeStep();
      }
      previousTranslationCompressionPlate = (1-
wallDamping)*translation*normalCompressionPlate +
previousTranslationCompressionPlate;
        p->se3.position= q*(p->se3.position +
previousTranslationCompressionPlate-zeroPoint)+zeroPoint;
        p->se3.orientation = q*p->se3.orientation;
         if (Ite>Omega::instance().getCurrentIteration() &&
Omega::instance().getCurrentIteration() % 20000 == 0)
         {
                string fileName="./outputdata/"+lexical_cast<string>
(outputFile)+".sp"+lexical_cast<string>
( Omega::instance().getCurrentIteration() );
            LOG_INFO ( "saving spheres: "<<fileName );
            Shop::saveSpheresToFile ( fileName );
         }
        if (Ite<=Omega::instance().getCurrentIteration() &&
(Omega::instance().getCurrentIteration()-Ite)% 2500 == 0)
         {
                string fileName="./outputdata/"+lexical_cast<string>
(outputFile)+".sp"+lexical_cast<string>
( Omega::instance().getCurrentIteration() );
            LOG_INFO ( "saving spheres: "<<fileName );
            Shop::saveSpheresToFile ( fileName );
         }
}


void CompressionPlate::applyCondition(MetaBody* ncb)
```

```
{

      shared_ptr<BodyContainer>& bodies = ncb->bodies;
      PhysicalParameters* p_CompressionPlate =
static_cast<PhysicalParameters*>((*bodies)[CompressionPlate_id]-
>physicalParameters.get());
            Vector3r wallForce (0, sigma_iso*width*depth, 0);
            if (CompressionPlate_activated)
                {
                 updateStiffness(ncb);
                 controlExternalStress(ncb, wallForce,
p_CompressionPlate, max_vel);
                }
}
YADE_PLUGIN();
```

VITA

Jingsong Chen was born in Anqing, Anhui Province, China on October, 1981. He graduated from Taihu middle school in July 1999. In September 1999, he started his undergraduate studies at Central south University in Changsha, China, and received his Bachelor Degree in Civil Engineering in 2003. After the completion of undergraduate study, he entered the master program at Central south University and received Master's Degree in geotechnical engineering in June 2006. In September 2006, he entered Tongji University and studied one year there for Ph.D. program. In 2007, he entered the University of Tennessee at Knoxville to pursue his Ph.D. degree in civil engineering. Under the guidance of Dr. Baoshan Huang, he performed research using discrete element method (DEM) to simulate asphalt mixture compaction and analyze heterogeneous air voids distribution with asphalt mixture specimen.